

SPECTROSCOPY AND PHOTOCHEMISTRY OF
PYRAZOLYL-BRIDGED BINUCLEAR IRIDIUM(I) COMPLEXES

Thesis by

Janet Layne Marshall

In Partial Fulfillment of the Requirements

for the Degree of

Doctor of Philosophy

California Institute of Technology

Pasadena, California

1987

(Submitted December 4, 1986)

Acknowledgements

I would like to thank my advisor, Harry Gray, for giving me the opportunity to pursue my graduate degree in his research group. His enthusiasm is greatly appreciated, and I hope that some of his knowledge has rubbed off on me.

Several members of the Gray group have been especially helpful. I would like to thank Mike, Al, and Tom for a number of insightful discussions and assistance with various experiments. Miriam deserves special thanks for proofreading this thesis and always having a sympathetic ear. Thanks to "my colleague" Tad for working with me on the study of intramolecular electron-transfer reactions of binuclear iridium(I) complexes during the past year. I appreciate Les' patience in getting me started on the laser and helping with the transient absorption experiments. In addition to the above-mentioned individuals, I have enjoyed both scientific and social interactions with friends and co-workers in the group. Special appreciation goes to Catherine for providing a full pot of coffee and a comfortable chair.

I wish to acknowledge Woody Woodruff and Ed Kober for their collaboration on the Raman experiments. I also want to thank Stephen Stobart for providing samples of the iridium complexes and getting us started on this project.

I have enjoyed my friendships with a number of people from the Bercaw, Collins, and Grubbs groups, and I have especially enjoyed the good times with Leigh, both here and at Carolina. I would like to thank my family for all the support, encouragement, and educational

assistance that they have provided. Jeff deserves special thanks for helping me scientifically, being a great friend, and letting me adopt Mabel and Margaret.

I would also like to acknowledge the Union Carbide Company, the Sun Oil Company, and the Atlantic Richfield Foundation for graduate fellowships.

to Jeff *to Jeff* *to Jeff* *to Jeff*

Abstract

Spectroscopic studies of a series of pyrazolyl-bridged and substituted-pyrazolyl-bridged binuclear iridium(I) complexes indicate that the description of the metal-metal interactions in previously studied D_{4h} d^8 - d^8 rhodium(I), iridium(I), and platinum(II) species may be extended to these lower symmetry (C_{2v}) d^8 - d^8 molecules. Specifically, the $^1A_1(d\sigma)^2(d\sigma^*)^2$ ground state exhibits weak metal-metal bonding, and the lowest excited states are a singlet (1B_2) and triplet (3B_2) derived from the $(d\sigma)^2(d\sigma^*)^1(p\sigma)^1$ electronic configuration. The 1B_2 and 3B_2 excited states, which are expected to feature strong metal-metal bonding, are luminescent at ambient temperature in fluid solution.

Electronic absorption and emission spectroscopic studies and photophysical investigations of the emissive singlet and triplet excited states of bis(1,5-cyclooctadiene)bis(μ -pyrazolyl)diiridium(I), $[\text{Ir}(\mu\text{-pz})(\text{COD})]_2$, and analogous substituted-pyrazolyl complexes are presented in Chapter 2. The absorption spectrum of $[\text{Ir}(\mu\text{-pz})(\text{COD})]_2$ exhibits an intense band attributable to $^1A_1 \rightarrow ^1B_2$ at 498 nm ($\epsilon = 8100 \text{ M}^{-1}\text{cm}^{-1}$). Both fluorescence ($\lambda_{\text{max}} = 558 \text{ nm}$, $\Phi_{\text{em}} = 0.0001$, $\tau < 20 \text{ ps}$) and phosphorescence ($\lambda_{\text{max}} = 684 \text{ nm}$, $\Phi_{\text{em}} = 0.0078$, $\tau = 250 \text{ ns}$) from the 1B_2 and 3B_2 excited states, respectively, are observed at ambient temperature for this complex. The absorption and emission spectra of the substituted-pyrazolyl complexes show similar features. In addition, ground-state resonance Raman studies of these complexes suggest the presence of a reasonable metal-metal bonding interaction in the

formally nonbonded binuclear center; excitation into the bands corresponding to the metal-metal localized $^1A_1 \rightarrow ^1B_2$ transition results in resonance-enhancement of vibrations at frequencies of 58 cm^{-1} to 80 cm^{-1} that are assigned to $\nu(\text{Ir-Ir})$.

The long lifetime of the $^3B_2(d\sigma^*p\sigma)$ excited state of $[\text{Ir}(\mu\text{-pz})\text{-}(\text{COD})]_2$ implies that it should be able to participate in bimolecular reactions. The results presented in Chapter 3 show that this strongly reducing excited state undergoes photoinduced electron transfer with a variety of substrates including reversible electron transfer to one-electron acceptors such as methyl viologen and pyridinium monocations. For pyridinium acceptors with reduction potentials ranging from -0.67 V to -1.85 V vs. SSCE, the rates of electron-transfer quenching range from a diffusion-limited rate of $2.0 \times 10^{10} \text{ M}^{-1}\text{s}^{-1}$ to $1.1 \times 10^6 \text{ M}^{-1}\text{s}^{-1}$ and obey Marcus-theory predictions for outer-sphere electron transfer in the "normal free-energy region." However, the rates do not decrease as predicted for the "inverted free-energy region." With acceptors such as halocarbons, the unproductive back-electron-transfer reaction can be circumvented, and net two-electron, photoinduced electron transfer yields iridium(II)-iridium(II) oxidative addition products.

Chapter 4 focuses on spectroscopic and photophysical investigations of pyrazolyl-bridged binuclear iridium(I) complexes containing carbon monoxide ligands. Spectroscopic studies of tetracarbonylbis(μ -pyrazolyl)diiridium(I), tetracarbonylbis(μ -3-methylpyrazolyl)diiridium(I), and tetracarbonylbis(μ -3,5-dimethylpyrazolyl)diiridium(I) reveal interesting features in the electronic absorption spectra at

ambient temperature and 77 K that may be assigned to $d\pi(xz,yz) \rightarrow [\sigma(p_z),\pi^*(CO)]$ transitions and predominantly metal-metal localized $\sigma^*(d_{z^2}) \rightarrow [\sigma(p_z),\pi^*(CO)]$ transitions that reflect the degree of metal-metal interaction. Photophysical studies of the emissive ${}^{1,3}B_2(d\sigma^*p\sigma)$ excited states suggest that a higher-energy d-d excited state may provide a pathway for thermal deactivation of these states.

Table of Contents

Acknowledgements		ii
Abstract		v
Chapter 1	Introduction	1
	References	9
Chapter 2	Spectroscopic Studies of Bis(1,5-cyclooctadiene)bis- (μ -pyrazolyl)diiridium(I) and Related Complexes	14
	Introduction	15
	Experimental	23
	Results and Discussion	33
	References and Notes	97
Chapter 3	Electron-Transfer Reactivity of the $^3B_2(d\sigma^* p\sigma)$ Excited State of $[Ir(\mu\text{-pz})(COD)]_2$	102
	Introduction	103
	Experimental	105
	Results and Discussion	116
	References and Notes	157
Chapter 4	Spectroscopic Studies of Tetracarbonylbis- (μ -pyrazolyl)diiridium(I) and Related Complexes	163
	Introduction	164
	Experimental	166
	Results and Discussion	172
	References and Notes	201

Chapter 1

Introduction

Interest in the chemistry of binuclear complexes has been, in part, due to the attractiveness of these complexes for the activation of organic and inorganic substrates by cooperative metal interactions.¹⁻³ Binuclear complexes offer multiple binding sites for substrates, multielectron redox capabilities, and for heteronuclear complexes, distinct metal centers that can interact differently with a given substrate.^{4,5} While numerous studies of the thermal reactivity of binuclear complexes with a variety of substrates have been undertaken, less attention has been given to the activation of organic and inorganic molecules by the electronic excited states of these complexes.⁶⁻⁹ Since a long-lived excited state of a complex is a unique species that can have different chemical and physical properties from those of the ground state, the possibility exists for reactivity with substrates by photoexcited binuclear complexes that is not observed thermally.^{10,11} In this regard, these complexes are promising for the conversion of visible light to chemical energy.¹²⁻¹⁴ Especially important to the study of both the photochemical and thermal reactivity of binuclear complexes is an understanding of the metal-metal bonding and the consequences of metal-metal bond-forming and bond-breaking reactions.

Since the mid-1970's, our group has been interested in the thermal chemistry, photophysics, and photochemistry of several binuclear d^8-d^8 complexes of second and third row transition metals. In particular, our research efforts have focused on the characterization and reactivity of the ground and luminescent excited states of complexes of rhodium(I) and iridium(I) with bridging isocyanide ligands and a

platinum(II) dimer with bridging pyrophosphite ligands.

Spectroscopic studies of monomeric, square-planar isocyanide complexes of rhodium(I) and iridium(I) showed the tendency of these species to form dimers and higher oligomers in concentrated solutions.¹⁵⁻¹⁷ With this in mind, a number of dimeric rhodium(I) complexes with a variety of bridging isocyanide ligands, including 1,3-diisocyanopropane (bridge) and 2,5-dimethyl-2,5-diisocyanohexane (TMB), were prepared.^{18,19} From spectroscopic studies of $[\text{Rh}_2(\text{bridge})_4]^{2+}$, a weak metal-metal interaction in the $^1A_{1g}$ (D_{4h}) ground state of the d^8-d^8 dimers was shown to arise from stabilization of the filled metal-metal bonding $1a_{1g}(d_z^2\sigma)$ and antibonding $1a_{2u}(d_z^2\sigma^*)$ orbitals by configurational mixing with unoccupied orbitals of the same symmetries [$2a_{1g}(p_z\sigma)$ and $2a_{2u}(p_z\sigma^*)$].^{20,21}

Additional studies of $[\text{Rh}_2(\text{bridge})_4]^{2+}$ and related rhodium isocyanide dimers revealed that the low-energy singlet ($^1A_{2u}$) and triplet ($^3A_{2u}$) excited states derived from the $(d\sigma)^2(d\sigma^*)^1(p\sigma)^1$ electronic configuration are luminescent at ambient temperature in solution.¹⁹⁻²² Ground-state and excited-state resonance Raman studies showed that the long-lived (8.5 μs , CH_3CN , $22 \pm 2^\circ\text{C}$) $^3A_{2u}$ excited state of $[\text{Rh}_2(\text{bridge})_4]^{2+}$ is strongly metal-metal bonding, as predicted by molecular orbital theory, with the rhodium-rhodium stretching frequency of 79 cm^{-1} in the $^1A_{1g}$ ground state increasing to 144 cm^{-1} in the $^3A_{2u}$ excited state.²³ Low-temperature, single-crystal absorption spectroscopic studies corroborated this prediction. The vibronically structured band centered at $\sim 670\text{ nm}$, corresponding to the $^1A_{1g} \rightarrow E_u(^3A_{2u})$ transition, shows a progression in a frequency of

$\sim 150 \text{ cm}^{-1}$, consistent with the rhodium-rhodium stretching frequency of 144 cm^{-1} obtained from the Raman studies. An analysis of the band shape suggested that the rhodium-rhodium distance decreases $\sim 0.3 \text{ \AA}$ in the ${}^3A_{2u}$ excited state.²⁴

Studies of the thermal chemistry of $[\text{Rh}_2(\text{bridge})_4]^{2+}$ revealed that it oxidatively adds substrates such as iodine, bromine, and chlorine to give the d^7-d^7 $[\text{Rh}_2(\text{bridge})_4(\text{X})_2]^{2+}$ dimers. Oxidative addition of methyl iodide produces a dimer where the methyl and iodide fragments have added across the metal-metal axis to give *trans*- $[\text{Rh}_2(\text{bridge})_4(\text{CH}_3)(\text{I})]^{2+}$.¹⁸

The photochemical reactivity of these rhodium isocyanide dimers is also interesting. The ${}^3A_{2u}$ excited states of $[\text{Rh}_2(\text{bridge})_4]^{2+}$ and $[\text{Rh}_2(\text{TMB})_4]^{2+}$ react by energy and electron transfer with a variety of substrates including both oxidative and reductive quenchers.²⁵ Furthermore, irradiation of $[\text{Rh}_2(\text{bridge})_4]^{2+}$ in aqueous HCl solution produces hydrogen, although the mechanism involves both thermal and photochemical production of hydrogen and is rather complex.^{8,20,26-30}

Studies of the ground and luminescent excited states of $[\text{Ir}_2(\text{TMB})_4]^{2+}$ reveal that this complex is structurally and electronically similar to the square-planar "face-to-face" rhodium isocyanide dimers. As discussed above, the metal-metal interaction increases dramatically in the luminescent ${}^1A_{2u}$ and ${}^3A_{2u}$ ($d\sigma^*p\sigma$) excited states of $[\text{Ir}_2(\text{TMB})_4]^{2+}$ from the relatively weak bonding interaction in the ${}^1A_{1g}$ ground state.^{30,31} This complex also thermally oxidatively adds halogens to give iridium(II)-iridium(II) metal-metal bonded species.³²

The square-planar "face-to-face" dimer of platinum(II) with bridg-

ing pyrophosphite ligands, $[\text{Pt}_2(\text{pop})_4]^{4-}$ ($\text{pop} = \text{P}_2\text{O}_5\text{H}_2^{2-}$), also has the same rich ground-state and excited-state properties and reactivity as the rhodium(I) and iridium(I) isocyanide dimers.^{33,34} In addition to the thermal oxidative addition of halogens to give the d^7-d^7 platinum(III)-platinum(III) dimers,³⁵⁻³⁷ partial oxidation of $[\text{Pt}_2(\text{pop})_4]^{4-}$ by chlorine water, bromine water, or triiodide leads to novel linear chain "-Pt(II)-Pt(III)-X-" mixed-valence complexes that are semiconducting solids.^{38,39} As with the studies of $[\text{Rh}_2(\text{bridge})_4]^{2+}$, both ground-state and excited-state resonance Raman⁴⁰ and single-crystal absorption and emission spectroscopic experiments⁴¹ of $[\text{Pt}_2(\text{pop})_4]^{4-}$ confirm the metal-metal interaction in the $^1\text{A}_{1g}$ ground state and a substantial increase in this bonding interaction in the highly luminescent $^3\text{A}_{2u}$ excited state. The $^3\text{A}_{2u}$ excited state reacts by electron transfer with a variety of oxidative and reductive quenchers,^{34,42} and irradiation of $[\text{Pt}_2(\text{pop})_4]^{4-}$ in the presence of halocarbons leads to net two-electron, photoinduced oxidative addition of these substrates.⁴³⁻⁴⁵ Recently, the $^3\text{A}_{2u}(d\sigma^*p\sigma)$ excited state of this complex has been shown to be extremely reactive in abstracting hydrogen atoms from a variety of substrates, including silicon, germanium, and tin hydrides.⁴⁶ This excited state also abstracts hydrogen atoms from a number of alcohols and photocatalytically converts isopropanol to acetone with visible and near-UV light.^{43,44,47}

Our interest in the spectroscopic properties of these d^8-d^8 dimers, the unique reactivity of the binuclear center in both thermal and photochemical reactions, and the metal-metal interactions in the

ground and excited states prompted us to examine the photophysical properties and photochemical reactivity of a class of lower-symmetry (C_{2v}) binuclear iridium(I) complexes. Our studies have focused on bis(μ -pyrazolyl)-bridged and bis(μ -substituted-pyrazolyl)-bridged iridium dimers with ancillary ligands such as 1,5-cyclooctadiene, carbon monoxide, and phosphines coordinated in a square-planar arrangement around each iridium atom.

We have been particularly interested in the properties of $[\text{Ir}(\mu\text{-pz})(\text{COD})]_2$ (pzH = pyrazole, COD = 1,5-cyclooctadiene) and several related iridium(I) dimers. The synthesis of $[\text{Ir}(\mu\text{-pz})(\text{COD})]_2$ was first published in a Spanish patent in 1981.⁴⁸ Shortly thereafter, a related preparation and X-ray crystal structure of this complex was reported by Stobart and co-workers.^{49,50} Given that the pyrazolyl ligand is able to bridge two metals over a wide range of intermetallic distances,⁵¹⁻⁵³ the short iridium-iridium separation of 3.216(1) Å for formally nonbonding iridium(I) centers suggests that this dimer is electronically similar to the square-planar "face-to-face" d^8 - d^8 dimers for which a weak ground-state metal-metal interaction has been documented (*vide supra*).

Stobart and co-workers have demonstrated that $[\text{Ir}(\mu\text{-pz})(\text{COD})]_2$ will oxidatively add halogens (I_2 , Br_2 , Cl_2) thermally to give symmetric iridium(II)-iridium(II) products. The oxidative addition of methyl iodide to $[\text{Ir}(\mu\text{-pz})(\text{COD})]_2$ parallels that of $[\text{Rh}_2(\text{bridge})_4]^{2+}$ in that the methyl and iodide fragments coordinate to opposing metal atoms. Because of its unique structure, $[\text{Ir}(\mu\text{-pz})(\text{COD})]_2$ can also oxidatively add substrates that must bind to both metal centers such

as the activated alkynes hexafluorobut-2-yne, methyl propiolate, and dimethylacetylenedicarboxylate.^{49,54,55}

The substitution chemistry of $[\text{Ir}(\mu\text{-pz})(\text{COD})]_2$ and related bis(1,5-cyclooctadiene)bis(μ -substituted-pyrazolyl)diiridium(I) complexes^{50,56} provides a route into several other binuclear complexes that also have rather short iridium-iridium separations. The reaction of $[\text{Ir}(\mu\text{-pz})(\text{COD})]_2$ with 1 atm. of carbon monoxide at ambient temperature is rapid and leads to formation of $[\text{Ir}(\mu\text{-pz})(\text{CO})_2]_2$.^{57,58} This complex reacts with a variety of phosphines (PR_3), replacing one carbonyl ligand from each metal center to give $[\text{Ir}(\mu\text{-pz})(\text{CO})(\text{PR}_3)]_2$, which has *trans* stereochemistry.⁵⁹ These complexes are also subject to thermal oxidative addition with a variety of substrates.^{56,60,61} Analogous reactions are observed for the substituted-pyrazolyl binuclear iridium(I) cyclooctadiene complexes.

Our studies have concentrated on investigating the metal-metal interactions in the ground and low-energy luminescent excited states of these complexes.⁶² By analogy to the square-planar "face-to-face" dimers of rhodium(I), iridium(I), and platinum(II) discussed earlier, the metal-metal interactions in these complexes of C_{2v} symmetry are interpreted in terms of a weakly metal-metal bonding ground state with the $(d\sigma)^2(d\sigma^*)^2$ electronic configuration. The luminescent excited states are described in terms of the $(d\sigma)^2(d\sigma^*)^1(p\sigma)^1$ electronic configuration and are expected to be strongly metal-metal bonding. Interestingly, the metal-metal interactions in these complexes can have both an angular as well as distance dependence by virtue of the "A-frame" shape. We are also interested in the photochemical re-

activity of these dimeric complexes since the lower symmetry and open shape, relative to the previously studied d^8-d^8 dimers, allows for greater access to the metals by potential substrates, enhancing the possibility of multielectron excited-state reactivity.

Specifically, Chapter 2 of this thesis describes several of the spectroscopic and photophysical properties of the ground and luminescent excited states of $[\text{Ir}(\mu\text{-pz})(\text{COD})]_2$ and four related substituted-pyrazolyl dimers. Chapter 3 addresses the electron-transfer reactivity of the triplet ($d\sigma^* p\sigma$) excited state of $[\text{Ir}(\mu\text{-pz})(\text{COD})]_2$ with a number of pyridinium acceptors and halocarbons. Chapter 4 presents spectroscopic studies of three of the iridium dimers containing carbonyl ligands: $[\text{Ir}(\mu\text{-pz})(\text{CO})_2]_2$, $[\text{Ir}(\mu\text{-3-CH}_3\text{pz})(\text{CO})_2]_2$, and $[\text{Ir}(\mu\text{-3,5-(CH}_3)_2\text{pz})(\text{CO})_2]_2$ (pzH = pyrazole, 3-CH₃pzH = 3-methylpyrazole, 3,5-(CH₃)₂pzH = 3,5-dimethylpyrazole). The wide range of metal-metal separations and, consequently, the metal-metal bonding interactions in the ground and excited states of these pyrazolyl-bridged binuclear iridium(I) complexes lead to unique spectroscopic and photophysical properties.

References

1. Poilblanc, R. *Inorg. Chim. Acta* 1982, 62, 75-86 and references therein.
2. Halpern, J. *Inorg. Chim. Acta* 1982, 62, 31-37 and references therein.
3. Poilblanc, R. *Nouv. J. Chim.* 1978, 2, 145-150.
4. McCleverty, J.A. *Inorg. Chim. Acta* 1982, 62, 67-73.
5. Chisholm, M.H. *ACS Symp. Ser.* 1980, 155, 17-39.
6. Wrighton, M.S.; Graff, J.L.; Luong, J.C.; Reichel, C.L.; Robbins, J.L. *ACS Symp. Ser.* 1980, 155, 85-110.
7. Nocera, D.G.; Maverick, A.W.; Winkler, J.R.; Che, C.-M.; Gray, H.B. *ACS Symp. Ser.* 1983, 211, 21-33.
8. Gray, H.B.; Maverick, A.W. *Science* 1981, 214, 1201-1205.
9. Maverick, A.W.; Che, C.-M.; Nocera, D.G.; Winkler, J.R.; Gray, H.B. in "Photochemical Conversion and Storage of Solar Energy"; Rabani, J., Ed.; Weizmann Science Press: Jerusalem, 1982; pp 161-173.
10. Balzani, V.; Bolletta, F.; Gandolfi, M.T.; Maestri, M. *Top. Curr. Chem.* 1978, 75, 1-64.
11. Balzani, V.; Scandola, F. in "Energy Resources through Photochemistry and Catalysis"; Gratzel, M., Ed.; Academic Press: New York, 1983; Chapter 1.
12. Rabani, J., Ed. "Photochemical Conversion and Storage of Solar Energy"; Weizmann Science Press: Jerusalem, 1982.
13. Gratzel, M., Ed. "Energy Resources through Photochemistry and Ca-

- talysis"; Academic Press: New York, 1983.
14. Connolly, J.S., Ed. "Photochemical Conversion and Storage of Solar Energy"; Academic Press: New York, 1981.
 15. Mann, K.R.; Gordon, J.G., II; Gray, H.B. *J. Am. Chem. Soc.* **1975**, *97*, 3553-3555.
 16. Mann, K.R.; Lewis, N.S.; Williams, R.M.; Gray, H.B.; Gordon, J.G., II *Inorg. Chem.* **1978**, *17*, 828-834.
 17. Geoffroy, G.L.; Bradley, M.G.; Keeney, M.E. *Inorg. Chem.* **1978**, *17*, 777-779.
 18. Lewis, N.S.; Mann, K.R.; Gordon, J.G., II; Gray, H.B. *J. Am. Chem. Soc.* **1976**, *98*, 7461-7463.
 19. Mann, K.R.; Thich, J.H.; Bell, R.A.; Coyle, C.L.; Gray, H.B. *Inorg. Chem.* **1980**, *19*, 2462-2468.
 20. Mann, K.R.; Gray, H.B. *Adv. Chem. Ser.* **1979**, *173*, 225-235.
 21. Rice, S.F.; Milder, S.J.; Gray, H.B.; Goldbeck, R.A.; Kliger, D.S. *Coord. Chem. Rev.* **1982**, *43*, 349-354.
 22. Miskowski, V.M.; Nobinger, G.L.; Kliger, D.S.; Hammond, G.S.; Lewis, N.S.; Mann, K.R.; Gray, H.B. *J. Am. Chem. Soc.* **1978**, *100*, 485-488.
 23. Dallinger, R.F.; Miskowski, V.M.; Gray, H.B.; Woodruff, W.H. *J. Am. Chem. Soc.* **1981**, *103*, 1595-1596.
 24. Rice, S.F.; Gray, H.B. *J. Am. Chem. Soc.* **1981**, *103*, 1593-1595.
 25. Milder, S.J.; Goldbeck, R.A.; Kliger, D.S.; Gray, H.B. *J. Am. Chem. Soc.* **1980**, *102*, 6761-6764.
 26. Mann, K.R.; Lewis, N.S.; Miskowski, V.M.; Erwin, D.K.; Hammond, G.S.; Gray, H.B. *J. Am. Chem. Soc.* **1977**, *99*, 5525-5526.

27. Gray, H.B.; Mann, K.R.; Lewis, N.S.; Thich, J.A.; Richman, R.M. *Adv. Chem. Ser.* **1978**, *168*, 44-56.
28. Miskowski, V.M.; Sigal, I.S.; Mann, K.R.; Gray, H.B.; Milder, S.J.; Hammond, G.S.; Ryason, P.R. *J. Am. Chem. Soc.* **1979**, *101*, 4383-4385.
29. Mann, K.R.; DiPierro, M.J.; Gill, T.P. *J. Am. Chem. Soc.* **1980**, *102*, 3965-3967.
30. Gray, H.B.; Miskowski, V.M.; Milder, S.J.; Smith, T.P.; Maverick, A.W.; Buhr, J.D.; Gladfelter, W.L.; Sigal, I.S.; Mann, K.R. in "Fundamental Research in Homogeneous Catalysis"; Tsutsui, M., Ed.; Plenum Press: New York, 1978; pp 819-834.
31. Smith, T.P. Ph.D. Dissertation, California Institute of Technology, Pasadena, 1982.
32. Miskowski, V.M.; Smith, T.P.; Loehr, T.M.; Gray, H.B. *J. Am. Chem. Soc.* **1985**, *107*, 7925-7934.
33. Sperline, R.P.; Dickson, M.K.; Roundhill, D.M. *J. Chem. Soc., Chem. Commun.* **1977**, 62-63.
34. Che, C.-M.; Butler, L.G.; Gray, H.B. *J. Am. Chem. Soc.* **1981**, *103*, 7796-7797.
35. Che, C.-M.; Schaefer, W.P.; Gray, H.B.; Dickson, M.K.; Stein, P.B.; Roundhill, D.M. *J. Am. Chem. Soc.* **1982**, *104*, 4253-4255.
36. Bryan, S.A.; Dickson, M.K.; Roundhill, D.M. *J. Am. Chem. Soc.* **1984**, *106*, 1882-1883.
37. Che, C.-M.; Butler, L.G.; Grunthaner, P.J.; Gray, H.B. *Inorg. Chem.* **1985**, *24*, 4662-4665.
38. Che, C.-M.; Herbstein, F.H.; Schaefer, W.P.; Marsh, R.E.; Gray,

- H.B. *J. Am. Chem. Soc.* **1983**, *105*, 4604-4607.
39. Clark, R.J.H.; Kurmoo, M.; Dawes, H.M.; Hursthouse, M.B. *Inorg. Chem.* **1986**, *25*, 409-412.
40. Che, C.-M.; Butler, L.G.; Gray, H.B.; Crooks, R.M.; Woodruff, W.H. *J. Am. Chem. Soc.* **1983**, *105*, 5492-5494.
41. Rice, S.F.; Gray, H.B. *J. Am. Chem. Soc.* **1983**, *105*, 4571-4575.
42. Heuer, W.B.; Totten, M.D.; Rodman, G.S.; Hebert, E.J.; Tracy, H.J.; Nagel, J.K. *J. Am. Chem. Soc.* **1984**, *106*, 1163-1164.
43. Marshall, J.L.; Stiegman, A.E.; Gray, H.B. *ACS Symp. Ser.* **1986**, *307*, 166-176.
44. Roundhill, D.M. *J. Am. Chem. Soc.* **1985**, *107*, 4354-4356.
45. Roundhill, D.M.; Atherton, S.F. *Inorg. Chem.* **1986**, *25*, 4071-4072.
46. Vlcek, A., Jr.; Gray, H.B. *J. Am. Chem. Soc.*, submitted.
47. Harvey, E.L.; Stiegman, A.E.; Vlcek, A., Jr.; Gray, H.B., manuscript in preparation.
48. Uson Lacal, R.; Oro Giral, L.A.; Ciriano Lopez, M.A.; Pinillos, M.T.; Royo Macia, M.; Pastor Martinez, E. Spanish Patent ES 497,900, 1981; *Chem. Abstr.* **1982**, *97*, 55306n.
49. Coleman, A.W.; Eadie, D.T.; Stobart, S.R.; Zaworotko, M.J.; Atwood, J.L. *J. Am. Chem. Soc.* **1982**, *104*, 922-923.
50. Beveridge, K.A.; Bushnell, G.W.; Stobart, S.R.; Atwood, J.L.; Zaworotko, M.J. *Organometallics* **1983**, *2*, 1447-1451.
51. Stobart, S.R.; Dixon, K.R.; Eadie, D.T.; Atwood, J.L.; Zaworotko, M.J. *Angew. Chem. Int. Ed. Engl.* **1980**, *19*, 931-932.
52. Trofimenko, S. *Chem. Rev.* **1972**, *72*, 497-509.
53. Trofimenko, S. *Prog. Inorg. Chem.* **1986**, *34*, 115-210.

54. Bushnell, G.W.; Decker, M.J.; Eadie, D.T.; Stobart, S.R.; Vefghi, R.; Atwood, J.L.; Zaworotko, M.J. *Organometallics* **1985**, *4*, 2106-2111.
55. Stobart, S.R.; Coleman, A.W.; Harrison, D.G.; Atwood, J.L.; Zaworotko, M.J. *J. Am. Chem. Soc.*, submitted.
56. Bushnell, G.W.; Fjeldsted, D.O.K.; Stobart, S.R.; Zaworotko, M.J.; Knox, S.A.R.; Macpherson, K.A. *Organometallics* **1985**, *4*, 1107-1114.
57. Nussbaum, S.; Rettig, S.J.; Storr, A.; Trotter, J. *Can. J. Chem.* **1985**, *63*, 692-702.
58. Harrison, D.G.; Stobart, S.R. *J. Chem. Soc., Chem. Commun.* **1986**, 285-286.
59. Beveridge, K.A.; Bushnell, G.W.; Dixon, K.R.; Eadie, D.T.; Stobart, S.R.; Atwood, J.L.; Zaworotko, M.J. *J. Am. Chem. Soc.* **1982**, *104*, 920-922.
60. Atwood, J.L.; Beveridge, K.A.; Bushnell, G.W.; Dixon, K.R.; Eadie, D.T.; Stobart, S.R.; Zaworotko, M.J. *Inorg. Chem.* **1984**, *23*, 4050-4057.
61. Powell, J.; Kuksis, A.; Nyburg, S.C.; Ng, W.W. *Inorg. Chim. Acta* **1982**, *64*, L211-L212.
62. Preliminary experiments were conducted by Dr. Terrance P. Smith and are reported in reference 31.

Chapter 2

Spectroscopic Studies of
Bis(1,5-cyclooctadiene)bis(μ -pyrazolyl)diiridium(I)
and Related Complexes

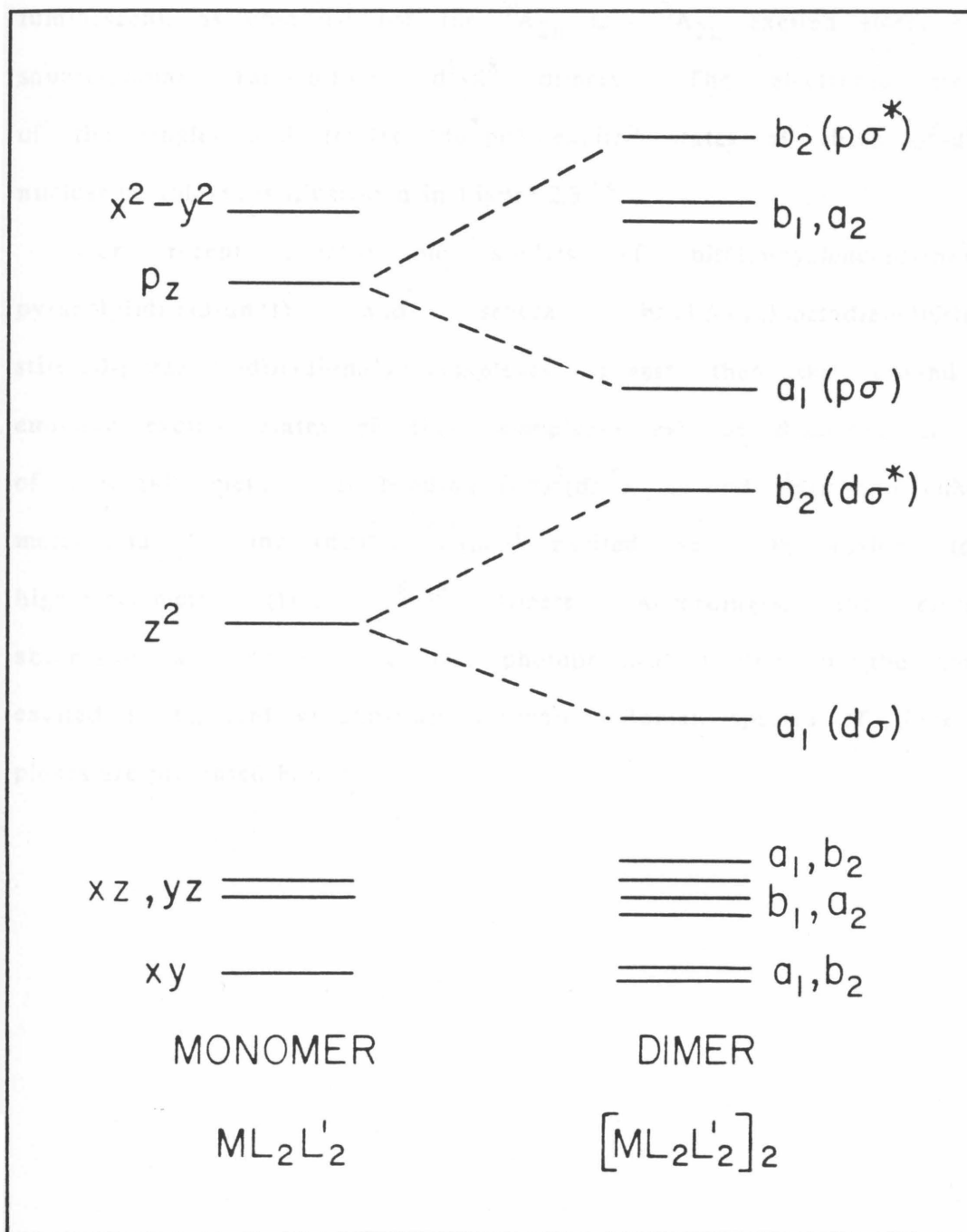
Introduction

Extensive spectroscopic studies of d^8-d^8 binuclear complexes of rhodium and iridium with bridging isocyanide ligands and $[\text{Pt}_2(\text{pop})_4]^{4-}$ ($\text{pop} = \text{P}_2\text{O}_5\text{H}_2^{2-}$) have established that the metal-metal interaction in the ${}^1A_{1g}(d\sigma)^2(d\sigma^*)^2$ (D_{4h}) ground state is weakly bonding and this interaction in the ${}^3A_{2u}(d\sigma)^2(d\sigma^*)^1(p\sigma)^1$ excited state approaches that of a single bond.¹⁻⁷ A molecular orbital diagram that describes the bonding in these dimers is shown in Figure 2.1.⁸ To a first approximation, the metal-metal interaction in the ground state is expected to be nonbonding since both the $a_{1g}(d\sigma)$ and $a_{2u}(d\sigma^*)$ orbitals are filled. However, configurational mixing of these orbitals with the unoccupied $a_{1g}(p\sigma)$ and $a_{2u}(p\sigma^*)$ orbitals serves to stabilize the former set and accounts for the weak metal-metal bonding interaction in the ${}^1A_{1g}$ ground state.^{2,3} As has been well-documented, a relatively low-energy, intense band in the absorption spectra of these "face-to-face" d^8-d^8 dimers of D_{4h} symmetry is assigned to the fully-allowed ${}^1A_{1g} \rightarrow {}^1A_{2u}$ transition. A weak band corresponding to the ${}^1A_{1g} \rightarrow {}^3A_{2u}$ transition is observed at lower energy. These complexes are emissive at ambient temperature in fluid solution, and both fluorescence from the ${}^1A_{2u}(d\sigma^*p\sigma)$ and phosphorescence from the ${}^3A_{2u}(d\sigma^*p\sigma)$ excited states are observed.^{1-3,5,7-14}

For lower-symmetry (C_{2v}) pyrazolyl-bridged iridium(I) dimers, a similar molecular orbital diagram for the interaction of two $\text{ML}_2\text{L}'_2$ fragments is shown in Figure 2.2.⁷ Both the $a_1(d\sigma)$ and $b_2(d\sigma^*)$ orbitals are filled, and by analogy to the higher-symmetry d^8-d^8 complexes,

Figure 2.1 Molecular orbital diagram for the interaction of two square-planar d^8 metal ions complexed with isocyanide ligands (D_{4h} symmetry).

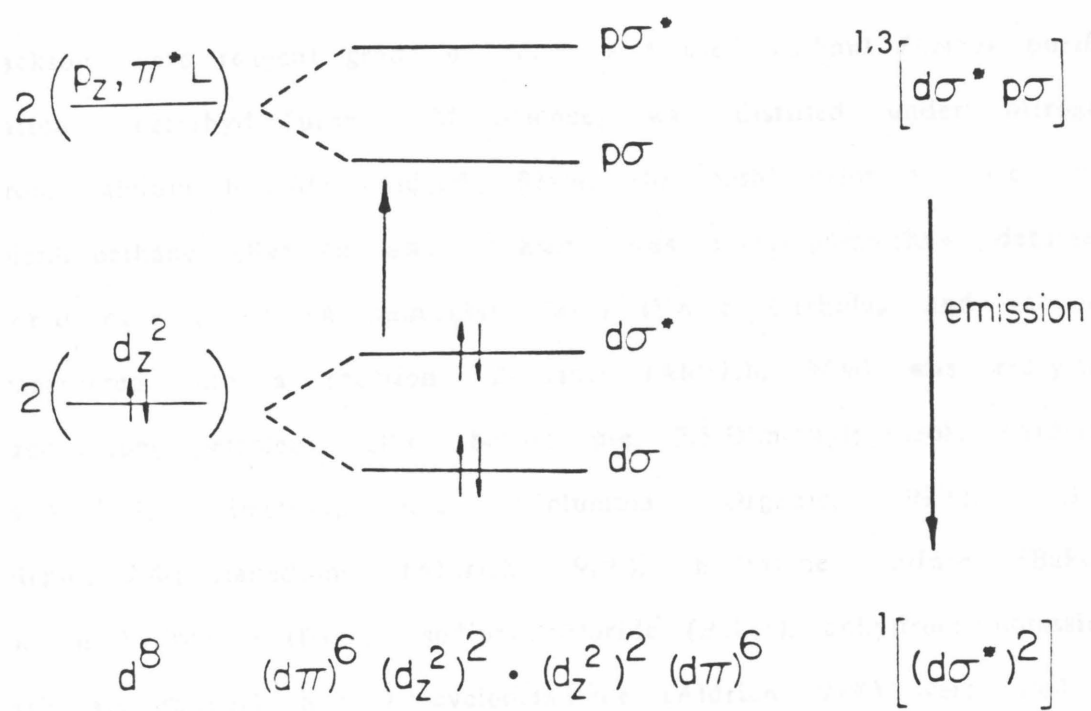
Figure 2.2 Molecular orbital diagram for pyrazolyl-bridged iridium(I) dimers of C_{2v} symmetry.



the ${}^1A_1(d\sigma)^2(d\sigma^*)^2$ ground state is expected to be weakly metal-metal bonding. The 1B_2 and 3B_2 excited states derived from 1A_1 by $b_2(d\sigma^*) \rightarrow a_1(p\sigma)$ excitation are expected to be strongly metal-metal bonding and luminescent, as observed for the ${}^1A_{2u}$ and ${}^3A_{2u}$ excited states of the square-planar "face-to-face" d^8-d^8 dimers. The electronic structure of the singlet and triplet $(d\sigma^* p\sigma)$ excited states of these d^8-d^8 binuclear complexes is illustrated in Figure 2.3.¹⁵

Our recent spectroscopic studies of bis(1,5-cyclooctadiene)bis(μ -pyrazolyl)diiridium(I) and several bis(1,5-cyclooctadiene)bis(μ -substituted-pyrazolyl)diiridium(I) complexes suggest that the ground and emissive excited states of these complexes can be described in terms of a weakly metal-metal bonding $(d\sigma)^2(d\sigma^*)^2$ ground state and enhanced metal-metal bonding $(d\sigma)^2(d\sigma^*)^1(p\sigma)^1$ excited states, by analogy to the higher-symmetry (D_{4h}) d^8-d^8 dimers. Accordingly, the electronic absorption and emission spectra, photophysical studies of the emissive excited states, and ground-state resonance Raman spectra of these complexes are presented herein.

Figure 2.3 Electronic structure of d^8-d^8 binuclear complexes which highlights the emissive excited states.



Experimental

Syntheses

Materials.

Petroleum ether (Baker), diethyl ether (Baker), methanol (Baker), 95% ethanol (U.S. Industrial), absolute ethanol (U.S. Industrial), benzene (Burdick and Jackson), and dichloromethane (Burdick and Jackson) were reagent grade or better and used without further purification. Tetrahydrofuran (EM Science) was distilled under nitrogen from calcium hydride (Aldrich, 95+%, -40 mesh) prior to use. 1,2-Dichloroethane (Burdick and Jackson) was freeze-pump-thaw degassed, stored over Linde 4A molecular sieves (Union Carbide), and vacuum-transferred into a reaction. Pyrazole (Aldrich, 98%) was recrystallized from petroleum ether before use. 3,5-Dimethylpyrazole (Aldrich, 99%), 3,4,5-trimethylpyrazole (Columbia Organic, 99%), 1,1,1-trifluoro-2,4-pentanedione (Aldrich, 98%), hydrazine sulfate (Baker), sodium hydroxide (Baker), sodium chloride (Baker), anhydrous potassium carbonate (Baker), and 1,5-cyclooctadiene (Aldrich, 99%) were used as received. Iridium trichloride trihydrate (Johnson Matthey), triethylamine (Aldrich, 99+%, Gold Label), Florisil (Spectrum Chemical, 60-100 mesh), and bromine (Baker) were used as received. Iodine (MCB) was sublimed before use.

Ligands.

3-(Trifluoromethyl)-5-methylpyrazole was synthesized by condensation of 1,1,1-trifluoro-2,4-pentanedione with hydrazine following a published procedure for the preparation of 3,5-dimethylpyrazole.¹⁶

Anal. Calcd for $C_5H_5N_2F_3$: C, 40.01; H, 3.36; N, 18.66. Found: C, 40.04; H, 3.40; N, 18.66.

Inorganic Complexes.

Di- μ -chloro-bis(1,5-cyclooctadiene)diiridium(I), $[Ir(COD)(Cl)]_2$, was synthesized by modification of a published procedure,¹⁷ improving the yield to 90% from the reported yield of 72%. A 250 mL, round-bottomed Schlenk flask was charged with $IrCl_3 \cdot 3H_2O$ (2.00 g, 5.67 mmol), 95% ethanol (34 mL), water (17 mL), and 1,5-cyclooctadiene (6.0 mL). The neck of the flask was fitted with a water-jacketed condenser, the sidearm of the flask was attached to a nitrogen or argon source, and a slow stream of inert gas was passed through the flask to a mineral oil bubbler attached to the top of the condenser. The solution was refluxed, with stirring, for 48 h during which time the orange-to-red product precipitated from solution. The solution was allowed to cool, and the solid $[Ir(COD)(Cl)]_2$ was collected by filtration, washed well with ice-cold methanol, and dried under vacuum. Yield: 1.71 g (90%). Anal. Calcd for $C_{16}H_{24}Cl_2Ir_2$: C, 28.61; H, 3.60; Cl, 10.56. Found: C, 28.64; H, 3.68; Cl, 10.45.

Bis(1,5-cyclooctadiene)bis(μ -pyrazolyl)diiridium(I), $[Ir(\mu\text{-pz})(COD)]_2$, was prepared using standard Schlenk techniques under an argon atmosphere by a procedure related to that of Stobart, *et al.*^{18,19} $[Ir(COD)(Cl)]_2$ (0.500 g, 0.744 mmol) was dissolved in tetrahydrofuran (50 mL) to give an orange-red solution. A colorless solution of pyrazole (0.110 g, 1.62 mmol) and excess triethylamine (0.73 mL, 5.2 mmol) in tetrahydrofuran (10 mL) was transferred via cannula to the solution of $[Ir(COD)(Cl)]_2$. The pyrazole/triethylamine residue

remaining in the flask was washed with tetrahydrofuran (5 mL) and also added to the reaction flask. The reaction mixture began to turn deep red upon addition of the pyrazole solution and was stirred at ambient temperature under argon for 1 h during which time a solid precipitated. The solvent was removed under vacuum, and the residue was transferred to a nitrogen atmosphere flush box. The $[\text{Ir}(\mu\text{-pz})(\text{COD})]_2$ was extracted into a minimum of benzene (80 mL) and filtered through a short column of Florisil with benzene as the eluting solvent. Slow evaporation of the benzene with a stream of argon yielded dark red, air-stable crystals of $[\text{Ir}(\mu\text{-pz})(\text{COD})]_2$ that were dried under vacuum. Yield: 0.510 g (93%). Anal. Calcd for $\text{C}_{22}\text{H}_{30}\text{N}_4\text{Ir}_2$: C, 35.95; H, 4.11; N, 7.62. Found: C, 36.24; H, 4.13; N, 7.64.

Bis(1,5-cyclooctadiene)bis(μ -3,5-dimethylpyrazolyl)diiridium(I), $[\text{Ir}(\mu\text{-3,5-(CH}_3)_2\text{pz})(\text{COD})]_2$, was prepared using standard Schlenk techniques under an argon atmosphere by a procedure related to that of Stobart, *et al.*²⁰ A solution of 3,5-dimethylpyrazole (0.250 g, 2.60 mmol) and excess triethylamine (1.0 mL, 7.2 mmol) in tetrahydrofuran (50 mL) was transferred via cannula to an orange-red tetrahydrofuran solution (50 mL) of $[\text{Ir}(\text{COD})(\text{Cl})]_2$ (0.865 g, 1.29 mmol). The dimethylpyrazole/triethylamine residue remaining in the flask was washed with additional tetrahydrofuran (10 mL) and added to the reaction mixture. The reaction solution was stirred under argon at ambient temperature for 48 h during which time the solution became deep purple and a solid precipitated. Since the complex is air-stable in solution, the reaction work-up was continued in the air by removal of the solvent on a rotary evaporator. The residue was washed with absolute

ethanol to remove the triethylammonium chloride by-product. The crude $[\text{Ir}(\mu\text{-}3,5\text{-}(\text{CH}_3)_2\text{pz})(\text{COD})]_2$ was dissolved in a 1:1 (v/v) mixture of dichloromethane/ethanol (200 mL). The dichloromethane was removed on a rotary evaporator, crystallizing the product from the ethanol. This solid was filtered and washed well with ethanol. The dichloromethane/ethanol crystallization was repeated, giving small purple-black, air-stable crystals of the desired product that were dried under vacuum. Yield: 0.925 g (91%). Anal. Calcd for $\text{C}_{26}\text{H}_{38}\text{N}_4\text{Ir}_2$: C, 39.48; H, 4.84; N, 7.08. Found: C, 39.37; H, 4.80; N, 7.10. Large purple-black needles of $[\text{Ir}(\mu\text{-}3,5\text{-}(\text{CH}_3)_2\text{pz})(\text{COD})]_2$ were grown by slow evaporation of a 1:1 (v/v) dichloromethane/ethanol solution.

Bis(1,5-cyclooctadiene)bis($\mu\text{-}3,4,5\text{-}$ trimethylpyrazolyl)diiridium(I), $[\text{Ir}(\mu\text{-}3,4,5\text{-}(\text{CH}_3)_3\text{pz})(\text{COD})]_2$, and bis(1,5-cyclooctadiene)-bis($\mu\text{-}3\text{-}$ (trifluoromethyl)-5-methylpyrazolyl)diiridium(I), $[\text{Ir}(\mu\text{-}3\text{-}\text{CF}_3\text{-}5\text{-}\text{CH}_3\text{pz})(\text{COD})]_2$, were prepared by procedures similar to that of Stobart, *et al.*²⁰ using Florisil as the chromatographic material, benzene as the eluting solvent, and a 1:1 (v/v) dichloromethane/ethanol solution as the recrystallization solvent. Since the compounds are air-stable in solution, the reaction work-ups were done in the air. Anal. Calcd for $\text{C}_{28}\text{H}_{42}\text{N}_4\text{Ir}_2$: C, 41.06; H, 5.17; N, 6.84. Found: C, 40.30; H, 4.92; N, 6.65. Anal. Calcd for $\text{C}_{26}\text{H}_{32}\text{N}_4\text{F}_6\text{Ir}_2$: C, 34.74; H, 3.59; N, 6.23. Found: C, 34.81; H, 3.64; N, 6.26.

Bis(1,5-cyclooctadiene)bis($\mu\text{-}3,5\text{-}$ bis(trifluoromethyl)pyrazolyl)diiridium(I), $[\text{Ir}(\mu\text{-}3,5\text{-}(\text{CF}_3)_2\text{pz})(\text{COD})]_2$, was obtained from Professor Stephen R. Stobart and used as received.

Bis(1,5-cyclooctadiene)bis(μ -pyrazolyl)(diiodide)diiridium(II), $[\text{Ir}(\mu\text{-pz})(\text{COD})(\text{I})]_2$, was prepared using standard Schlenk techniques under an argon atmosphere by the method of Stobart, *et al.*^{21,22} A solution of iodine (0.037 g, 0.146 mmol) in tetrahydrofuran (5 mL) was transferred via cannula to a stirring solution of $[\text{Ir}(\mu\text{-pz})(\text{COD})]_2$ (0.100 g, 0.136 mmol) in tetrahydrofuran (20 mL). Upon mixing, the reaction solution turned deep purple and small crystals of $[\text{Ir}(\mu\text{-pz})(\text{COD})(\text{I})]_2$ began to precipitate. After the solution was stirred for 15 min, hexane (30 mL) was added to further precipitate the product. The air-stable solid was filtered, washed well with hexane (4 x 10 mL), and dried under vacuum. Yield: 0.120 g (89%). Anal. Calcd for $\text{C}_{22}\text{H}_{30}\text{N}_4\text{I}_2\text{Ir}_2$: C, 26.72; H, 3.06; N, 5.67. Found: C, 26.88; H, 3.03; N, 5.84.

Bis(1,5-cyclooctadiene)bis(μ -pyrazolyl)(dibromide)diiridium(II), $[\text{Ir}(\mu\text{-pz})(\text{COD})(\text{Br})]_2$, was prepared using standard Schlenk techniques under an argon atmosphere by a method analogous to that for $[\text{Ir}(\mu\text{-pz})(\text{COD})(\text{I})]_2$.²¹ A solution of bromine (5 μL , 0.1 mmol) in tetrahydrofuran (5 mL) was added to a stirring tetrahydrofuran (20 mL) solution of $[\text{Ir}(\mu\text{-pz})(\text{COD})]_2$ (0.075 g, 0.102 mmol). Upon mixing, the reaction solution darkened and solid $[\text{Ir}(\mu\text{-pz})(\text{COD})(\text{Br})]_2$ began to precipitate. The reaction was stirred at ambient temperature for 15 min and hexane (30 mL) was added to further precipitate the product. The air-stable, brown solid was washed well with hexane and dried under vacuum. Yield: 0.078 g (85%). Anal. Calcd for $\text{C}_{22}\text{H}_{30}\text{N}_4\text{Br}_2\text{Ir}_2$: C, 29.53; H, 3.38; N, 6.26. Found: C, 28.74; H, 3.22; N, 6.00.

Bis(1,5-cyclooctadiene)bis(μ -pyrazolyl)(dichloride)diiridium(II),

$[\text{Ir}(\mu\text{-pz})(\text{COD})(\text{Cl})]_2$, was prepared by the method of Caspar^{2,3} by photolysis of $[\text{Ir}(\mu\text{-pz})(\text{COD})]_2$ in 1,2-dichloroethane. Anal. Calcd for $\text{C}_{22}\text{H}_{30}\text{N}_4\text{Cl}_2\text{Ir}_2 \cdot 0.75 \text{C}_2\text{H}_4\text{Cl}_2$: C, 32.08; H, 3.77; N, 6.39. Found: C, 31.82; H, 3.60; N, 6.72.

Bis(1,5-cyclooctadiene)bis(μ -pyrazolyl)dirhodium(I), $[\text{Rh}(\mu\text{-pz})(\text{COD})]_2$, was obtained from Dr. Jonathan V. Caspar and used as received.

Physical Measurements

Materials.

Solvents for the spectroscopic (electronic absorption, electronic emission, transient absorption, resonance Raman) and emission lifetime measurements were purified, if necessary, degassed with a minimum of five freeze-pump-thaw cycles on a high-vacuum line (limiting pressure $< 10^{-3}$ torr), and bulb-to-bulb distilled into glass round-bottomed storage flasks equipped with Teflon vacuum valves. The solvents were stored over either alumina (Woelm N, Activity Grade 1, obtained from ICN Nutritional Biochemicals), Linde 4A molecular sieves (Union Carbide), or sodium metal (Baker)/benzophenone (MCB). The alumina and molecular sieves were activated by heating under dynamic vacuum ($< 10^{-3}$ torr) for 24 h. Acetonitrile (Burdick and Jackson, UV Grade), cyclohexane (Aldrich, 99+%, Gold Label), and benzene (Burdick and Jackson) were used as received and stored over alumina, molecular sieves, and sodium/benzophenone, respectively. Tetrahydrofuran (EM Science) was distilled under nitrogen from calcium hydride (Aldrich, 95+%, -40 mesh) and stored over sodium/benzophenone. 2-Methyltetrahydrofuran (Aldrich), purified by the method outlined for

tetrahydrofuran,^{2,4} was first distilled from a 0.5 % suspension of cuprous chloride (Allied), followed by distillation from potassium hydroxide pellets (Baker), and then distilled from calcium hydride before vacuum-transfer onto sodium/benzophenone. The characteristic deep purple-blue color of the benzophenone ketyl in the benzene, tetrahydrofuran, and 2-methyltetrahydrofuran solvents' storage flasks signified that the solvents were deoxygenated and dry.

For the measurement of several of the absorption spectra and the molar extinction coefficients of the iridium dimers that are air-stable in solution, either tetrahydrofuran that was freshly distilled under nitrogen from calcium hydride or cyclohexane that was from a freshly opened bottle of Gold Label grade were used.

Ruthenium tris(2,2'-bipyridine) di(hexafluorophosphate), $[\text{Ru}(\text{bpy})_3](\text{PF}_6)_2$, was obtained from Dr. Michael D. Hopkins and recrystallized from a solution of acetonitrile (Burdick and Jackson) and toluene (Baker) before use.

Electronic Absorption Spectroscopy.

Electronic absorption spectra were measured using either a Cary 17 or a Hewlett-Packard 8450A spectrophotometer. Spectra were obtained of solutions prepared on a high-vacuum line (limiting pressure $< 10^{-3}$ torr) in a cell consisting of a 10 mL Pyrex bulb, a 1 cm pathlength quartz cuvette, and a Teflon vacuum valve. For molar extinction coefficient measurements, the solvent was distilled from the appropriate storage flask to a calibrated volumetric cylinder before transfer to the cell. Several spectra of the complexes that are air-stable in solution were measured of samples prepared in the air in 1 cm

pathlength quartz cuvettes. The absorption spectra of these complexes in aerated solvents are identical to those in degassed solvents.

Electronic Emission Spectroscopy.

Electronic emission spectra were measured using an emission spectrophotometer constructed at Caltech that has been described previously.⁵ Spectra recorded at ambient temperature were obtained for solutions that were prepared on a high-vacuum line (limiting pressure $< 10^{-3}$ torr) in a cell consisting of a 10 mL Pyrex bulb, a 1 cm pathlength quartz fluorescence cell, and a Teflon vacuum valve. For the measurements at 77 K, solutions were prepared in the same manner in a glass NMR tube attached to a Teflon vacuum valve. Solvent was bulb-to-bulb distilled into the cell or tube containing the compound from the appropriate solvent storage flask. Highly dilute solutions were used for the quantum yield measurements.^{2 5} An acetonitrile solution of $[\text{Ru}(\text{bpy})_3](\text{PF}_6)_2$, which has a quantum yield for emission of 0.062 at ambient temperature,^{2 6} was used as the standard. For these measurements, the excitation wavelength was the 436 nm Hg line from a medium-pressure Hg/Xe arc lamp that was filtered with an Oriel 5645 interference filter. For the 77 K emission measurements, the NMR tubes were held in a liquid-nitrogen-filled quartz finger dewar. The emission intensities were corrected for spectrometer response by point-by-point multiplication of analog spectra by the appropriate correction factors.^{2 7}

Emission Lifetime and Transient Absorption Measurements.

Emission lifetime measurements were conducted with a Nd:YAG pulsed laser system that has been described previously^{2 8} using 532 nm excita-

tion. The solutions for the measurements at ambient temperature were prepared by the procedure used for the emission measurements. The solutions for the variable temperature and 77 K lifetime measurements were prepared in NMR tubes by the same procedure. All of the emission intensity decays exhibited first-order kinetics over at least 3 half-lives. For the measurements at 77 K, the NMR tubes were held in a liquid-nitrogen-filled quartz finger dewar. For the variable temperature measurements between 190 and 300 K, a continuous-flow nitrogen gas dewar was used. The sample temperature was monitored with a calibrated copper/constantan thermocouple. The laser was operated at a low power output to minimize local sample heating.

The transient absorption experiments were performed using the same laser system with changes in the optical train as described elsewhere.²⁸ The spectra were obtained point-by-point in the visible region of the spectrum except at wavelengths near the laser line (532 nm). The solutions were prepared on a high-vacuum line (limiting pressure $< 10^{-3}$ torr) in a cell consisting of a 10 mL Pyrex bulb, a 1 cm quartz cuvette, and a Teflon vacuum valve by bulb-to-bulb distillation of the solvent into the cell containing the iridium complex.

Resonance Raman Spectroscopy.

Resonance Raman spectra obtained at Caltech were recorded with a Spex 14024 spectrometer equipped with 2400 lines/mm holographic gratings, a thermoelectric cooled Hamamatsu R955 photomultiplier tube, and a Spex SCAMP data system. Laser excitation was provided by a Spectra-Physics 171-18 (Ar^+) laser. Typical signal averaging used 9, 16 or 25 scans. Spectra were recorded of solutions prepared on a high-vacuum

line (limiting pressure $< 10^{-3}$ torr) in a 1 mm pathlength cell equipped with a Teflon vacuum valve by distillation of solvent into the cell from the appropriate storage flask.

Resonance Raman spectra of the iridium dimers with improved resolution at low frequencies (for $\Delta\bar{\nu}$ between 50 and 100 cm^{-1}) were measured by Dr. Edward M. Kober at Los Alamos National Laboratory.

Additional Measurements.

Elemental analyses were obtained by Mr. Larry Henling at the Caltech Analytical Laboratory. The elemental analysis for $[\text{Ir}(\text{COD})\text{-(Cl)}]_2$ was obtained by Spang Microanalytical Laboratory, Eagle Harbor, Michigan.

Results and Discussion

The synthesis and thermal chemistry of a variety of pyrazolyl-bridged and substituted-pyrazolyl-bridged binuclear iridium(I) complexes have been investigated in several laboratories.²⁹⁻³¹ In particular, Stobart and co-workers have contributed to this effort through extensive studies of a number of these complexes containing 1,5-cyclooctadiene, carbon monoxide, and phosphine ligands.^{18-22,32-38} The complexes of cyclooctadiene are especially interesting since the metal-metal separation can be influenced dramatically by the steric demands of the bridging ligands.^{20,33} The X-ray crystal structure determinations of several of these binuclear complexes reveal that the iridium-iridium distances are rather short, consistent with a weak metal-metal bonding interaction in the 1A_1 ground state. The structural characterization of bis(1,5-cyclooctadiene)bis(μ -pyrazolyl)diiridium(I), $[\text{Ir}(\mu\text{-pz})(\text{COD})]_2$ (pzH = pyrazole, COD = 1,5-cyclooctadiene), reveals that this complex adopts a conformation similar to that of a number of "A-frame" complexes³⁹ with an iridium-iridium separation of 3.216(1) Å, as shown in Figure 2.4.^{21,33} Related iridium dimers, containing pyrazolyl ligands that are substituted in the 3- and 5-positions of the heterocyclic ring by methyl or trifluoromethyl groups, have even shorter metal-metal separations because of steric repulsions between the hydrogen atoms of the cyclooctadiene ligands and the substituents on the pyrazolyl bridges.^{20,33} Table 2.1 lists the iridium-iridium distances of several of these complexes that have been structurally characterized.

Figure 2.4 Structure of $[\text{Ir}(\mu\text{-pz})(\text{COD})]_2$.

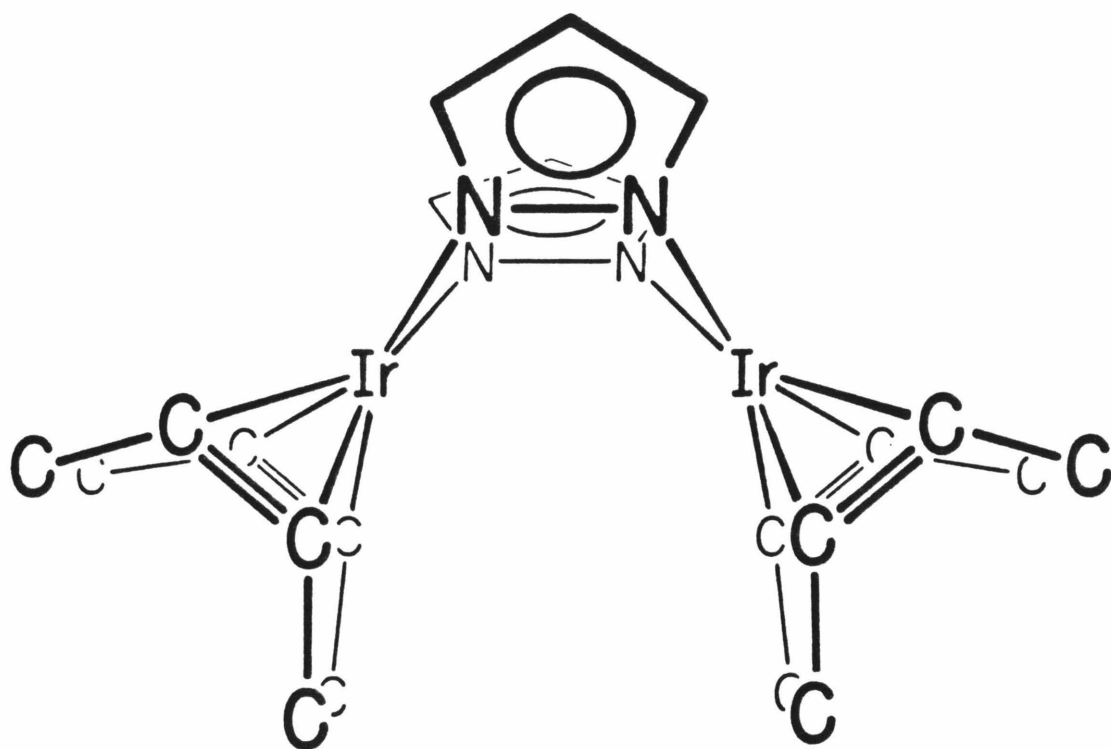


Table 2.1 Metal-metal distances for pyrazolyl-bridged binuclear iridium(I) cyclooctadiene complexes.

Iridium Complex	Ir-Ir Distance (Å)	Reference
$[\text{Ir}(\mu\text{-pz})(\text{COD})]_2$	3.216(1)	21, 33
$[\text{Ir}(\mu\text{-3,4,5-(CH}_3)_3\text{pz})(\text{COD})]_2$	3.096(1)	20
$[\text{Ir}(\mu\text{-3-CF}_3\text{-5-CH}_3\text{pz})(\text{COD})]_2$	3.066(1)	33
$[\text{Ir}(\mu\text{-3,5-(CF}_3)_2\text{pz})(\text{COD})]_2$	3.073(1)	33

pzH = pyrazole

3,4,5-(CH₃)₃pzH = 3,4,5-trimethylpyrazole

3-CF₃-5-CH₃pzH = 3-(trifluoromethyl)-5-methylpyrazole

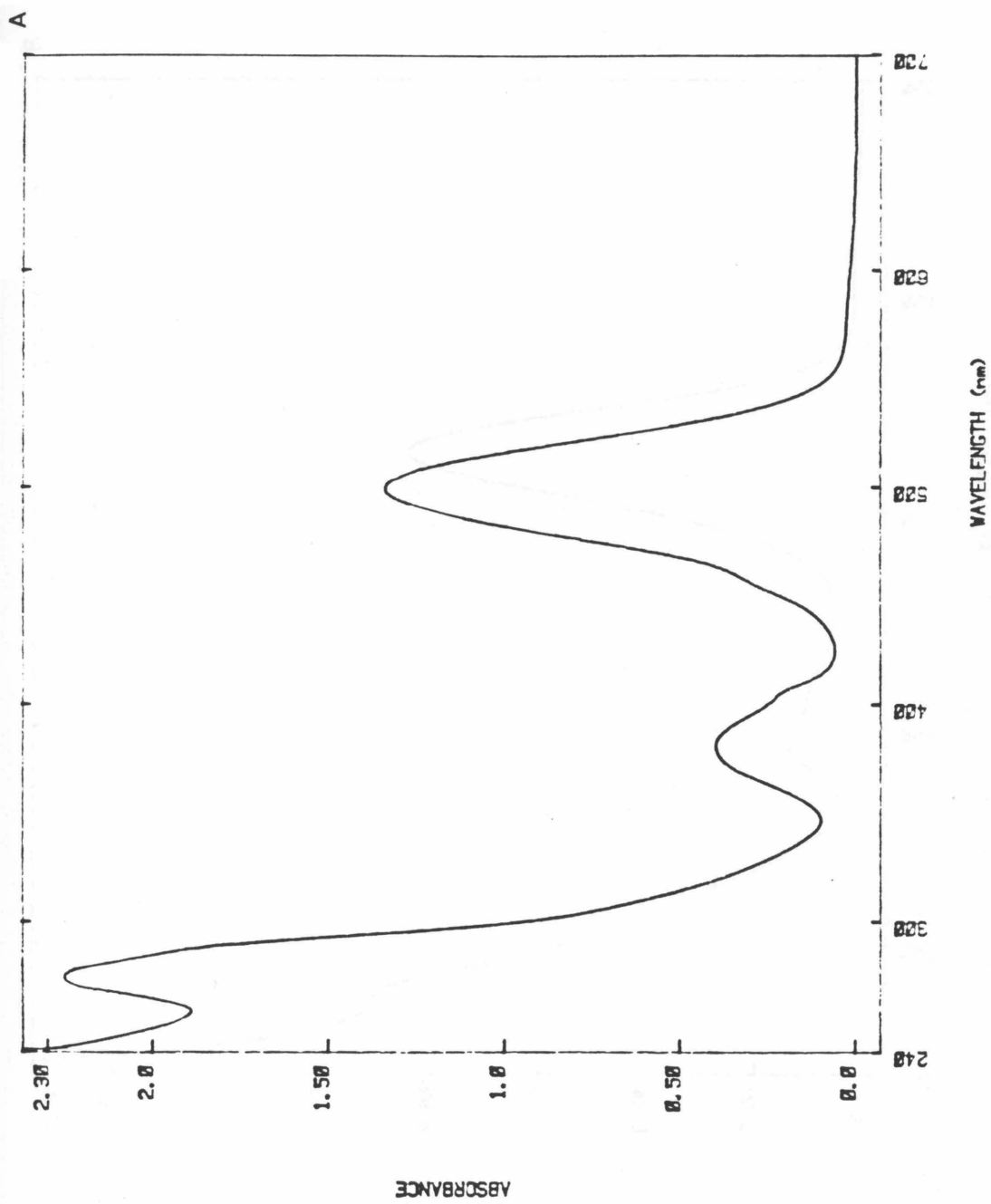
3,5-(CF₃)₂pzH = 3,5-bis(trifluoromethyl)pyrazole

COD = 1,5-cyclooctadiene

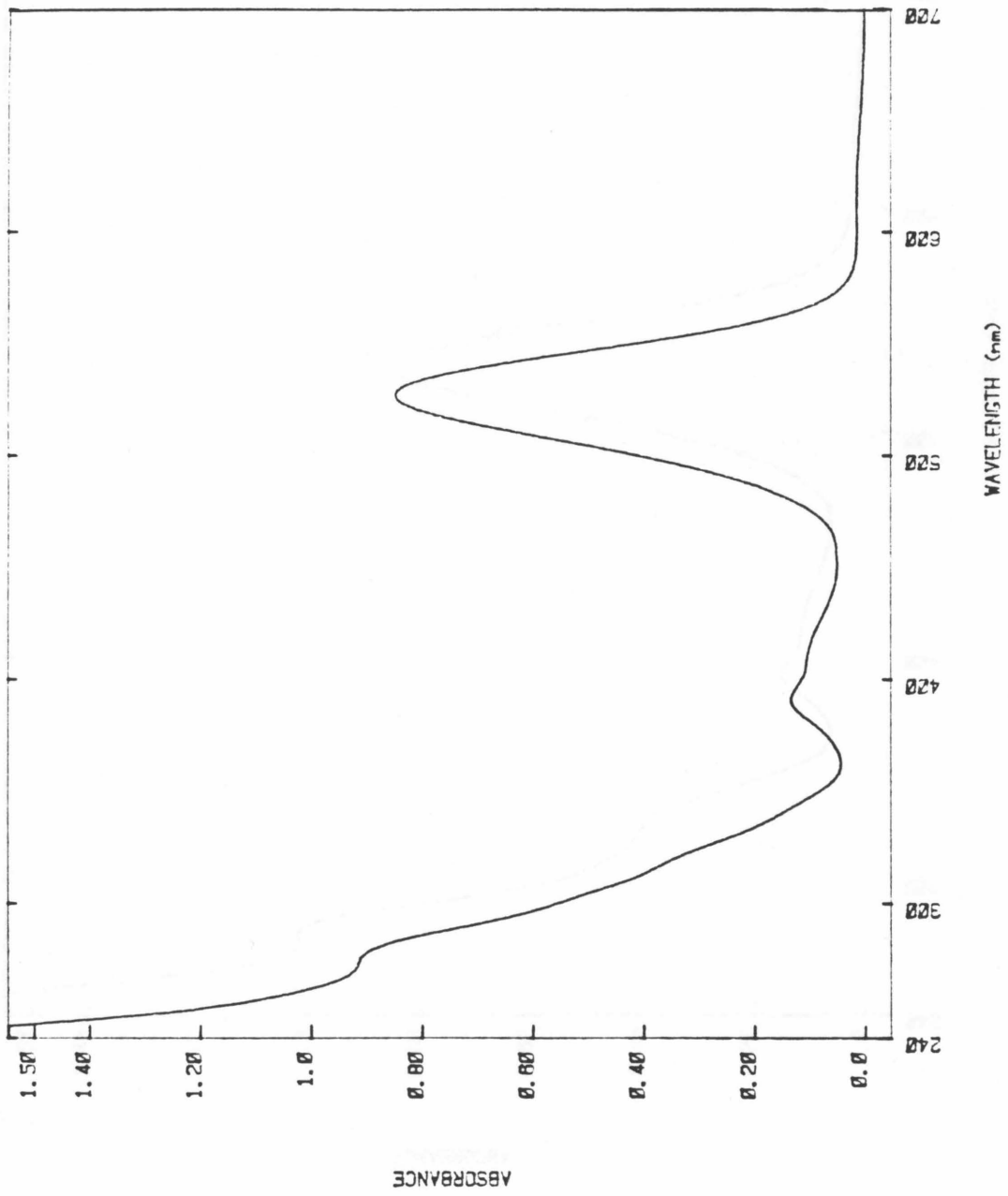
The four iridium complexes listed in Table 2.1 and a similar complex that has not been structurally characterized, $[\text{Ir}(\mu\text{-}3,5\text{-}(\text{CH}_3)_2\text{pz})(\text{COD})]_2$ ($3,5\text{-}(\text{CH}_3)_2\text{pzH}$ = 3,5-dimethylpyrazole, COD = 1,5-cyclooctadiene), are all intensely colored in solution and in the solid state, ranging from pink to deep purple. The electronic absorption spectra of these five binuclear iridium complexes are shown in Figure 2.5. The corresponding band maxima and molar extinction coefficients are listed in Table 2.2.⁴⁰ The spectra of these complexes are qualitatively similar; the intense band around 498 to 529 nm in each spectrum is logically assigned to the $^1\text{A}_1 \rightarrow ^1\text{B}_2$ ($d\sigma^* \rightarrow p\sigma$) transition, by analogy to similar spectral features observed for the "face-to-face" $d^8\text{-}d^8$ dimers.^{1-3,5,7-10,13} A weak band at lower energy is observed for all of these complexes and is assigned to the corresponding triplet $^1\text{A}_1 \rightarrow ^3\text{B}_2$ ($d\sigma^* \rightarrow p\sigma$) transition. The general shift of these bands to lower energy with substitution of the pyrazolyl bridge, from those of $[\text{Ir}(\mu\text{-pz})(\text{COD})]_2$, is consistent with the smaller splitting between the $b_2(d\sigma^*)$ and $a_1(p\sigma)$ orbitals for the complexes with shorter metal-metal separations. The features at higher energy most likely correspond to $d\pi(xz,yz) \rightarrow p\sigma$ transitions, as proposed for the higher-energy spectral features of the rhodium(I) and iridium(I) isocyanide complexes.⁷⁻⁹

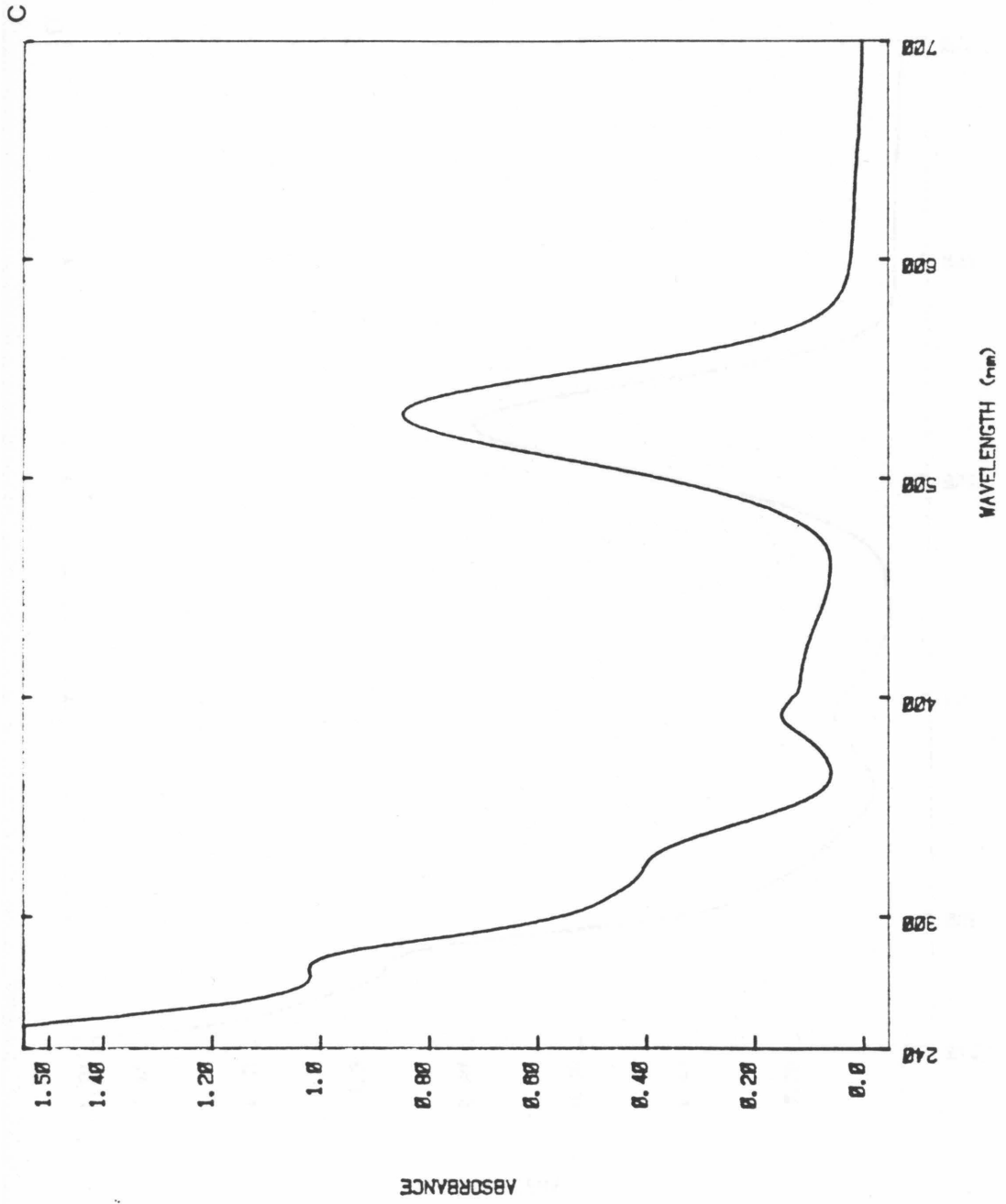
These binuclear iridium(I) complexes exhibit both fluorescence and phosphorescence at ambient temperature in fluid solution from the $^1\text{B}_2(d\sigma^* p\sigma)$ and $^3\text{B}_2(d\sigma^* p\sigma)$ excited states, respectively. The emission spectra are shown in Figure 2.6, and the corresponding emission quantum yields and band maxima for the luminescent excited states are

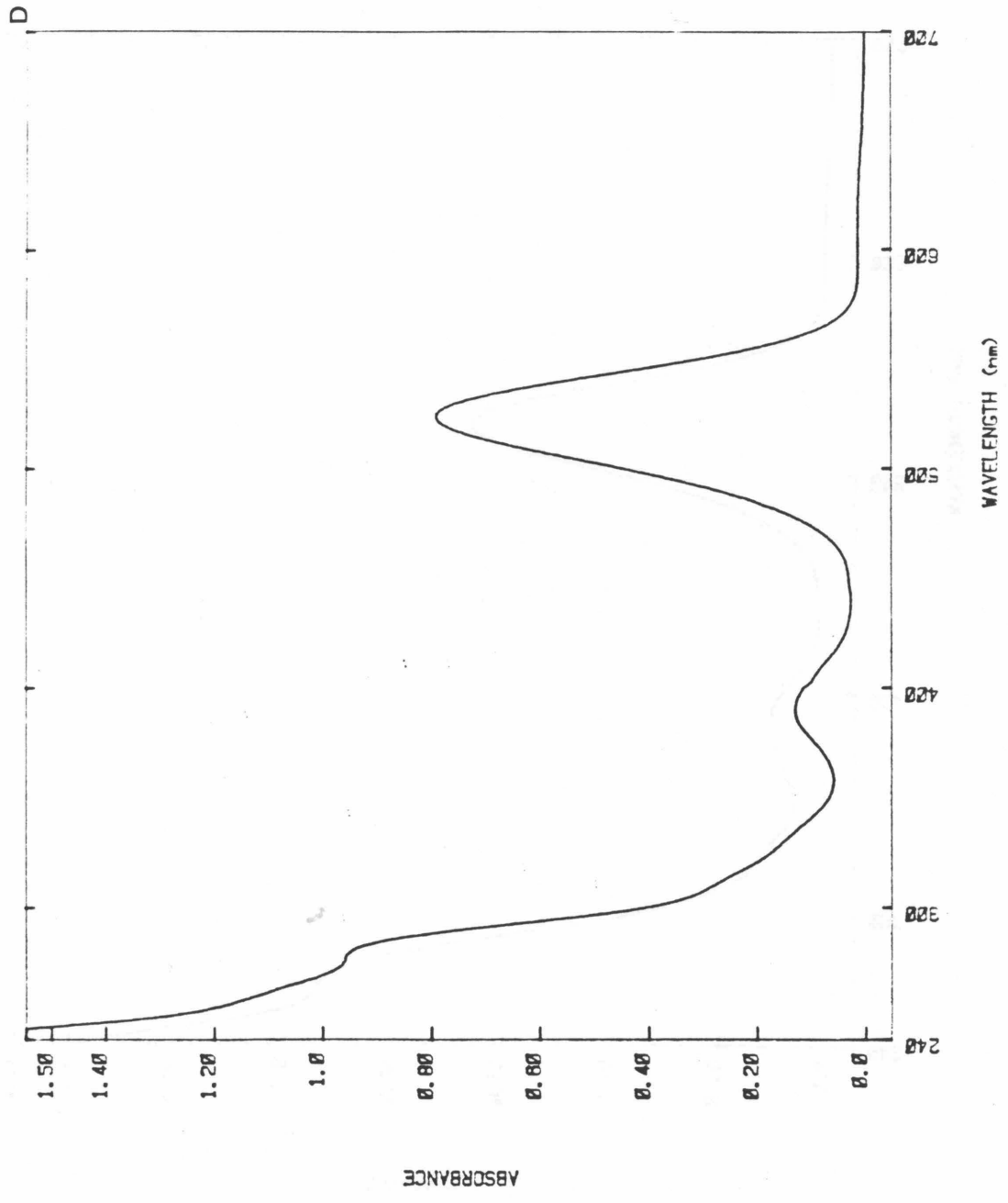
Figure 2.5 Electronic absorption spectra of (a) $[\text{Ir}(\mu\text{-pz})(\text{COD})]_2$, (b) $[\text{Ir}(\mu\text{-3,5-(CH}_3)_2\text{pz})(\text{COD})]_2$, (c) $[\text{Ir}(\mu\text{-3,4,5-(CH}_3)_3\text{-pz})(\text{COD})]_2$, (d) $[\text{Ir}(\mu\text{-3-CF}_3\text{-5-CH}_3\text{pz})(\text{COD})]_2$, (e) $[\text{Ir}(\mu\text{-3,5-(CF}_3)_2\text{pz})(\text{COD})]_2$ (tetrahydrofuran solutions, $22 \pm 2^\circ\text{C}$).



B







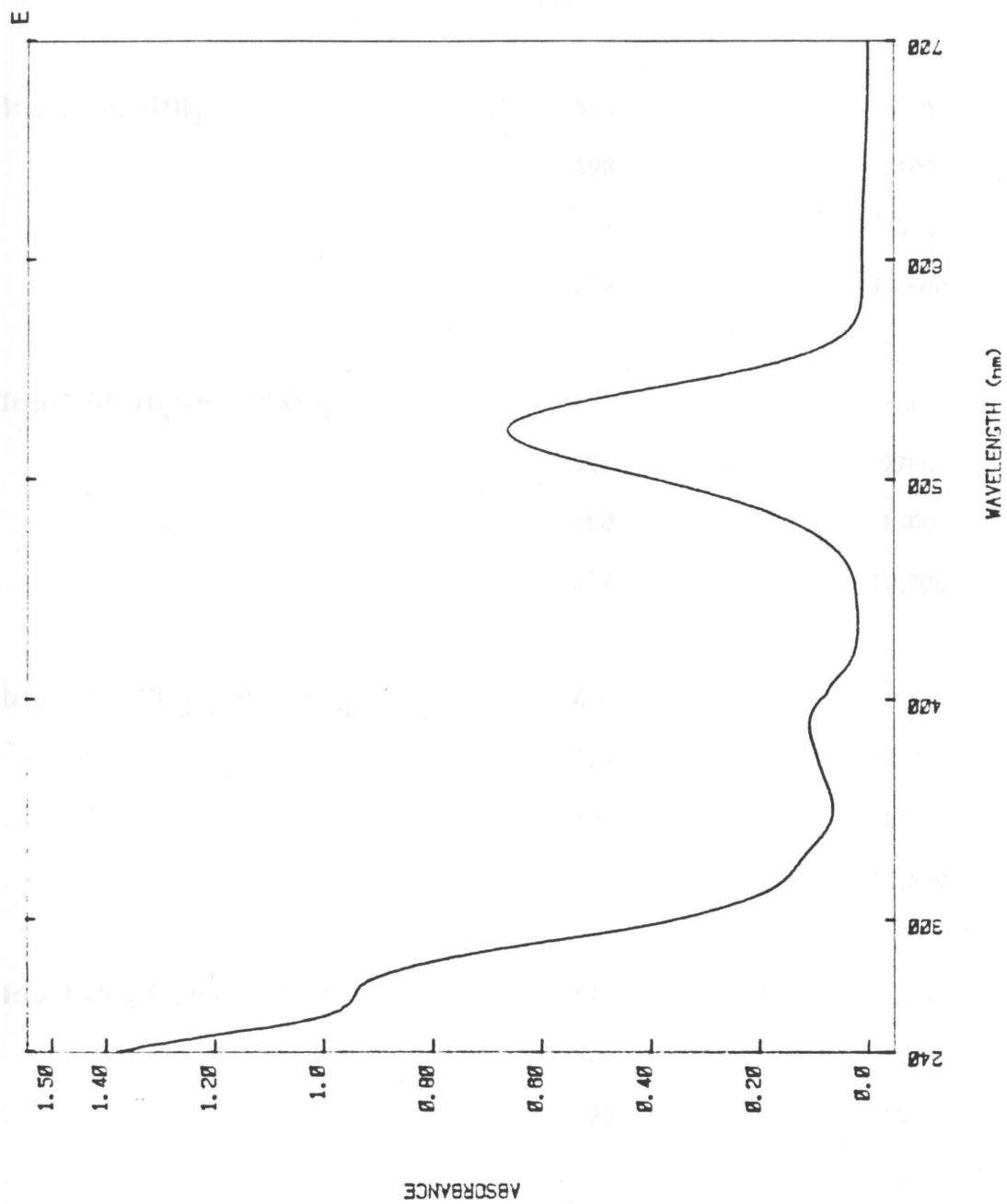


Table 2.2 Electronic absorption spectral data for pyrazolyl-bridged binuclear iridium(I) cyclooctadiene complexes.

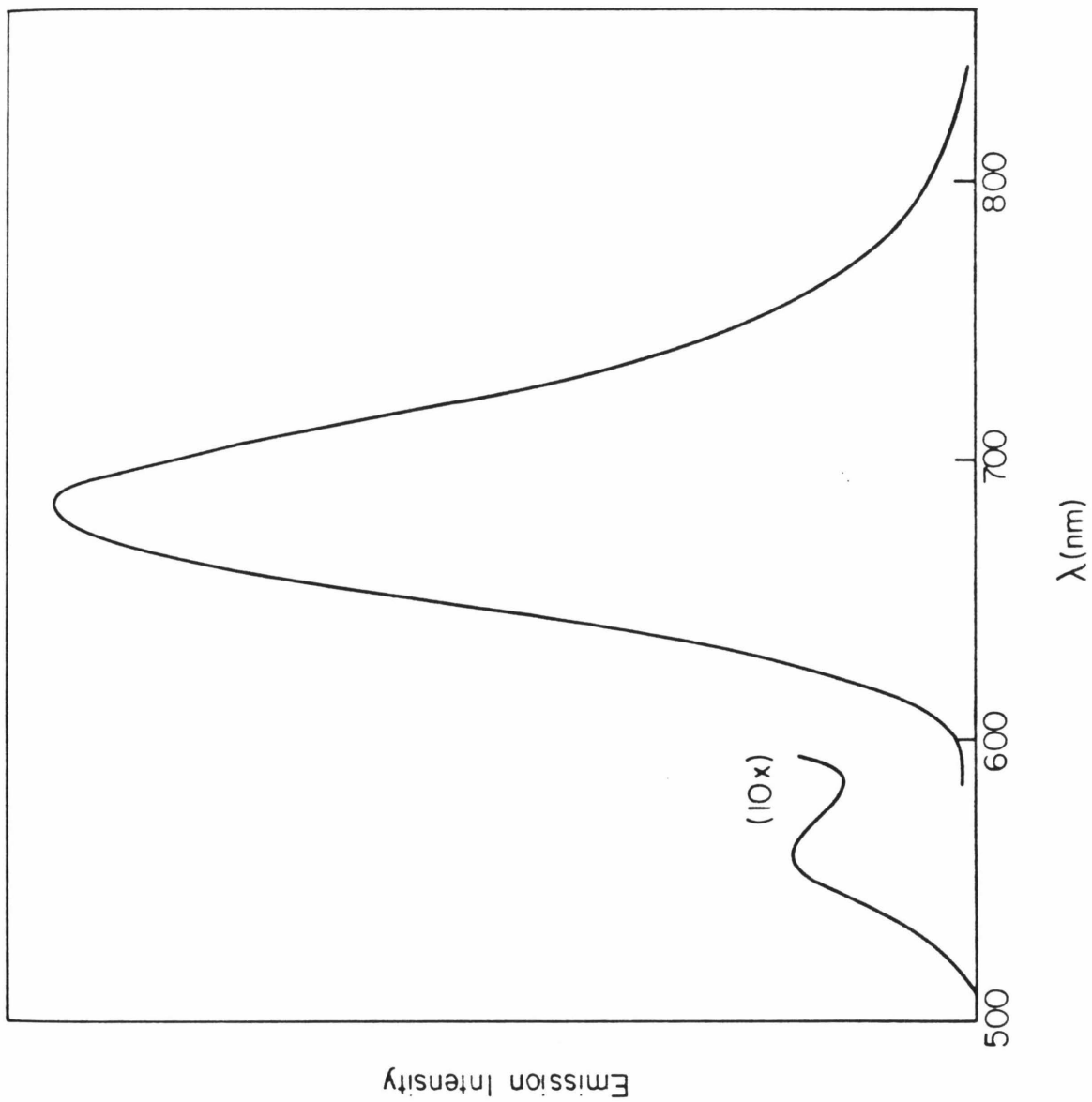
Iridium Complex	λ_{\max} (nm) ^a	ϵ (M ⁻¹ cm ⁻¹) ^b
[Ir(μ -pz)(COD)] ₂	585	150
	498	8100
	381	2500
	274	13,600
[Ir(μ -3,5-(CH ₃) ₂ pz)(COD)] ₂	625	180
	528	9700
	390	1500
	274	10,700
[Ir(μ -3,4,5-(CH ₃) ₃ pz)(COD)] ₂	630	180
	529	9800
	392	1700
	277	11,800
[Ir(μ -3-CF ₃ -5-CH ₃ pz)(COD)] ₂	610	180
	524	10,900
	390	1800
	276	13,200

[Ir(μ -3,5-(CF ₃) ₂ pz)(COD)] ₂	610	160
	522	9700
	388	1600
	266	13,600

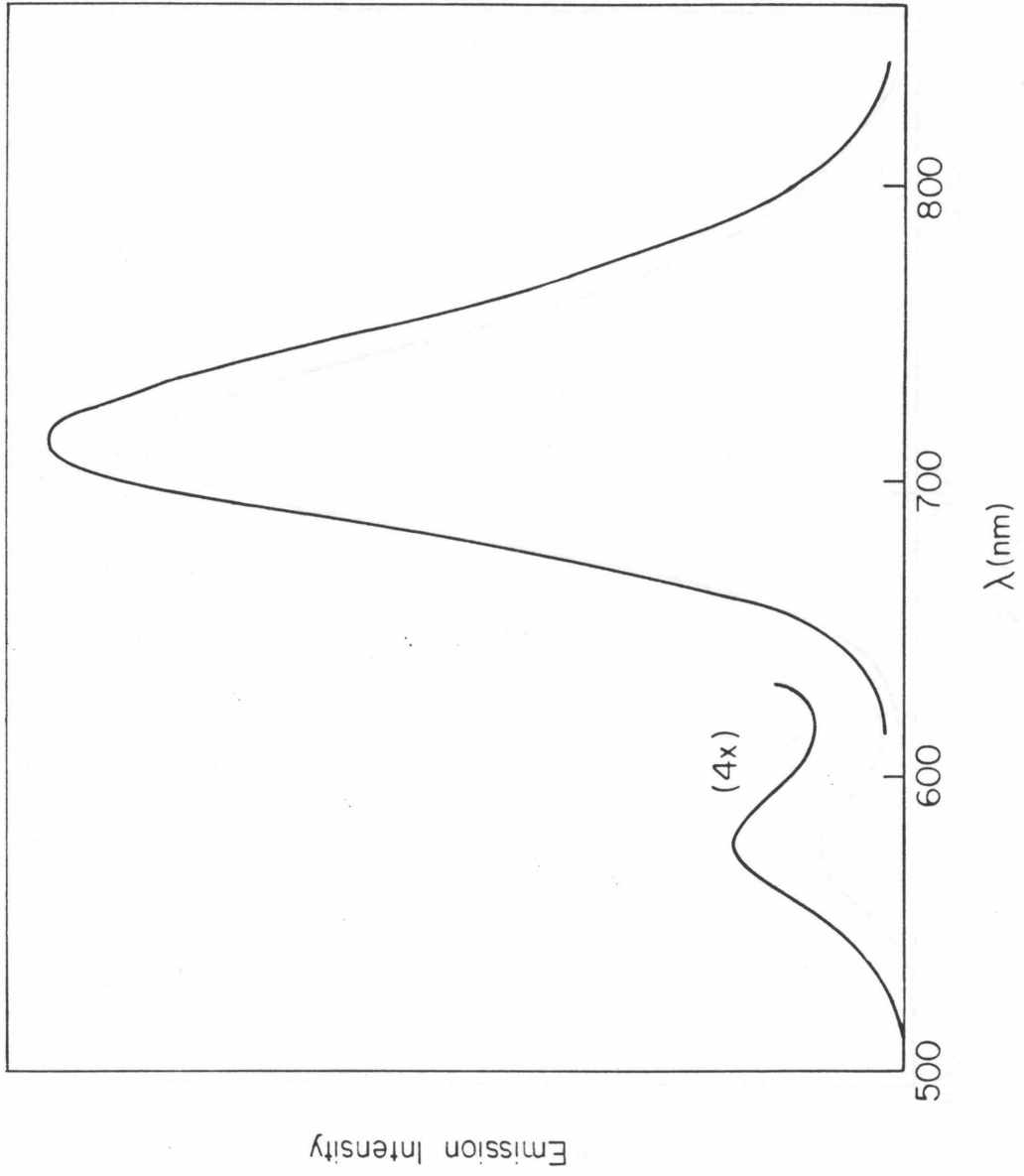
- a. The band maxima of the $^1A_1 \rightarrow ^3B_2$ transition for these complexes are difficult to determine precisely because of the low intensity and broad shape of the bands.
- b. The extinction coefficients were measured for tetrahydrofuran solutions of the complexes and are accurate to $\pm 5\%$.

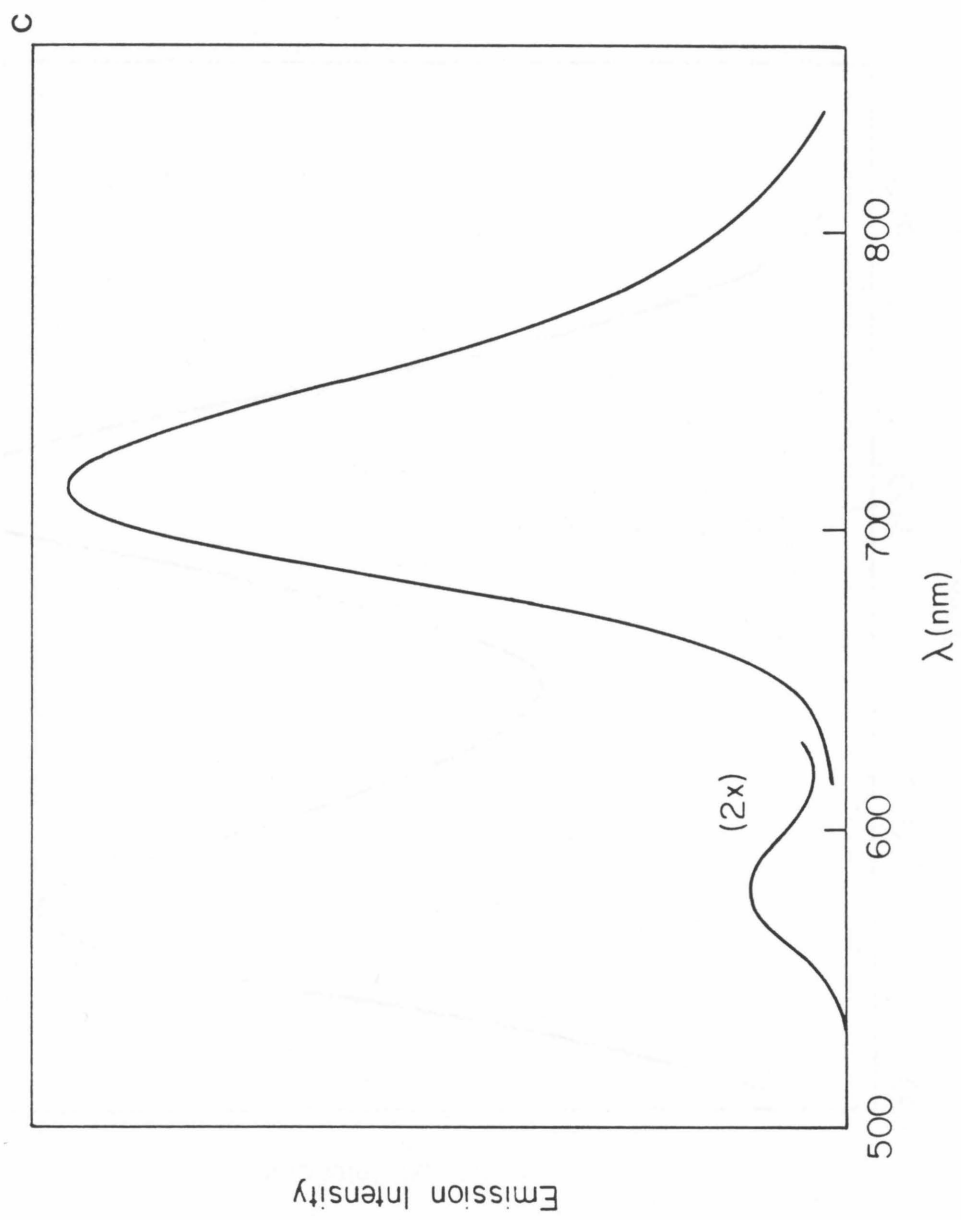
Figure 2.6 Corrected emission spectra of (a) $[\text{Ir}(\mu\text{-pz})(\text{COD})]_2$, (b) $[\text{Ir}(\mu\text{-3,5-(CH}_3)_2\text{pz})(\text{COD})]_2$, (c) $[\text{Ir}(\mu\text{-3,4,5-(CH}_3)_3\text{pz})(\text{COD})]_2$, (d) $[\text{Ir}(\mu\text{-3-CF}_3\text{-5-CH}_3\text{pz})(\text{COD})]_2$, (e) $[\text{Ir}(\mu\text{-3,5-(CF}_3)_2\text{pz})(\text{COD})]_2$ (acetonitrile solutions, $22 \pm 2^\circ\text{C}$).

A

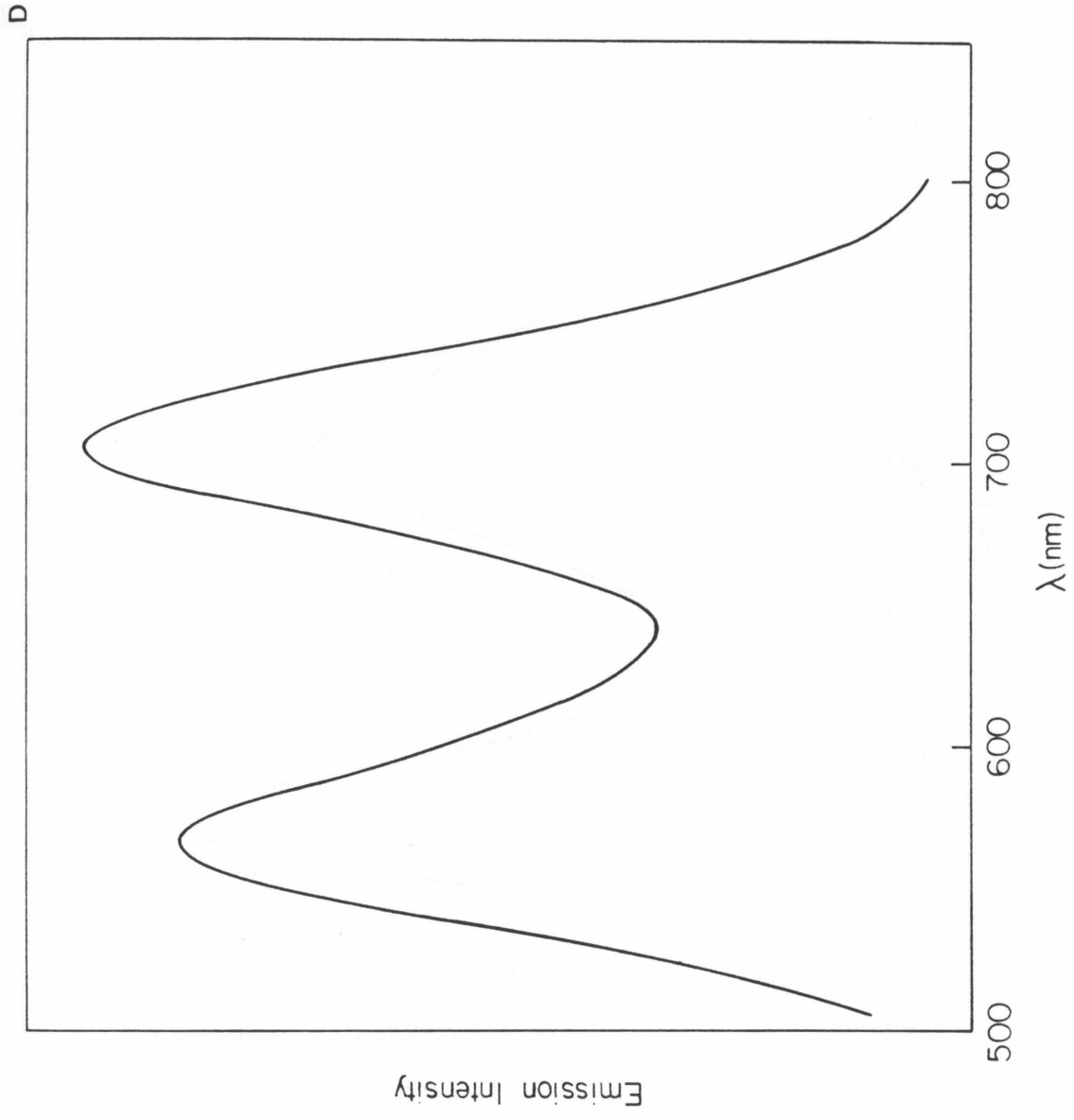


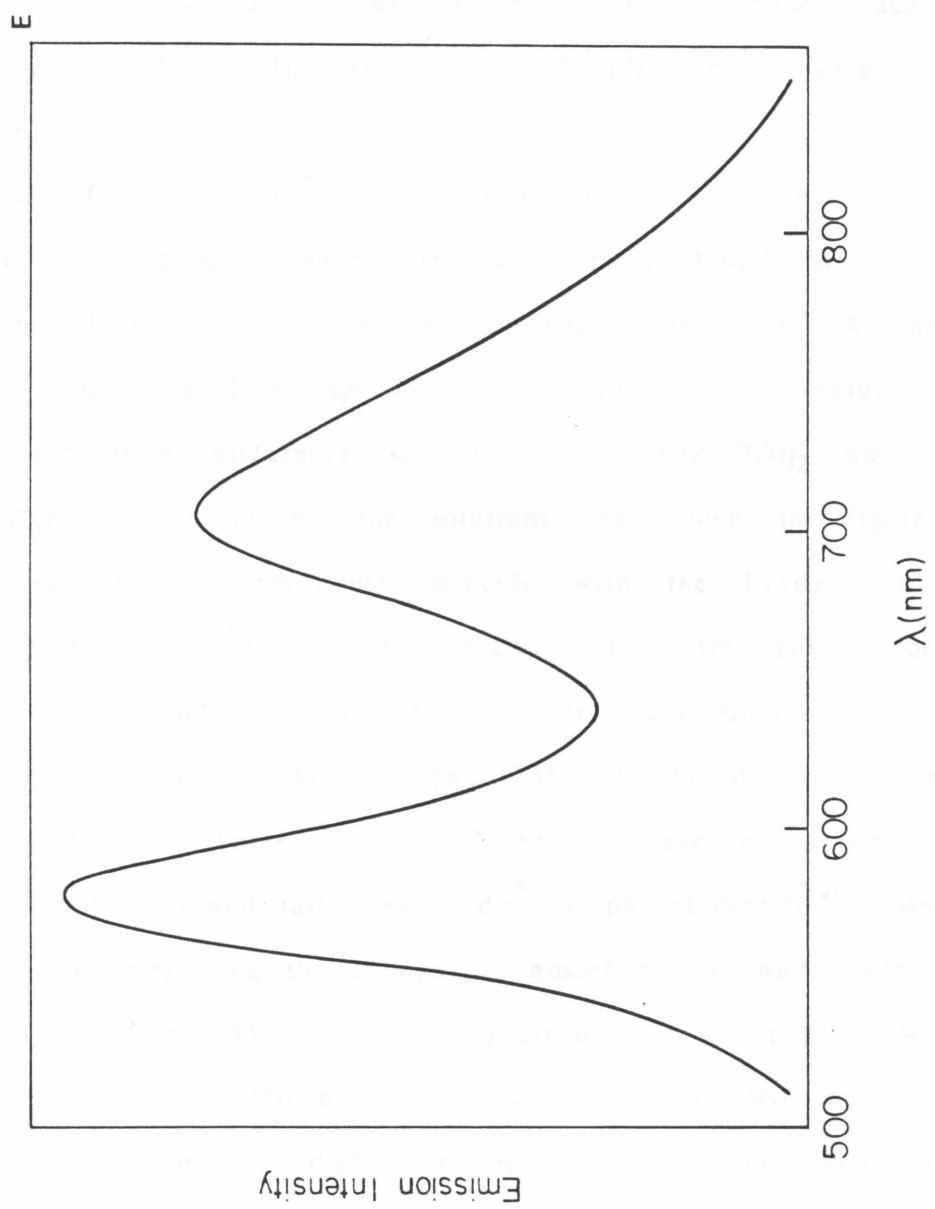
B





c





listed in Table 2.3.⁴¹ The small Stokes shifts between the absorption and emission bands (${}^1A_1 \leftrightarrow {}^1B_2$, 1500 - 2200 cm^{-1} ; ${}^1A_1 \leftrightarrow {}^3B_2$, 1900 - 2500 cm^{-1}), the excited-state lifetimes (*vide infra*), and the similarities between the physical properties of these luminescent excited states and the ${}^{1,3}A_{2u}(d\sigma^* p\sigma)$ excited states of the "face-to-face" d^8 - d^8 dimers of rhodium(I), iridium(I), and platinum(II) support this assignment.

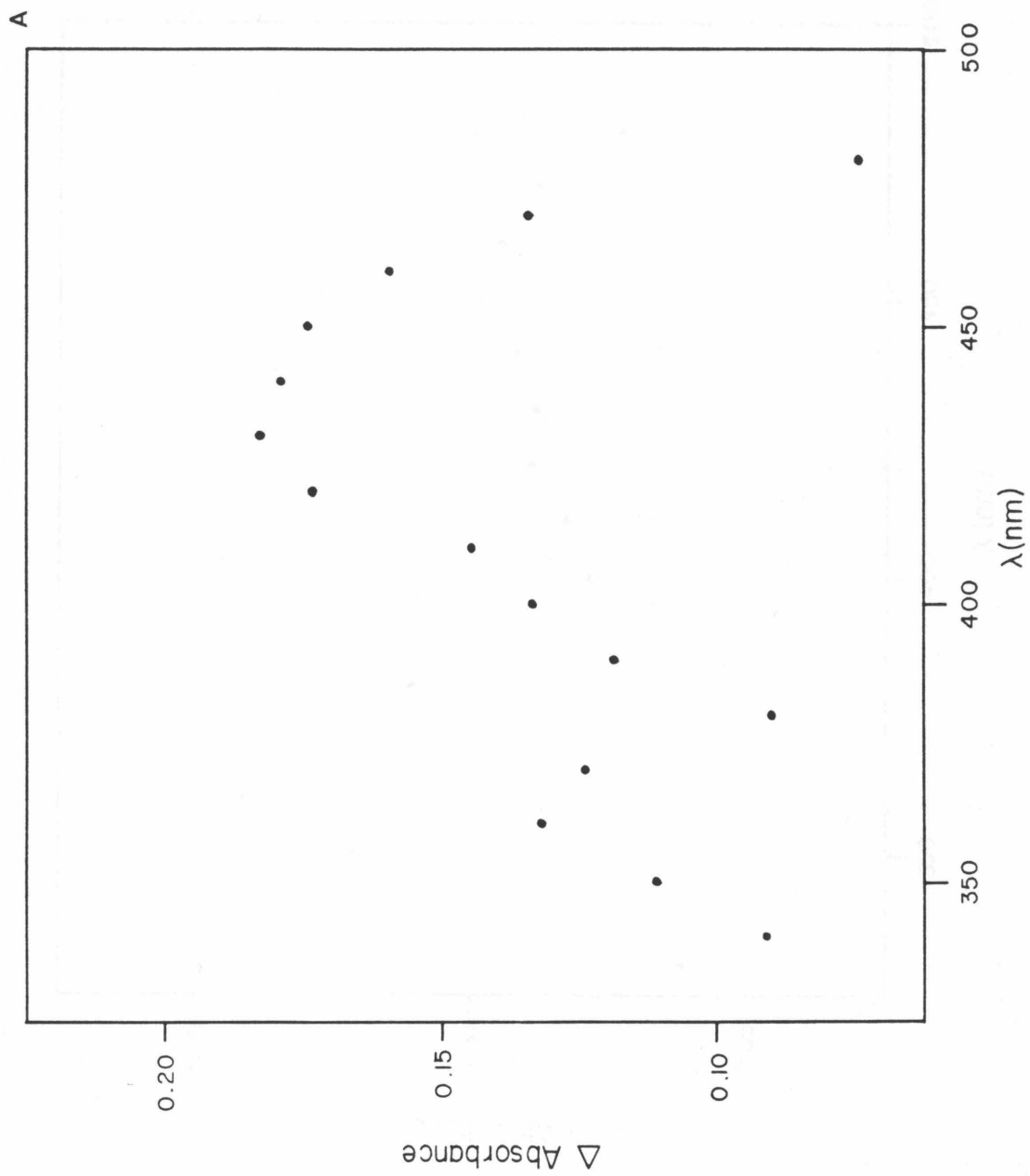
Several of the ${}^3B_2(d\sigma^* p\sigma)$ excited states of the pyrazolyl-bridged iridium(I) cyclooctadiene dimers are sufficiently long-lived in fluid solution to observe the changes in absorbance from the 1A_1 ground state by nanosecond laser spectroscopy at ambient temperature. The transient absorption difference spectra of $[\text{Ir}(\mu\text{-pz})(\text{COD})]_2$ and $[\text{Ir}(\mu\text{-3,4,5-(CH}_3)_3\text{pz})(\text{COD})]_2$ in benzene solutions are shown in Figure 2.7. The lifetimes of the transients coincide with the lifetimes of the phosphorescent ${}^3B_2(d\sigma^* p\sigma)$ excited states. The transient absorption difference spectra of these two complexes are very similar to that of the ${}^3A_{2u}(d\sigma^* p\sigma)$ excited state of $[\text{Rh}_2(\text{TMB})_4]^{2+}$ (TMB = 2,5-dimethyl-2,5-diisocyanohexane) where two broad features are also observed to the blue of the ground-state singlet $d\sigma^* \rightarrow p\sigma$ absorption.⁴² Because of problems in measuring the changes in absorbance at wavelengths near the laser excitation (532 nm), the spectrum of $[\text{Ir}(\mu\text{-pz})(\text{COD})]_2$ was not measured for $\lambda > 480$ nm. Recently, Dr. Jay R. Winkler measured the transient absorption difference spectrum of this complex in cyclohexane solution over a larger wavelength range, and a bleaching at ~ 500 nm that corresponds to the singlet $d\sigma^* \rightarrow p\sigma$ transition of the ground state was observed.⁴²

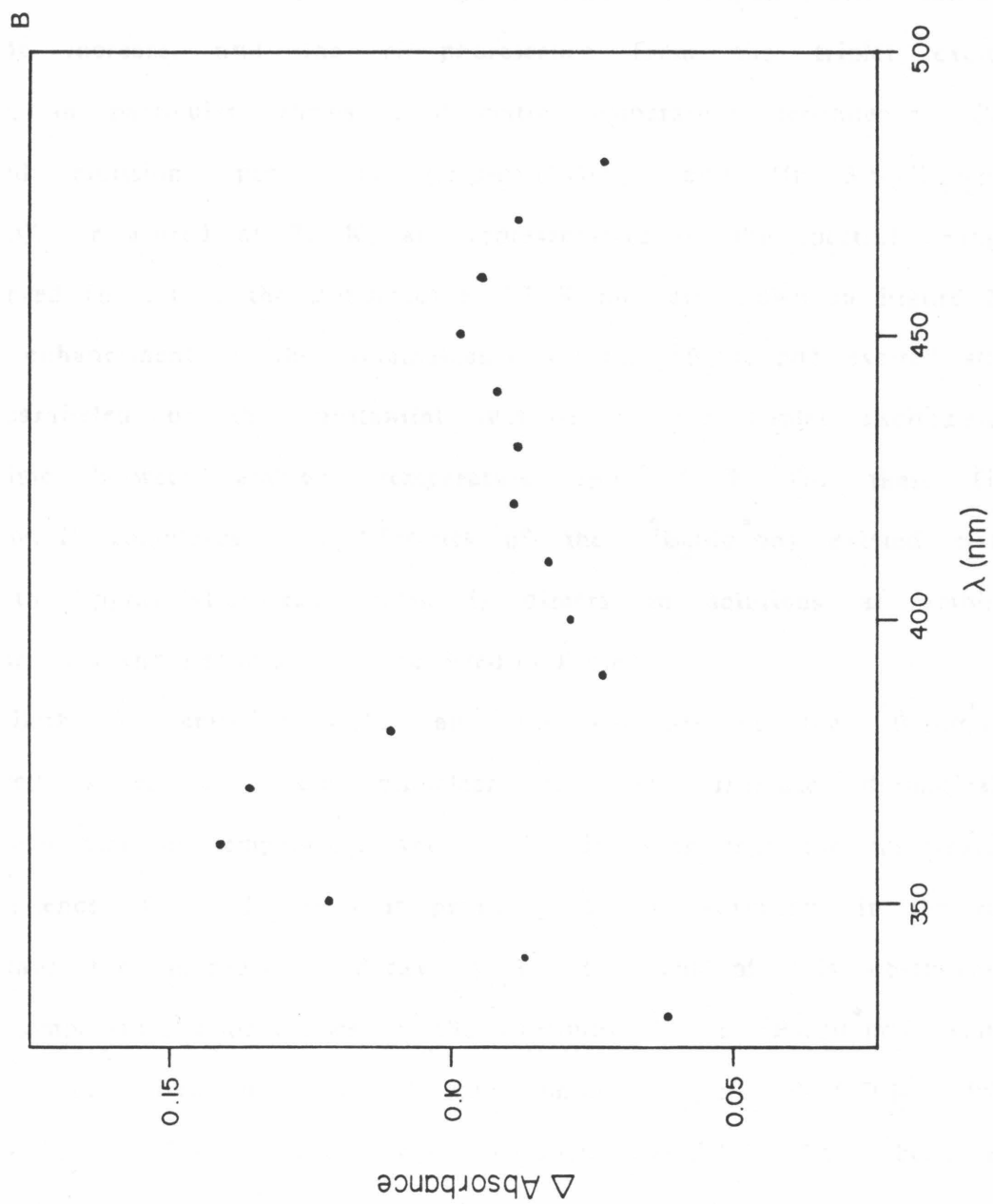
Table 2.3 Emission band maxima and quantum yields for the fluorescent $^1B_2(d\sigma^*p\sigma)$ and phosphorescent $^3B_2(d\sigma^*p\sigma)$ excited states of pyrazolyl-bridged binuclear iridium(I) cyclo-octadiene complexes.

Iridium Complex ^a	Emission Band Maxima (nm) ^b		Quantum Yields ^c	
	$^1B_2(d\sigma^*p\sigma)$	$^3B_2(d\sigma^*p\sigma)$	1B_2	3B_2
(μ -pz)	558	684	0.0001	0.0078
(μ -3,5-(CH ₃) ₂ pz)	579	715	0.0001	0.0038
(μ -3,4,5-(CH ₃) ₃ pz)	580	717	0.0001	0.0035
(μ -3-CF ₃ -5-CH ₃ pz)	567	705	0.0003	0.0003
(μ -3,5-(CF ₃) ₂ pz)	579	705	0.0006	0.0006

- a. The complex designations are abbreviated and represent [Ir(μ -pz)(COD)]₂ and the substituted-pyrazolyl analogues.
- b. The emission band maxima and quantum yields were measured of acetonitrile solutions of these complexes.
- c. An acetonitrile solution of [Ru(bpy)₃](PF₆)₂, which has a quantum yield for emission of 0.062,²⁶ was used as the standard. The numbers are accurate to $\pm 20\%$.

Figure 2.7 Transient absorption difference spectra of (a) $[\text{Ir}(\mu\text{-pz})(\text{COD})]_2$ and (b) $[\text{Ir}(\mu\text{-3,4,5-(CH}_3)_3\text{pz})(\text{COD})]_2$ (benzene solutions, $22 \pm 2^\circ\text{C}$, $[\text{Ir}_2] = 10^{-4}\text{ M}$, $\lambda_{\text{ex}} = 532\text{ nm}$).

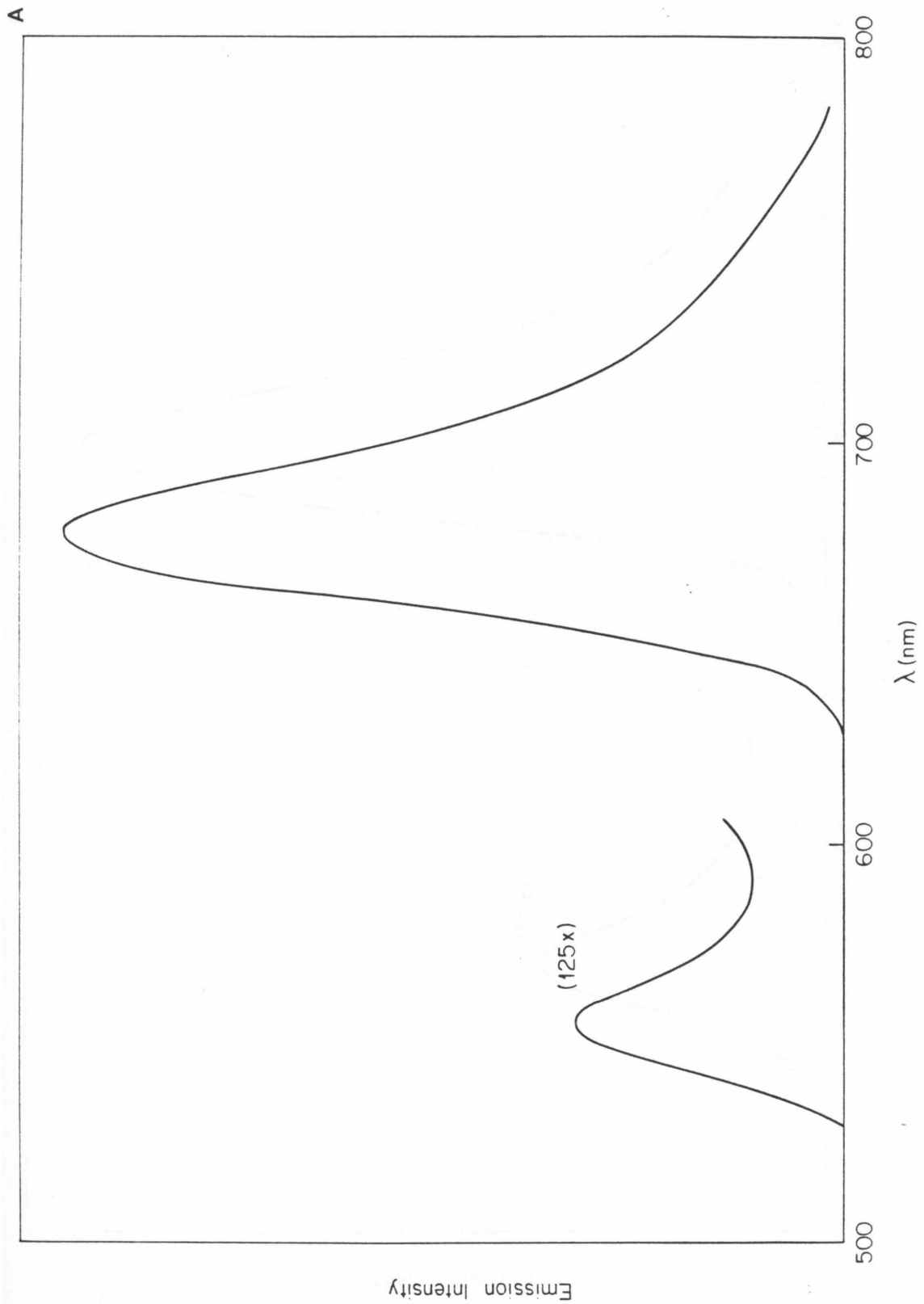




The emission intensities of the $^1B_2(d\sigma^*p\sigma)$ and $^3B_2(d\sigma^*p\sigma)$ excited states of these pyrazolyl-bridged iridium complexes are temperature dependent. Upon cooling to 77 K, the fluorescence and phosphorescence bands sharpen and shift to slightly higher energies. The emission yields increase, and the phosphorescence from the triplet excited state, in particular, shows a dramatic temperature dependence. Corrected emission spectra of $[\text{Ir}(\mu\text{-pz})(\text{COD})]_2$ and $[\text{Ir}(\mu\text{-3,5-(CF}_3)_2\text{pz})(\text{COD})]_2$, measured at 77 K, are representative of the spectral changes observed for all of the complexes at 77 K and are shown in Figure 2.8. The enhancement in the luminescence of the $^3B_2(d\sigma^*p\sigma)$ excited state is paralleled by the substantial increase in the triplet excited-state lifetime between ambient temperature and 77 K for these five iridium(I) complexes. The lifetimes of the $^3B_2(d\sigma^*p\sigma)$ excited states of the pyrazolyl-bridged iridium(I) dimers in solutions at ambient temperature and glasses at 77 K are listed in Table 2.4.

Both the emission yields and the lifetimes of the $^3B_2(d\sigma^*p\sigma)$ excited states of these binuclear complexes increase dramatically between ambient temperature and 77 K, implying that the temperature dependence of the lifetimes is primarily due to variations in the rate constant for nonradiative decay (k_{nr}). In light of this observation, the temperature dependences of the lifetimes of the $^3B_2(d\sigma^*p\sigma)$ excited states for three of the iridium complexes, $[\text{Ir}(\mu\text{-pz})(\text{COD})]_2$, $[\text{Ir}(\mu\text{-3,4,5-(CH}_3)_3\text{pz})(\text{COD})]_2$, and $[\text{Ir}(\mu\text{-3-CF}_3\text{-5-CH}_3\text{pz})(\text{COD})]_2$, have been examined in detail. From the relationship between the observed lifetime (τ_{obs}), the quantum yield for emission (Φ_{em}), and the rate constants for radiative and nonradiative decay (k_r , k_{nr}) of an excited state,

Figure 2.8 Corrected emission spectra of (a) $[\text{Ir}(\mu\text{-pz})(\text{COD})]_2$ and (b) $[\text{Ir}(\mu\text{-3,5-(CF}_3)_2\text{pz})(\text{COD})]_2$ at 77 K (2-methyltetrahydrofuran glasses).



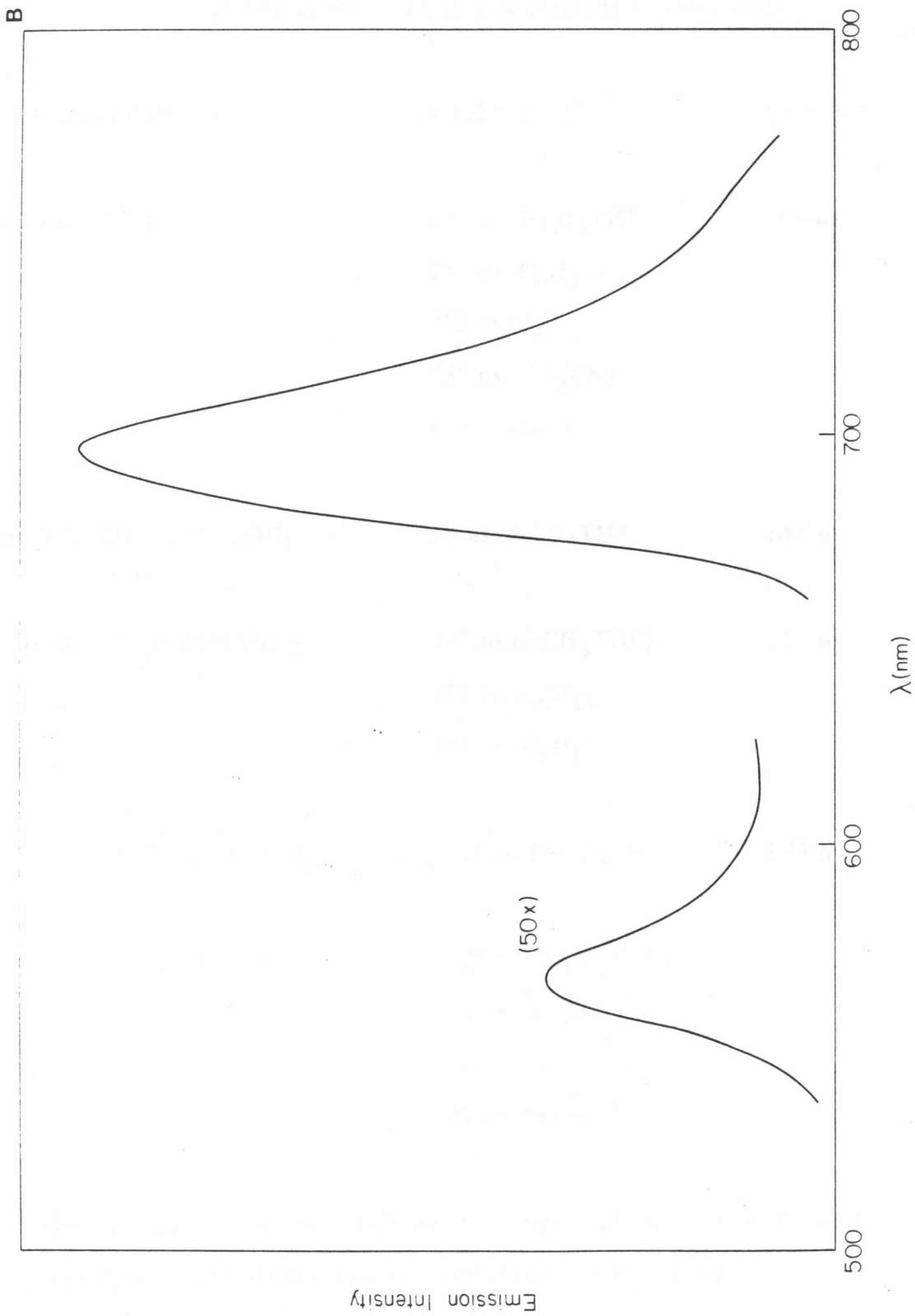


Table 2.4 Lifetimes of the ${}^3B_2(d\sigma^*p\sigma)$ excited states of pyrazolyl-bridged binuclear iridium(I) cyclooctadiene complexes.

Iridium Complex	τ ($22 \pm 2^\circ\text{C}$) ^a	τ (77 K) ^b
[Ir(μ -pz)(COD)] ₂	245 ns (2-CH ₃ THF)	2.68 μs
	250 ns (C ₆ H ₁₂)	
	280 ns (C ₆ H ₆)	
	250 ns (CH ₃ CN)	
	640 ns (solid)	
[Ir(μ -3,5,-(CH ₃) ₂ pz)(COD)] ₂	80 ns (2-CH ₃ THF)	1.57 μs
[Ir(μ -3,4,5-(CH ₃) ₃ pz)(COD)] ₂	100 ns (2-CH ₃ THF)	1.52 μs
	100 ns (C ₆ H ₁₂)	
	100 ns (C ₆ H ₆)	
[Ir(μ -3-CF ₃ -5-CH ₃ pz)(COD)] ₂	< 20 ns (2-CH ₃ THF) ^c	1.73 μs
[Ir(μ -3,5-(CF ₃) ₂ pz)(COD)] ₂	< 20 ns (2-CH ₃ THF) ^c	1.80 μs
	< 20 ns (C ₆ H ₁₂) ^c	
	< 20 ns (CH ₃ CN) ^c	
	100 ns (solid)	

a. The lifetimes were measured in a variety of solvents (2-CH₃THF = 2-methyltetrahydrofuran, C₆H₁₂ = cyclohexane, CH₃CN = aceto-

nitrile, C_6H_6 = benzene) and are accurate to $\pm 5\%$.

- b. The lifetimes were measured in 2-methyltetrahydrofuran glasses and are accurate to $\pm 5\%$.
- c. The measurement of this excited-state lifetime is instrument-limited.

given in equations (1) and (2), the values of k_r and k_{nr} can be calculated for the triplet excited states of these three complexes and are listed in Table 2.5.

$$\tau_{\text{obs}} = 1/(k_r + k_{nr}) \quad (1)$$

$$\Phi_{\text{em}} = k_r/(k_{nr} + k_r) \quad (2)$$

The observed lifetimes (τ_{obs}) of the ${}^3B_2(d\sigma^*p\sigma)$ excited states are approximately equal to $(1/k_{nr})$, and the data for the temperature dependence of τ_{obs} for these three complexes, shown in Figure 2.9, can be fit to a modified-Arrhenius expression of the form given in equation (3). In this expression, k_{nr}° and $k_{nr}' \exp(-E_a/k_bT)$ represent the nonradiative rate at low and high temperatures, respectively.

$$(1/\tau_{\text{obs}}) \approx k_{nr} = k_{nr}^{\circ} + k_{nr}' \exp(-E_a/k_bT) \quad (3)$$

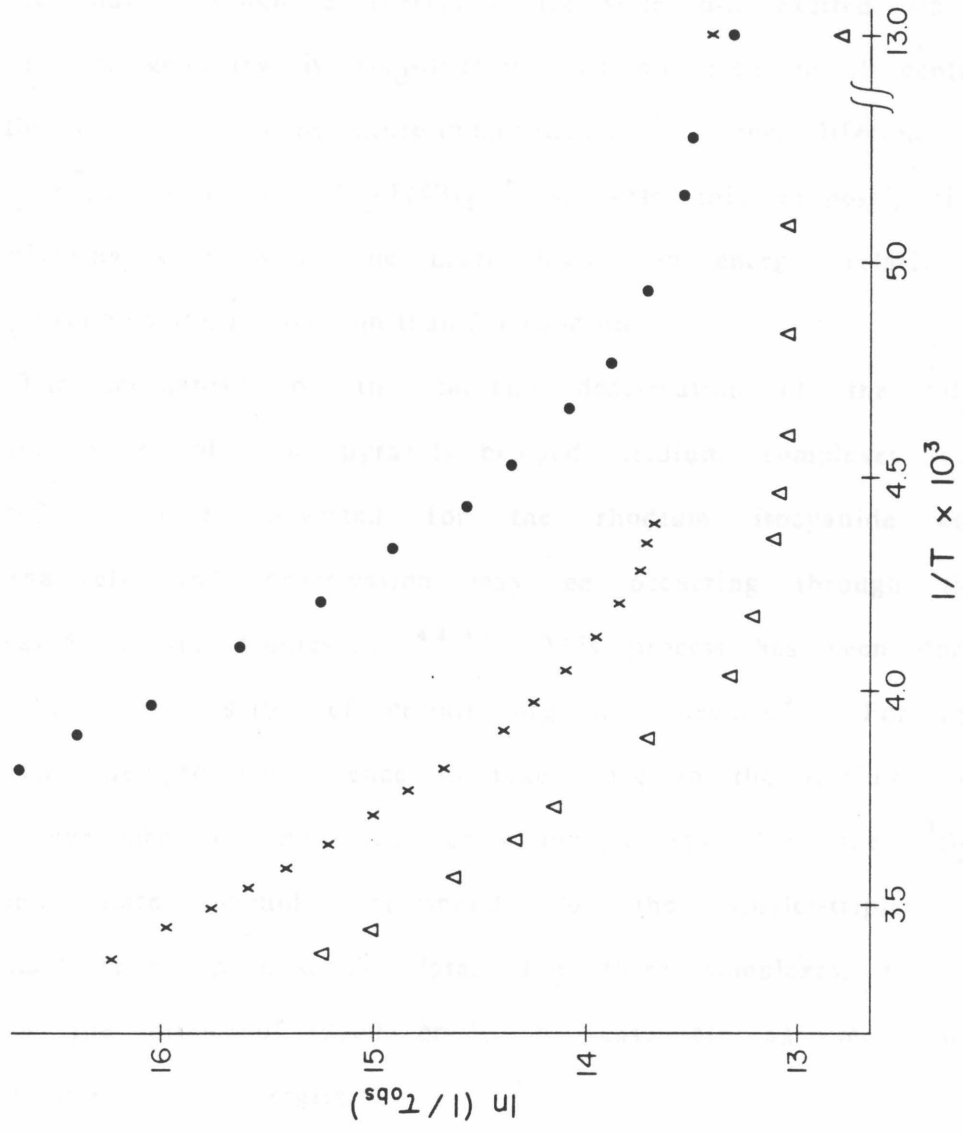
The term E_a is the activation energy for the thermally-accessible non-radiative pathway leading to deactivation of the excited state, and the calculated values of E_a for the ${}^3B_2(d\sigma^*p\sigma)$ excited states of $[\text{Ir}(\mu\text{-pz})(\text{COD})]_2$, $[\text{Ir}(\mu\text{-3,4,5-(CH}_3)_3\text{pz})(\text{COD})]_2$, and $[\text{Ir}(\mu\text{-3-CF}_3\text{-5-CH}_3\text{pz})(\text{COD})]_2$ are 2600, 2500, and 2300 cm^{-1} , respectively.

Although the mechanism for the deactivation of the ${}^3B_2(d\sigma^*p\sigma)$ excited state is not understood, similar temperature-dependent behavior has been observed for the ${}^3A_{2u}(d\sigma^*p\sigma)$ excited state of several of the binuclear rhodium(I) bridging isocyanide complexes.^{2,8} In

Table 2.5 Calculated values of the radiative (k_r) and nonradiative (k_{nr}) decay rate constants for the ${}^3B_2(d\sigma^*p\sigma)$ excited states of selected pyrazolyl-bridged binuclear iridium(I) cyclooctadiene complexes at $22 \pm 2^\circ\text{C}$.

Iridium Complex	k_r (s^{-1})	k_{nr} (s^{-1})
$[\text{Ir}(\mu\text{-pz})(\text{COD})]_2$	3.1×10^4	4.0×10^6
$[\text{Ir}(\mu\text{-3,4,5-(CH}_3)_3\text{pz})(\text{COD})]_2$	3.5×10^4	1.0×10^7
$[\text{Ir}(\mu\text{-3-CF}_3\text{-5-CH}_3\text{pz})(\text{COD})]_2$	$> 1.5 \times 10^4$	$> 5.0 \times 10^7$

Figure 2.9 Arrhenius plots of the ${}^3B_2(d\sigma^*p\sigma)$ excited-state lifetimes for $[\text{Ir}(\mu\text{-pz})(\text{COD})]_2$ (Δ), $[\text{Ir}(\mu\text{-3,4,5-(CH}_3)_3\text{pz})(\text{COD})]_2$ (X), and $[\text{Ir}(\mu\text{-3-CF}_3\text{-5-CH}_3\text{pz})(\text{COD})]_2$ (\bullet).



contrast, the lifetime of the ${}^3A_{2u}(d\sigma^*p\sigma)$ excited state of $[\text{Ir}_2(\text{TMB})_4]^{2+}$ is temperature independent between ambient temperature and 77 K.⁷ A nonradiative pathway that has been suggested to account for these observations involves deactivation of the phosphorescent excited state through a thermally accessible d-d excited state whose equilibrium geometry is D_{2d} -distorted around each metal center.^{2,8,43} Furthermore, the temperature-independence of the lifetime of the ${}^3A_{2u}(d\sigma^*p\sigma)$ state of $[\text{Ir}_2(\text{TMB})_4]^{2+}$ supports this proposal, since this deactivating state would be much higher in energy, relative to the ${}^3A_{2u}$ excited state, for iridium than for rhodium.

The mechanism of the thermal deactivation of the ${}^3B_2(d\sigma^*p\sigma)$ excited state of the pyrazolyl-bridged iridium complexes could be related to that suggested for the rhodium isocyanide complexes. Alternatively, this deactivation may be occurring through thermally-activated delayed fluorescence.^{44,45} This process has been documented for the excited states of certain organic molecules.⁴⁶ For thermally-activated delayed fluorescence to take place in the iridium complexes, the experimentally measured activation energy for the ${}^3B_2(d\sigma^*p\sigma)$ excited state should correspond to the singlet-triplet splitting obtained from spectroscopic data. For these complexes, this splitting is on the order of 2500 cm^{-1} , in reasonable agreement with the measured activation energies.

The ${}^1B_2(d\sigma^*p\sigma)$ excited states of these iridium complexes are very short-lived at ambient temperature in solution in accord with the low fluorescence quantum yields for this state. Picosecond laser spectroscopic studies by Dr. Jay R. Winkler have shown that the lifetime of

the ${}^1B_2(d\sigma^*p\sigma)$ excited state of $[\text{Ir}(\mu\text{-pz})(\text{COD})]_2$ is < 20 ps.^{4,2} This value is much lower than that observed for the lifetimes of the ${}^1A_{2u}(d\sigma^*p\sigma)$ excited state for two of the rhodium isocyanide d^8-d^8 dimers $[\text{Rh}_2(\text{bridge})_4]^{2+}$ (bridge = 1,3-diisocyanopropane), $\tau({}^1A_{2u}) = 1.1$ ns;² $[\text{Rh}_2(\text{TMB})_4]^{2+}$, $\tau({}^1A_{2u}) = 820$ ps)^{4,2} but is consistent with the much lower fluorescence quantum yield. For instance, if the radiative decay rates for the ${}^1A_{2u}$ state of $[\text{Rh}_2(\text{TMB})_4]^{2+}$ and the 1B_2 state of $[\text{Ir}(\mu\text{-pz})(\text{COD})]_2$ are similar, the lower fluorescence quantum yield for the iridium dimer (0.0001) implies that the lifetime of the 1B_2 excited state is on the order of 2 ps, given that the ${}^1A_{2u}$ excited state of $[\text{Rh}_2(\text{TMB})_4]^{2+}$ has a lifetime of 820 ps and $\Phi_{\text{em}} = 0.046$.^{4,2}

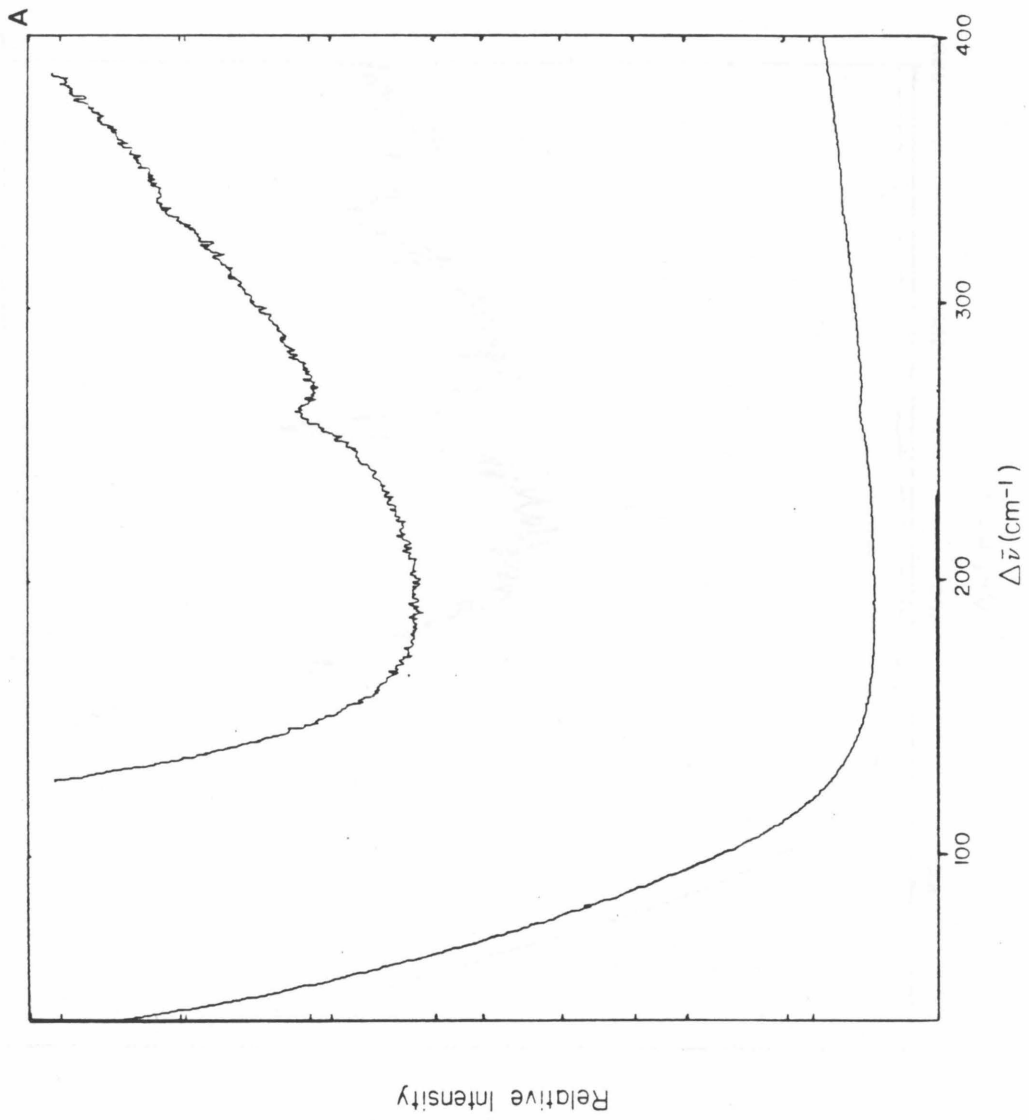
Resonance Raman spectroscopic studies of the d^8-d^8 dimers $[\text{Rh}_2(\text{bridge})_4]^{2+}$ and $[\text{Pt}_2(\text{pop})_4]^{4-}$ have shown that a substantial metal-metal bonding interaction is present in the ${}^1A_{1g}(d\sigma)^2(d\sigma^*)^2$ ground state of these binuclear complexes.^{4,6} Excitation into the bands corresponding to the metal-localized ${}^1A_{1g} \rightarrow {}^1A_{2u}$ transition in these dimers results in resonance-enhancement of the metal-metal stretching vibrations, which are observed at 79 cm^{-1} for the rhodium complex and at 118 cm^{-1} for $[\text{Pt}_2(\text{pop})_4]^{4-}$. In addition, time-resolved resonance Raman studies of these complexes have confirmed that a strong metal-metal bonding interaction exists in the ${}^3A_{2u}(d\sigma)^2(d\sigma^*)^1(p\sigma)^1$ excited state.^{4,6}

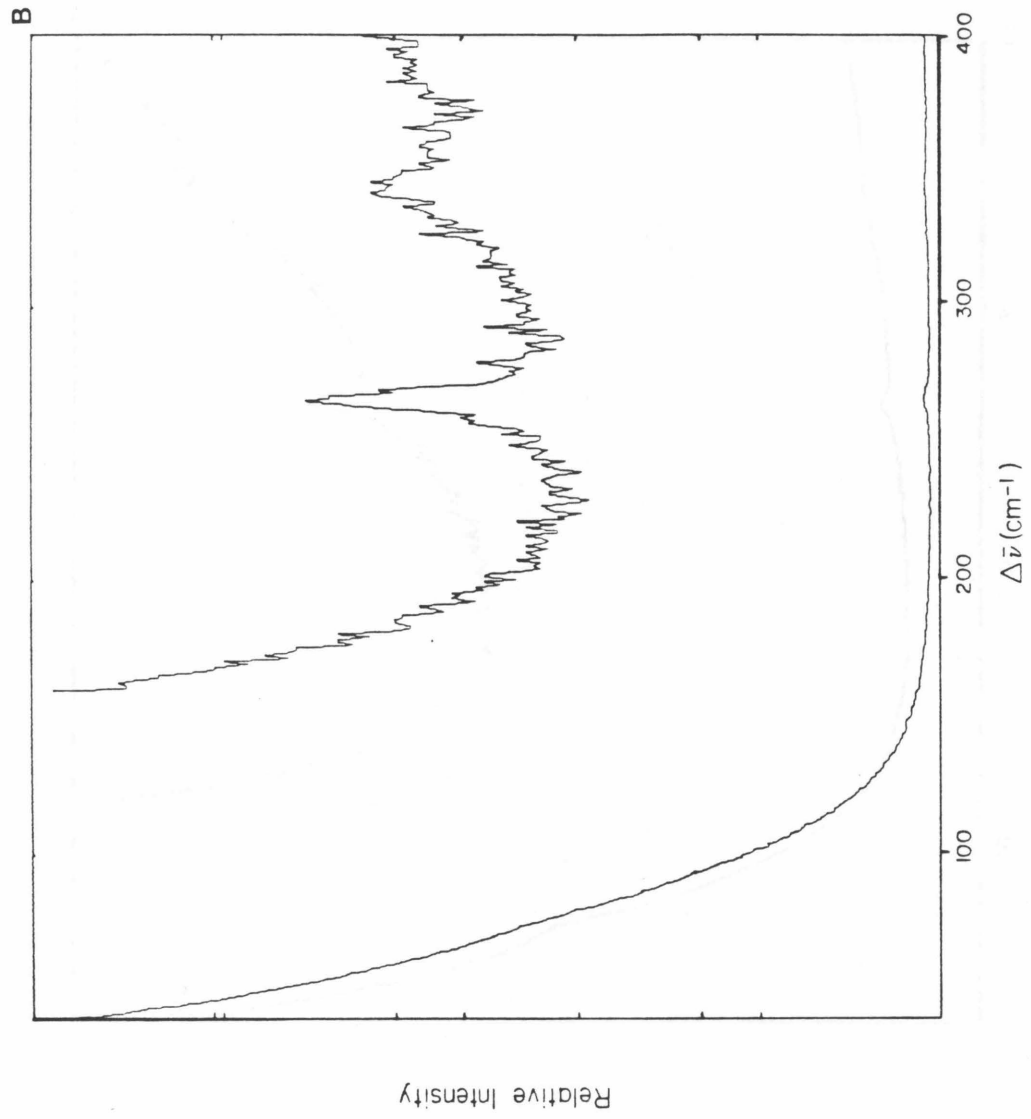
Resonance Raman spectroscopic studies of the pyrazolyl-bridged iridium(I) cyclooctadiene complexes suggest that a metal-metal bonding interaction is also present in the ground state of these lower-symmetry d^8-d^8 dimers. Excitation into the bands corresponding to the

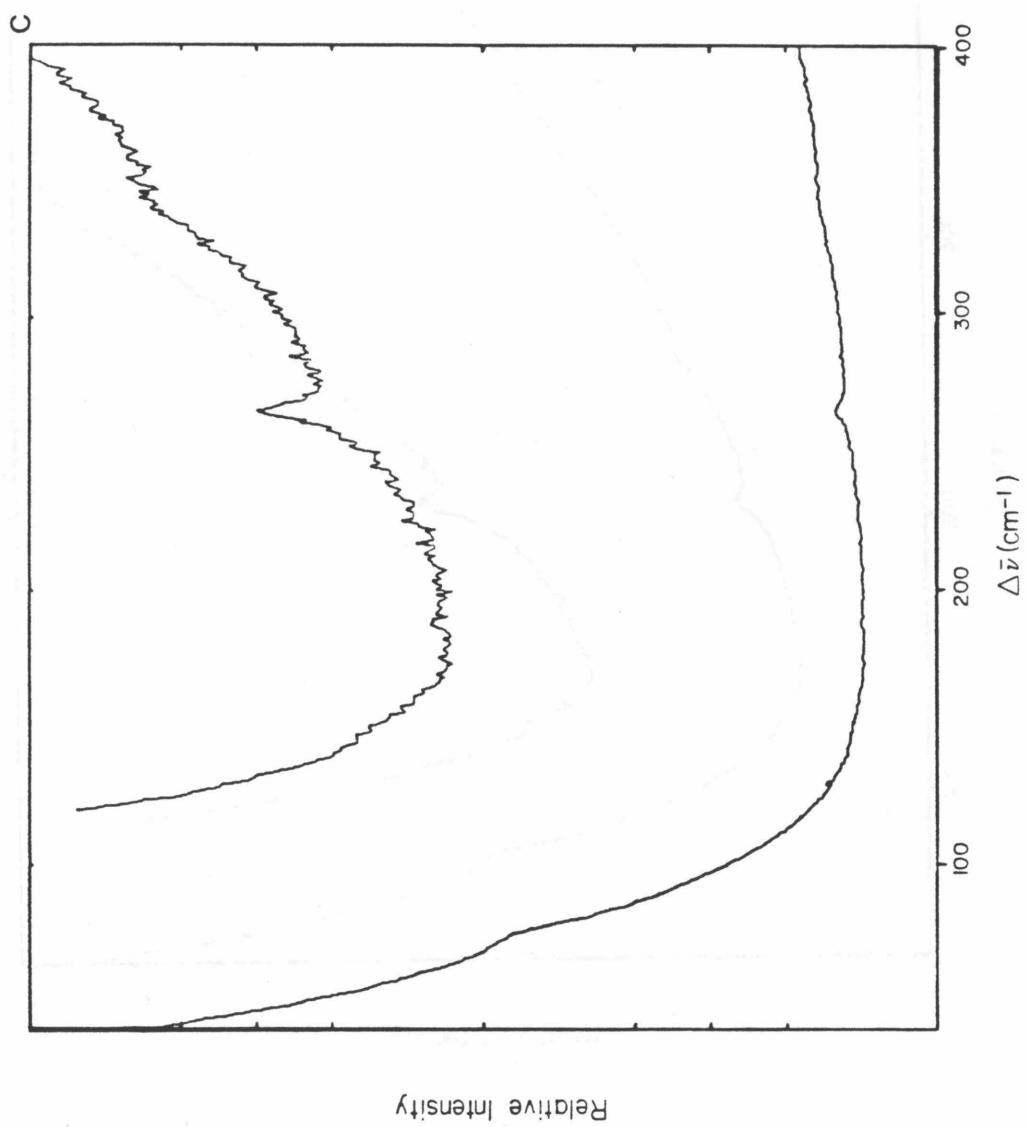
metal-localized ${}^1A_1 \rightarrow {}^1B_2$ transition results in resonance-enhancement of vibrations at low frequencies that may be assigned to the iridium-iridium stretch. In addition, several other bands that are observed in the resonance Raman spectra are less-strongly resonance-enhanced upon excitation into this transition and are likely candidates for metal-ligand stretching vibrations. The resonance Raman spectra of $[\text{Ir}(\mu\text{-pz})(\text{COD})]_2$, $[\text{Ir}(\mu\text{-3,4,5-(CH}_3)_3\text{pz})(\text{COD})]_2$, and $[\text{Ir}(\mu\text{-3,5-(CF}_3)_2\text{pz})(\text{COD})]_2$ in benzene solutions were measured at Caltech and are shown in Figure 2.10. Recently, Dr. Edward M. Kober at Los Alamos National Laboratory measured the resonance Raman spectra of these complexes in tetrahydrofuran solutions and obtained much better resolution in the low-frequency region of the spectrum. The resonance Raman spectra of $[\text{Ir}(\mu\text{-3-CF}_3\text{-5-CH}_3\text{pz})(\text{COD})]_2$ and $[\text{Ir}(\mu\text{-3,5-(CH}_3)_2\text{pz})(\text{COD})]_2$ in tetrahydrofuran solutions were also measured, and these spectra are shown in Figure 2.11.⁴⁷ For the spectrum of $[\text{Ir}(\mu\text{-pz})(\text{COD})]_2$ in tetrahydrofuran and the spectra of the three iridium complexes in benzene solutions, the low-frequency features are poorly-resolved because of the Rayleigh scattering of the laser line. Also, all of the spectra show a substantial baseline slope because of emission from the fluorescent excited state.

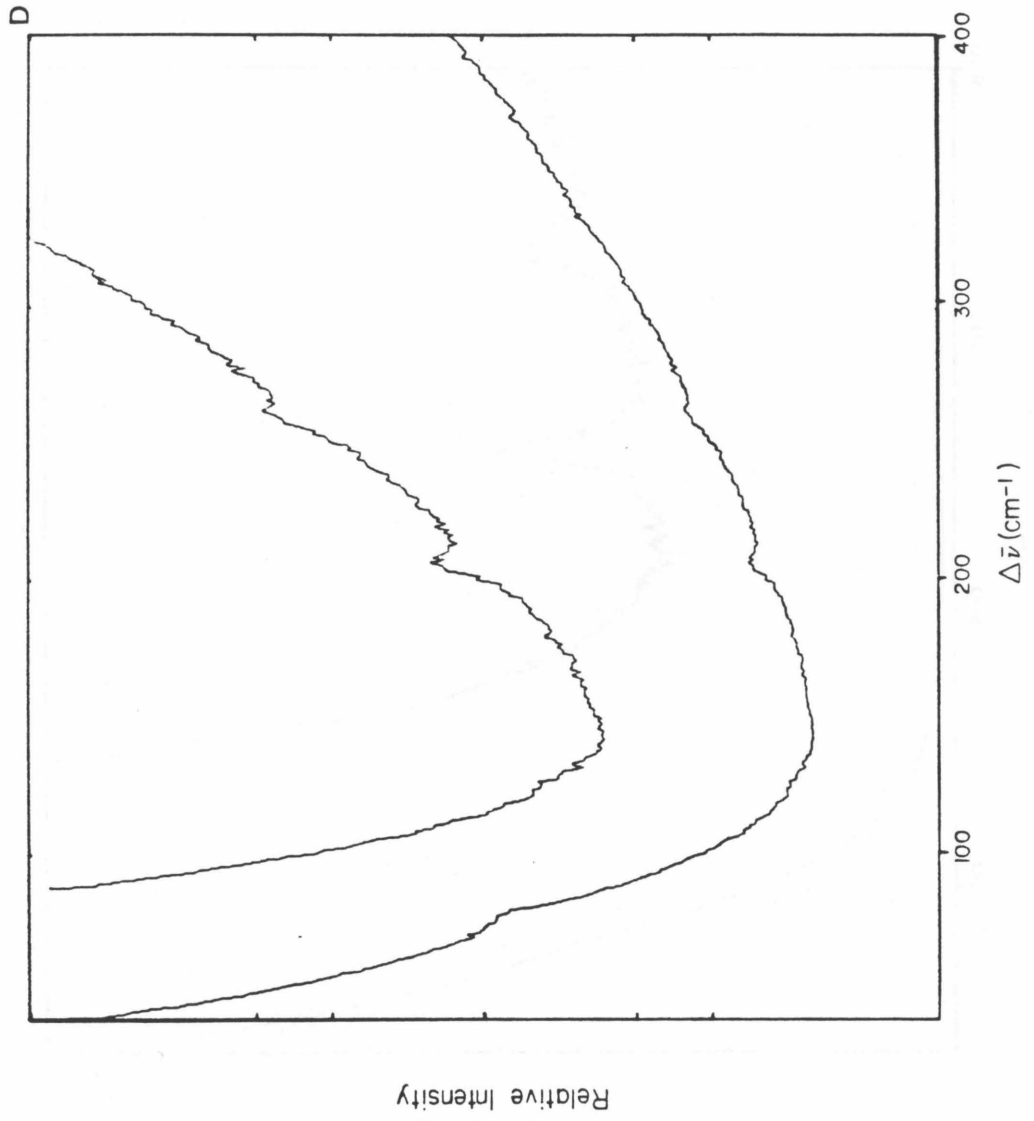
Several features that are common to the spectra of the binuclear iridium complexes are suggested to correspond to the iridium-iridium, iridium-alkene, and iridium-nitrogen stretching vibrations and are listed in Table 2.6. The relative trend in the metal-metal stretching frequencies is consistent with the metal-metal separations in the complexes that have been structurally characterized. Specifically, the

Figure 2.10 Resonance Raman spectra of (a) $[\text{Ir}(\mu\text{-pz})(\text{COD})]_2$, $\lambda_{\text{ex}} = 496.5$ nm, 16 scans, $[\text{Ir}_2] = 9 \times 10^{-4}$ M, benzene solution; (b) $[\text{Ir}(\mu\text{-3,4,5-(CH}_3)_3\text{pz})(\text{COD})]_2$, $\lambda_{\text{ex}} = 496.5$ nm, 9 scans, $[\text{Ir}_2] = 7 \times 10^{-4}$ M, benzene solution; (c) $[\text{Ir}(\mu\text{-3,4,5-(CH}_3)_3\text{pz})(\text{COD})]_2$, $\lambda_{\text{ex}} = 514.5$ nm, 16 scans, $[\text{Ir}_2] = 7 \times 10^{-4}$ M, benzene solution; (d) $[\text{Ir}(\mu\text{-3,5-(CF}_3)_2\text{pz})(\text{COD})]_2$, $\lambda_{\text{ex}} = 514.5$ nm, 16 scans, $[\text{Ir}_2] = 6 \times 10^{-4}$ M, benzene solution; (e) $[\text{Ir}(\mu\text{-3,5-(CF}_3)_2\text{pz})(\text{COD})]_2$, $\lambda_{\text{ex}} = 496.5$ nm, 25 scans, $[\text{Ir}_2] = 6 \times 10^{-4}$ M, benzene solution.









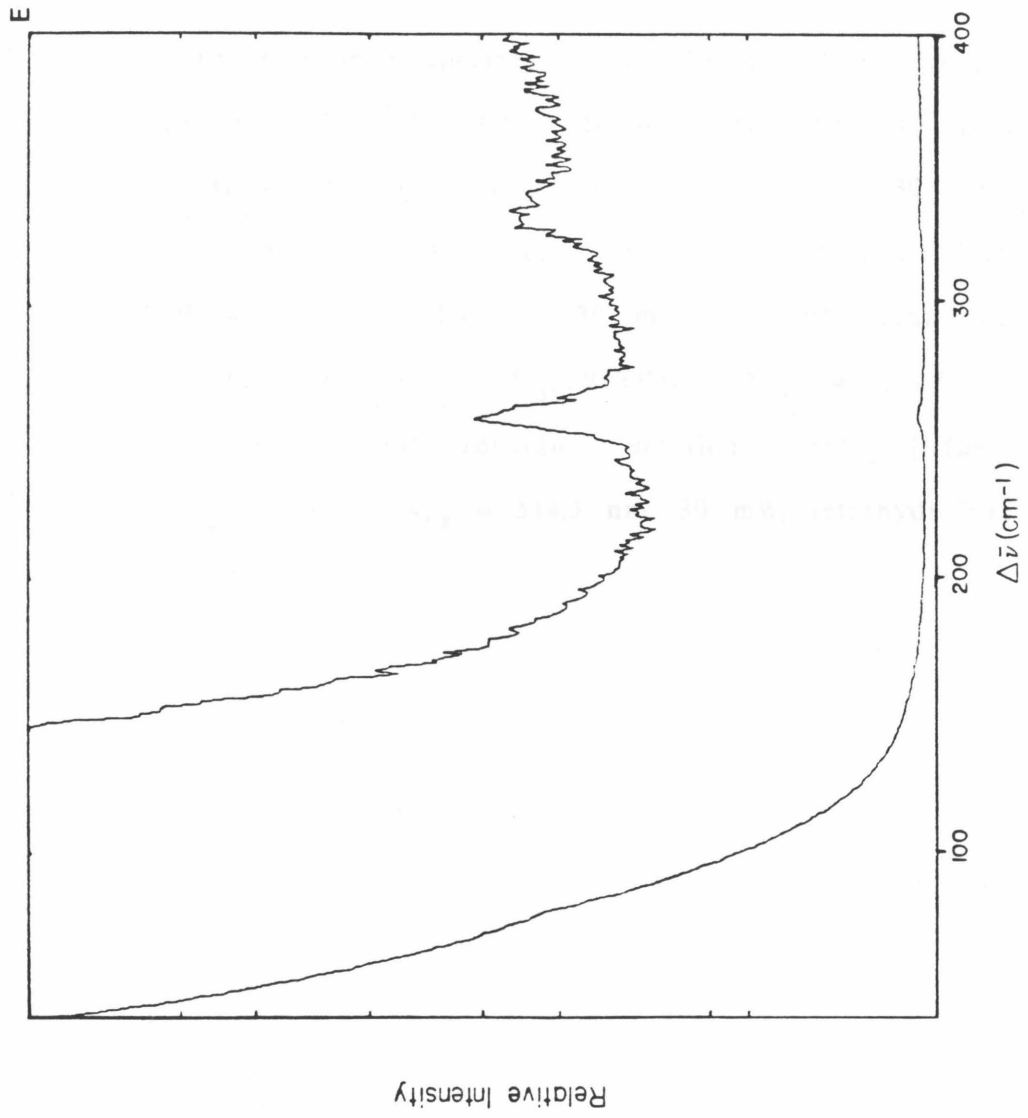
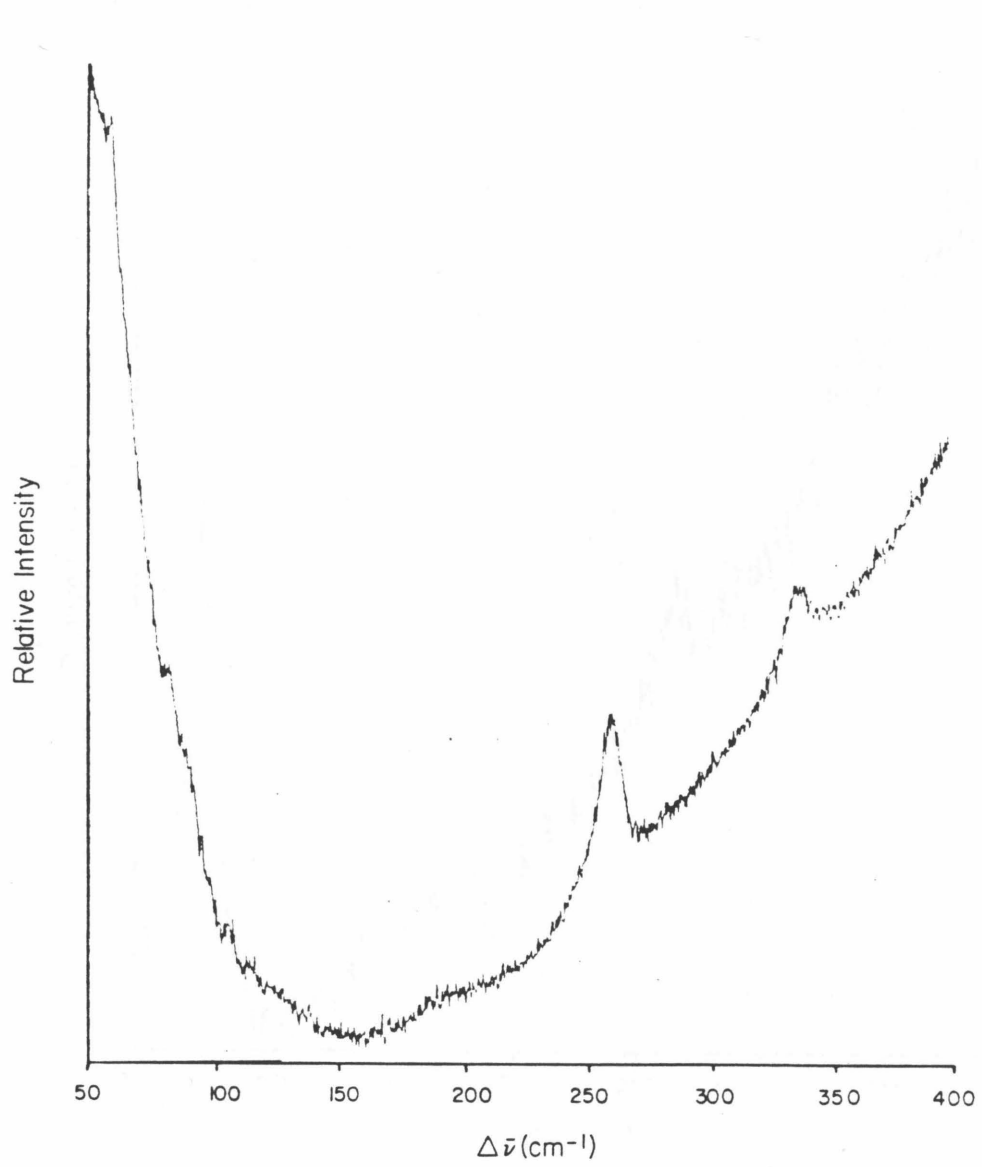
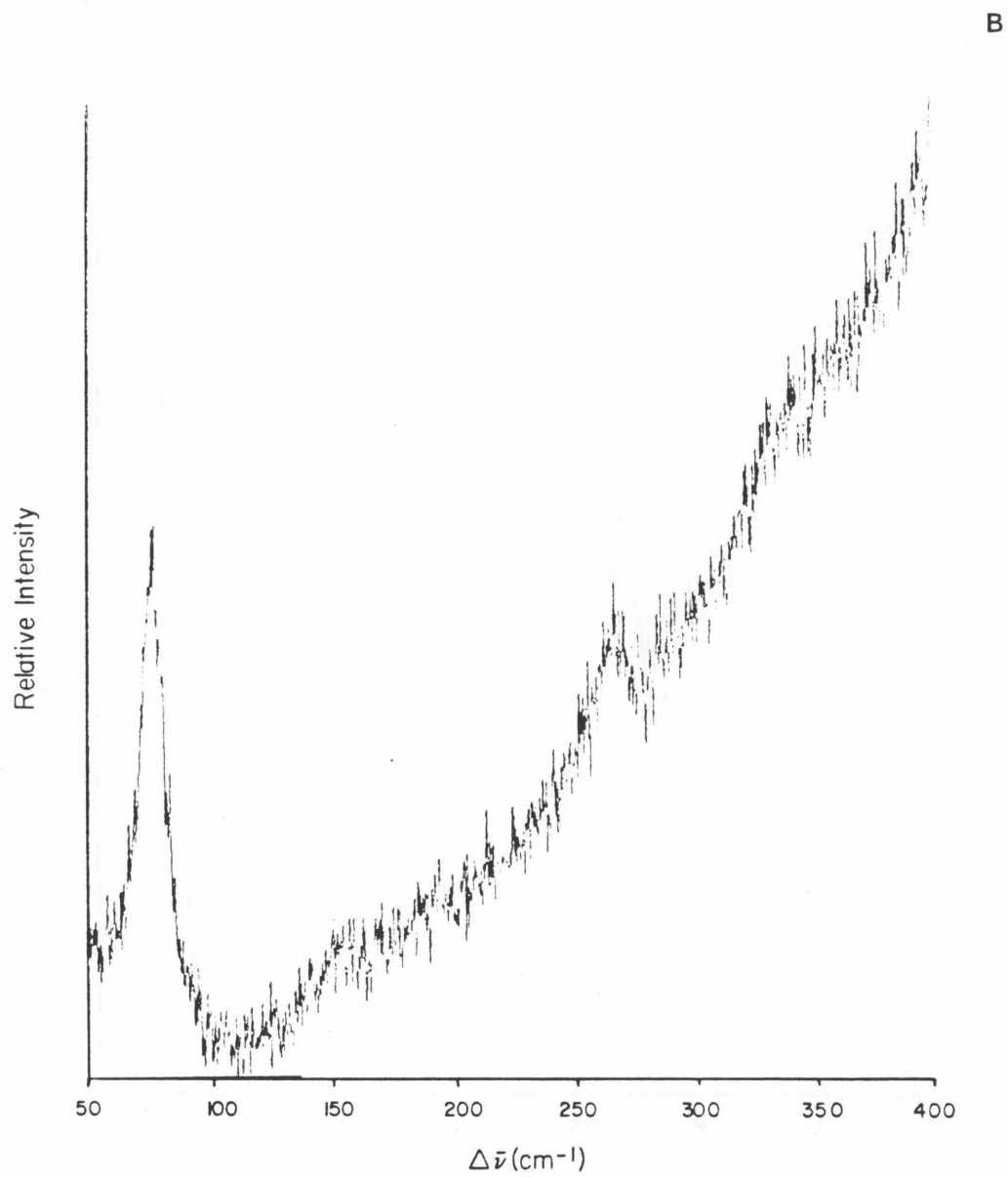
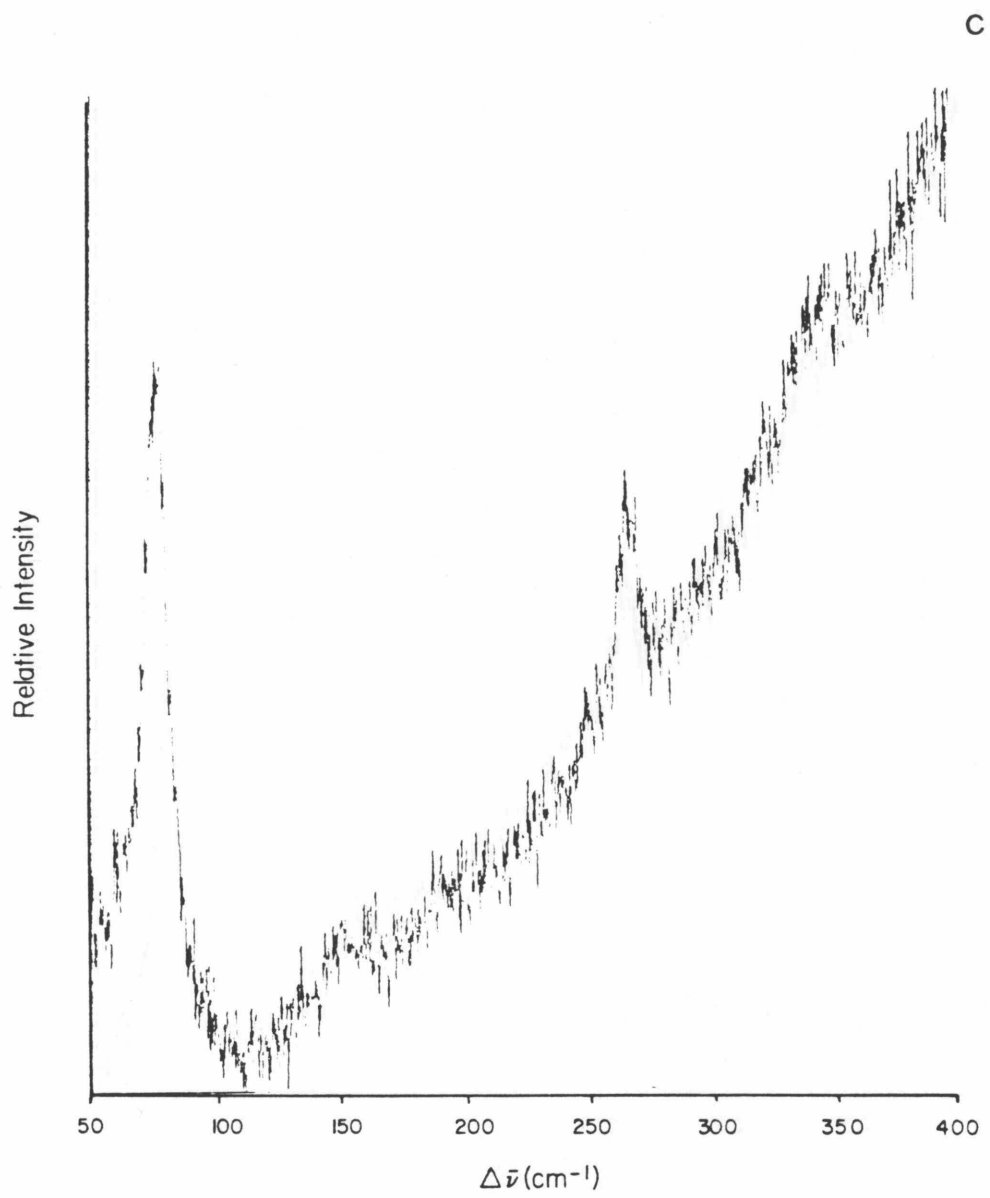
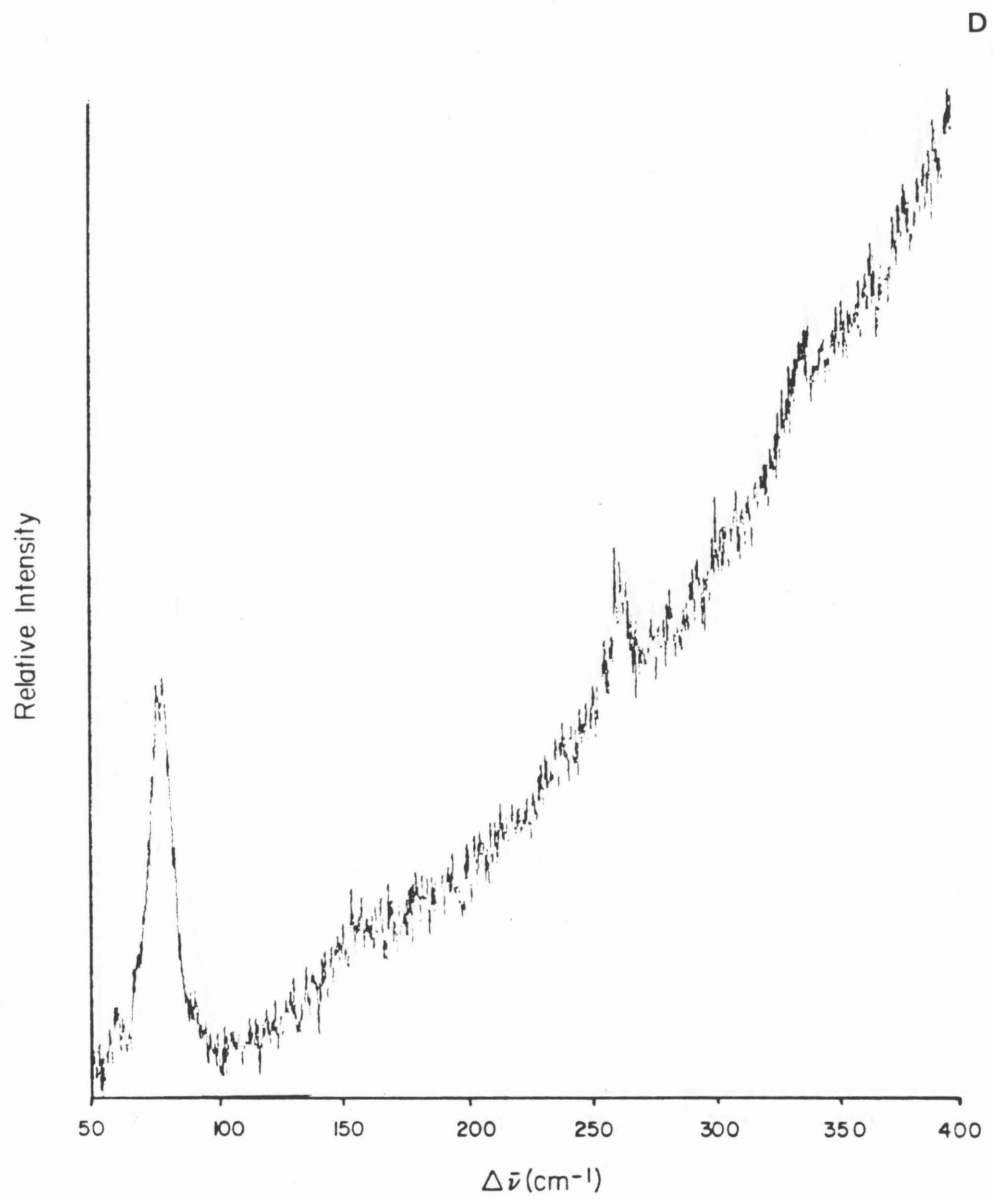


Figure 2.11 Resonance Raman spectra of (a) $[\text{Ir}(\mu\text{-pz})(\text{COD})]_2$, $\lambda_{\text{ex}} = 488.0$ nm, 35 mW, tetrahydrofuran solution; (b) $[\text{Ir}(\mu\text{-}3,5\text{-(CH}_3)_2\text{pz})(\text{COD})]_2$, $\lambda_{\text{ex}} = 514.5$ nm, 30 mW, tetrahydrofuran solution; (c) $[\text{Ir}(\mu\text{-}3,4,5\text{-(CH}_3)_3\text{pz})(\text{COD})]_2$, $\lambda_{\text{ex}} = 514.5$ nm, 30 mW, tetrahydrofuran solution; (d) $[\text{Ir}(\mu\text{-}3\text{-CF}_3\text{-}5\text{-CH}_3\text{pz})(\text{COD})]_2$, $\lambda_{\text{ex}} = 514.5$ nm, 30 mW, tetrahydrofuran solution; (e) $[\text{Ir}(\mu\text{-}3,5\text{-(CF}_3)_2\text{pz})(\text{COD})]_2$, $\lambda_{\text{ex}} = 514.5$ nm, 30 mW, tetrahydrofuran solution.









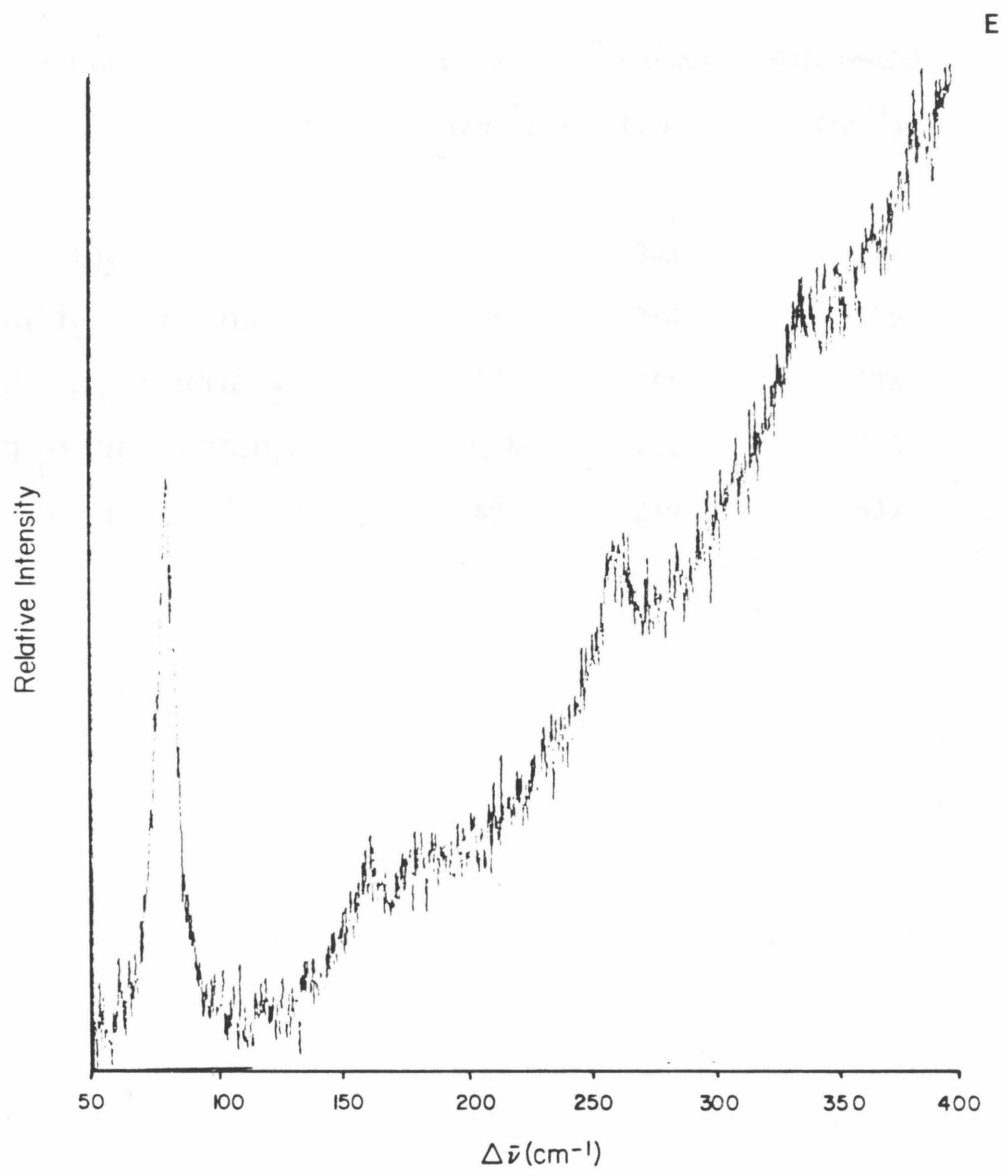


Table 2.6 Vibrational stretching frequencies measured by resonance Raman spectroscopy for pyrazolyl-bridged binuclear iridium(I) cyclooctadiene complexes.

Iridium Complex	$\nu(\text{Ir-Ir})$ (cm^{-1})	$\nu(\text{Ir-N})$ (cm^{-1})	$\nu(\text{Ir-(}\pi\text{-C=C)})$ (cm^{-1})
$[\text{Ir}(\mu\text{-pz})(\text{COD})]_2$	58	263	337
$[\text{Ir}(\mu\text{-3,5-(CH}_3)_2\text{pz})(\text{COD})]_2$	76	264	336
$[\text{Ir}(\mu\text{-3,4,5-(CH}_3)_3\text{pz})(\text{COD})]_2$	77	266	343
$[\text{Ir}(\mu\text{-3-CF}_3\text{-5-CH}_3\text{pz})(\text{COD})]_2$	76, 79	262	338
$[\text{Ir}(\mu\text{-3,5-(CF}_3)_2\text{pz})(\text{COD})]_2$	80	259	333

3,5-disubstituted-pyrazolyl-bridged complexes all have values of $\nu(\text{Ir}-\text{Ir})$ from 76 to 80 cm^{-1} , whereas the iridium-iridium stretching frequency for $[\text{Ir}(\mu\text{-pz})(\text{COD})]_2$ is at 58 cm^{-1} , consistent with the substantially longer metal-metal separation in this complex.

The spectrum of the complex $[\text{Ir}(\mu\text{-3-CF}_3\text{-5-CH}_3\text{pz})(\text{COD})]_2$ shows closely-spaced features at 76 cm^{-1} and 79 cm^{-1} that most likely correspond to the iridium-iridium stretching vibrations for the diastereomers that arise from the asymmetry in the bridging ligand.²⁰ The crystal structure of this complex is disordered with respect to CH_3/CF_3 site occupancy,³³ and this has been suggested to result from co-crystallization of the diastereomers. The electronic absorption and emission spectral properties of these isomers must be extremely similar since no unusual effects are observed in the spectra and the emission lifetime decays are all single-exponential.

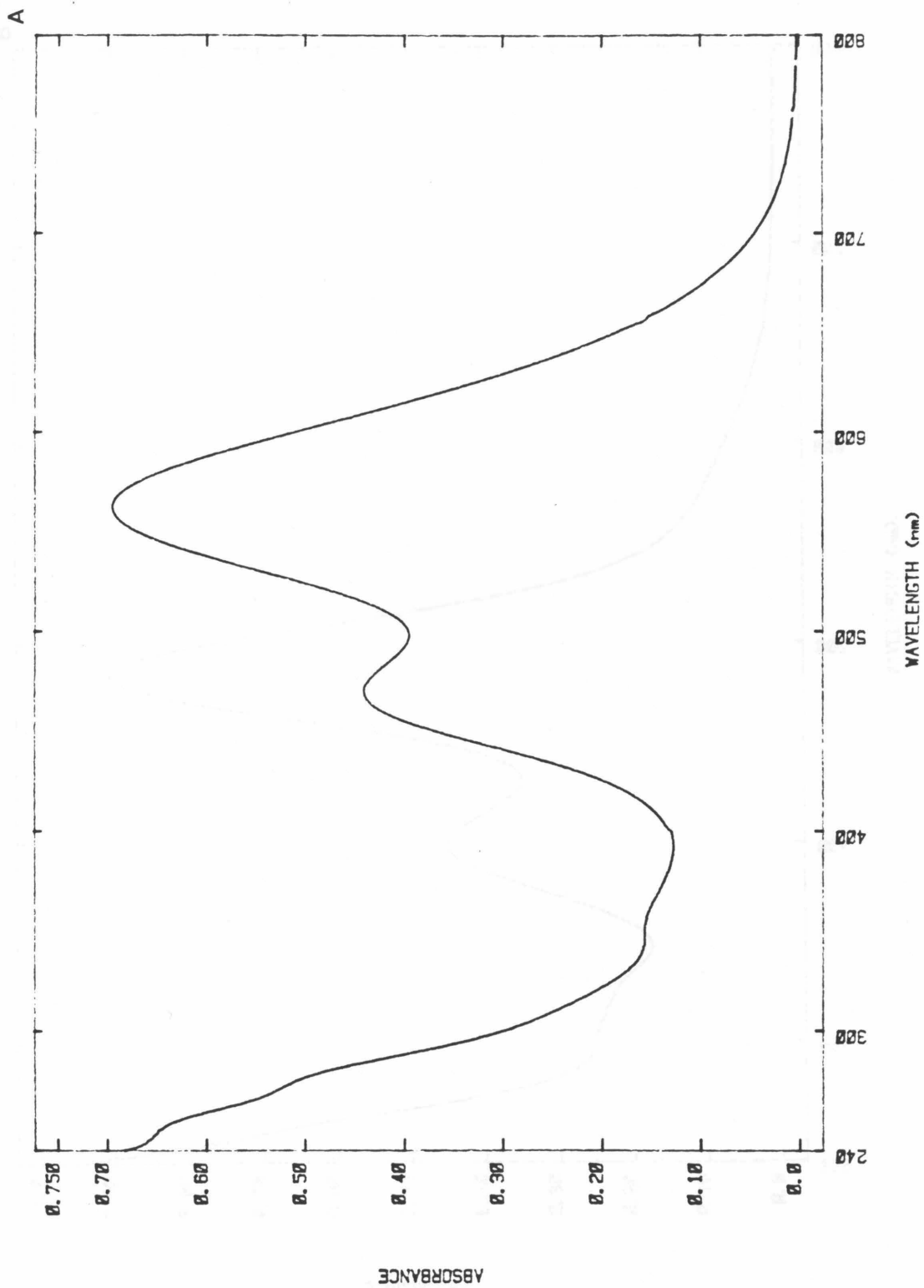
The weak feature at $\sim 2 \nu(\text{Ir}-\text{Ir})$ that is observed in the resonance Raman spectrum of each of these complexes is probably the first overtone of the iridium-iridium stretching vibration. The feature at $\sim 260 \text{ cm}^{-1}$ that is observed is assigned to the iridium-nitrogen stretching vibration, by analogy to previous studies of iridium-pyridine complexes where bands at similar frequencies in the far-infrared spectra have been assigned to the iridium-nitrogen stretching vibration.⁴⁸ Likewise, the features at $\sim 340 \text{ cm}^{-1}$ are reasonable for the iridium-alkene stretch. For example, far-infrared spectroscopic studies of $[\text{Ir}(\text{COD})(\text{Cl})]_2$ have suggested that a band at 411 cm^{-1} corresponds to the metal-alkene stretch.⁴⁹ Also, the symmetric iridium-alkene stretch for the π -bonded allyl group in $\text{Ir}(\pi\text{-C}_3\text{H}_5)_3$ has

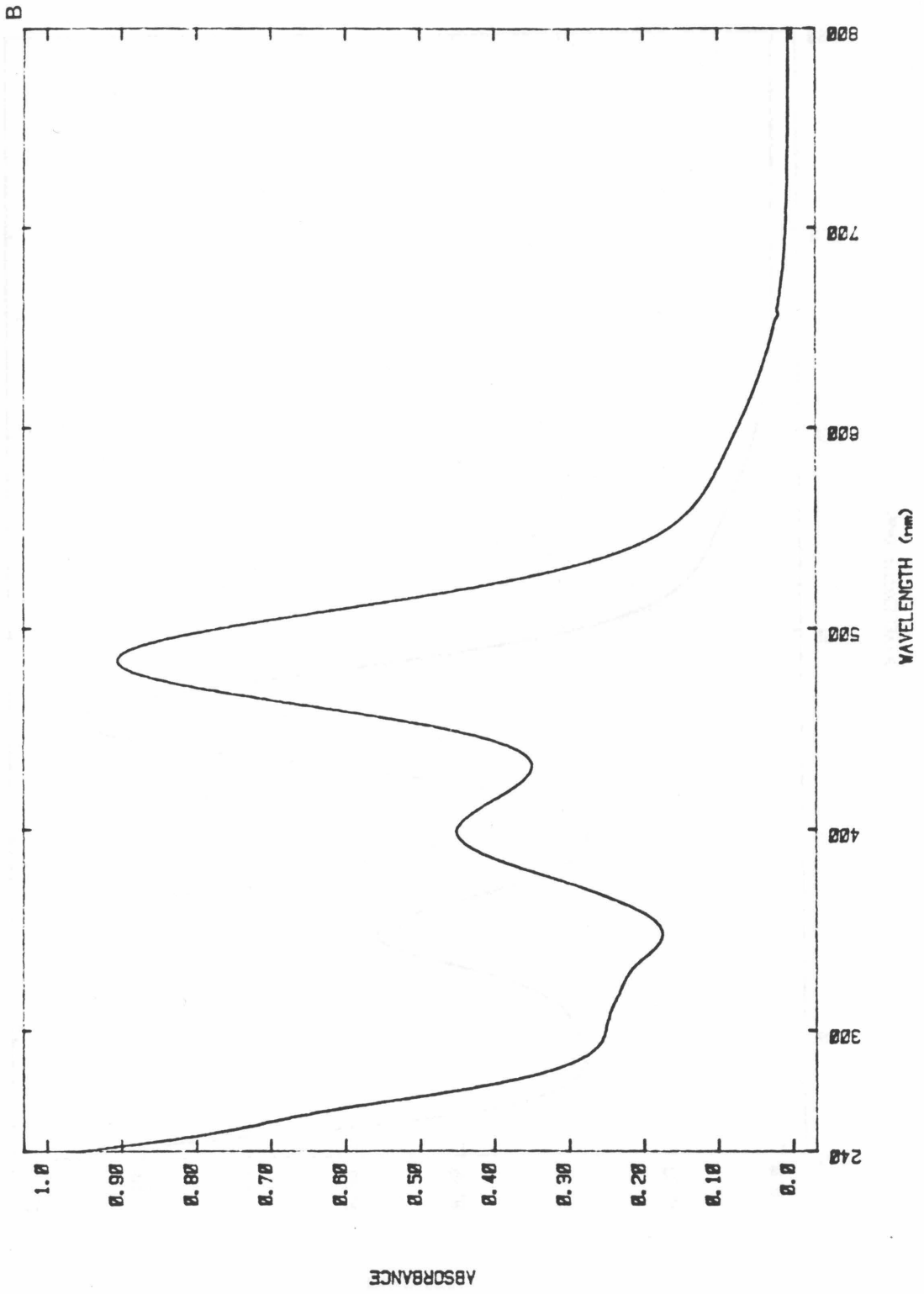
a frequency of 350 cm^{-1} , as measured by Raman spectroscopy.⁵⁰

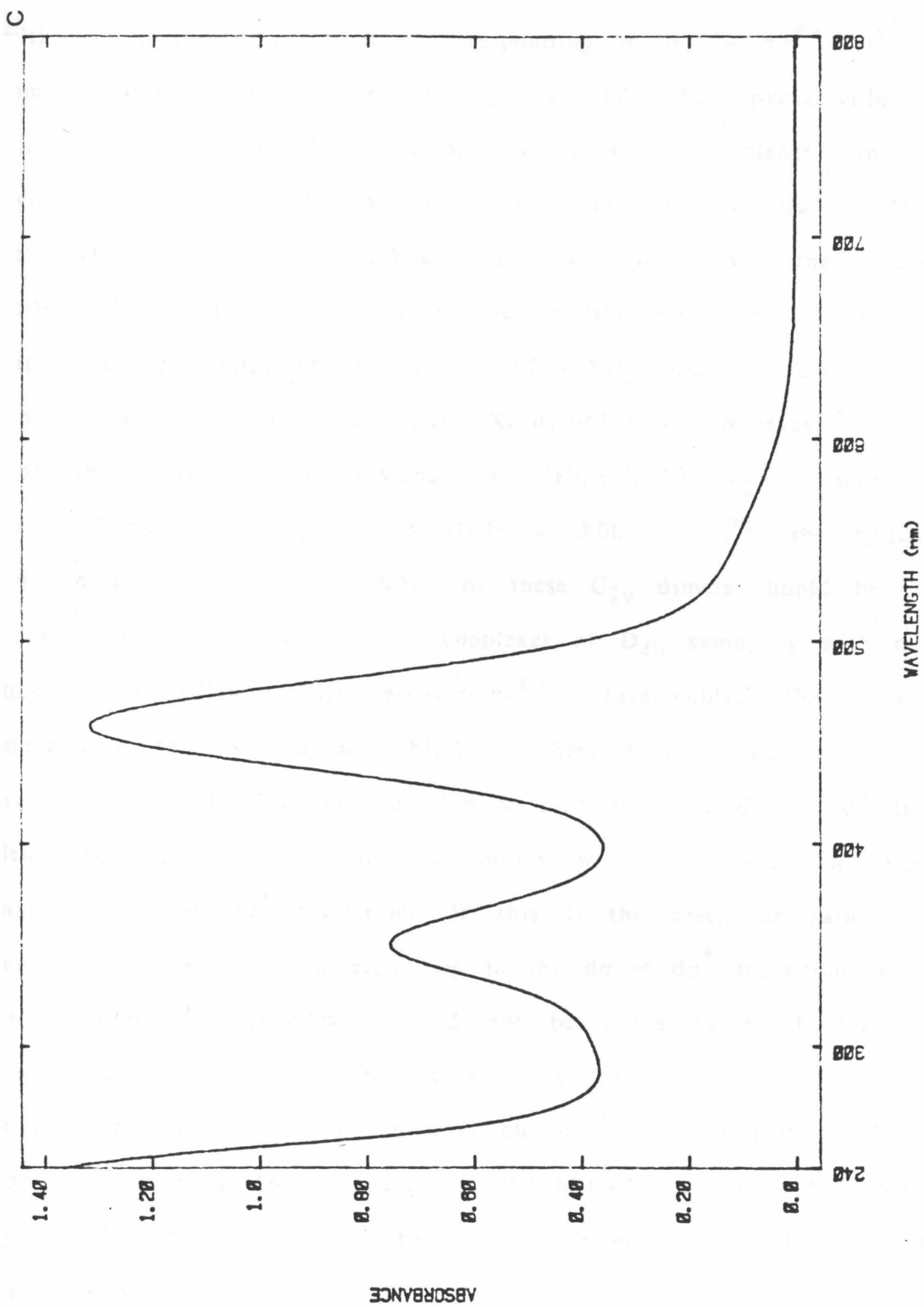
The values of $\nu(\text{Ir-Ir})$ for these iridium(I) binuclear complexes are suggestive of a weak bonding interaction in the 1A_1 ground state, as predicted from configurational mixing of the filled $a_1(d\sigma)$ and $b_2(d\sigma^*)$ orbitals with the unoccupied $a_1(p\sigma)$ and $b_2(p\sigma^*)$ orbitals. Analogous to the ground-state resonance Raman studies of $[\text{Rh}_2(\text{bridge})_4]^{2+}$ and $[\text{Pt}_2(\text{pop})_4]^{4-}$, the frequencies for the metal-metal stretching vibration of these lower-symmetry iridium dimers are less than that expected for a full metal-metal single bond⁵¹⁻⁵³ but are consistent with a weak bonding interaction. In addition, the presence of metal-ligand stretching vibrations in the resonance Raman spectra of these pyrazolyl-bridged iridium(I) cyclooctadiene complexes is consistent with the observation of the rhodium-carbon stretching vibration in the resonance Raman spectra of $[\text{Rh}_2(\text{bridge})_4]^{2+}$.⁴

As mentioned in Chapter 1, Stobart and co-workers have investigated the thermal chemistry of these pyrazolyl-bridged dimers.^{19,22,37} The complex $[\text{Ir}(\mu\text{-pz})(\text{COD})]_2$ is easily oxidized by a variety of substrates, including iodine, bromine, and chlorine, and the products of oxidative addition of X_2 are the $X\text{-Ir(II)-Ir(II)-X}$ metal-metal bonded dimers.^{19,22} The complexes $[\text{Ir}(\mu\text{-pz})(\text{COD})(\text{I})]_2$, $[\text{Ir}(\mu\text{-pz})(\text{COD})(\text{Br})]_2$, and $[\text{Ir}(\mu\text{-pz})(\text{COD})(\text{Cl})]_2$ are intensely colored, and their electronic absorption spectra are shown in Figure 2.12. The $d^8\text{-}d^8$ $[\text{Rh}_2(\text{bridge})_4]^{2+}$, $[\text{Rh}_2(\text{TMB})_4]^{2+}$, and $[\text{Ir}_2(\text{TMB})_4]^{2+}$ complexes also react thermally with iodine, bromine, and chlorine to give doubly-oxidized binuclear complexes.^{7,53,54} The $[\text{Rh}_2(\text{bridge})_4(\text{X})_2]^{2+}$, $[\text{Rh}_2(\text{TMB})_4(\text{X})_2]^{2+}$, and $[\text{Ir}_2(\text{TMB})_4(\text{X})_2]^{2+}$ complexes are also colored,

Figure 2.12 Electronic absorption spectra of (a) $[\text{Ir}(\mu\text{-pz})(\text{COD})\text{-}(\text{I})]_2$, $\epsilon(562 \text{ nm}) = 20,300 \text{ M}^{-1}\text{cm}^{-1}$, $\epsilon(470 \text{ nm}) = 12,900 \text{ M}^{-1}\text{cm}^{-1}$, tetrahydrofuran solution; (b) $[\text{Ir}(\mu\text{-pz})(\text{COD})\text{-}(\text{Br})]_2$, $\epsilon(484 \text{ nm}) = 17,000 \text{ M}^{-1}\text{cm}^{-1}$, $\epsilon(399 \text{ nm}) = 8450 \text{ M}^{-1}\text{cm}^{-1}$, tetrahydrofuran solution; (c) $[\text{Ir}(\mu\text{-pz})(\text{COD})\text{-}(\text{Cl})]_2$, $\epsilon(458 \text{ nm}) = 15,100 \text{ M}^{-1}\text{cm}^{-1}$, $\epsilon(351 \text{ nm}) = 8670 \text{ M}^{-1}\text{cm}^{-1}$, tetrahydrofuran solution.







and the two bands in the absorption spectra of these dihalide complexes have been assigned to $d\sigma \rightarrow d\sigma^*$ and $d\pi \rightarrow d\sigma^*$ transitions, with the higher-energy feature corresponding to $d\sigma \rightarrow d\sigma^*$.^{7,53,54} In some respects, the absorption spectra of the pyrazolyl-bridged iridium(II) dimers resemble the spectra of these complexes. In particular, the two broad features in the absorption spectra of $[\text{Ir}(\mu\text{-pz})(\text{COD})(\text{X})]_2$ ($\text{X} = \text{I}, \text{Br}, \text{Cl}$) shift to lower energy with the reducing ability of the halogen. However, the relative intensities of the two bands in the spectra of the $[\text{Ir}(\mu\text{-pz})(\text{COD})(\text{X})]_2$ complexes are reversed from those of the higher-symmetry X-M(II)-M(II)-X complexes.⁵³ Given that the iridium-iridium distance in $[\text{Ir}(\mu\text{-pz})(\text{COD})(\text{I})]_2$ is long for an iridium-iridium single bond ($\text{Ir-Ir} = 3.085(3) \text{ \AA}$),²² the splitting between the $d\sigma$ and $d\sigma^*$ orbitals of these C_{2v} dimers should be considerably less than that for the complexes of D_{4h} symmetry with more "normal" metal(II)-metal(II) separations.⁵³ Presumably, the relative energies of the $d\pi$ and $d\sigma$ orbitals of these dimers could be reversed from those of the "face-to-face" dimers, such that the $d\sigma \rightarrow d\sigma^*$ transition in the pyrazolyl-bridged complexes would be lower in energy than the $d\pi \rightarrow d\sigma^*$ transition. If this is the case, the rather low energies for the bands corresponding to the $d\sigma \rightarrow d\sigma^*$ transition in the $[\text{Ir}(\mu\text{-pz})(\text{COD})(\text{X})]_2$ complexes would not be unreasonable. Furthermore, this metal-metal localized transition is expected to be substantially mixed with the axial ligand-to-metal charge transfer transition ($\text{L}\sigma \rightarrow d\sigma^*$), as observed for the D_{4h} X-M(II)-M(II)-X complexes,^{7,53} which agrees with the shift of this band to higher energy with less reducing halide ligands.

Several other observations, related to the studies of the pyrazolyl-bridged iridium(I) dimers outlined above, deserve mention. The rhodium analogue of $[\text{Ir}(\mu\text{-pz})(\text{COD})]_2$ was originally prepared by Trofimenko in 1971,⁵⁵ and an X-ray crystal structure determination of this complex was recently completed by Stobart and co-workers.³³ Interestingly, $[\text{Rh}(\mu\text{-pz})(\text{COD})]_2$ adopts the same conformation as $[\text{Ir}(\mu\text{-pz})(\text{COD})]_2$, with a rhodium-rhodium separation of 3.267(2) Å. In contrast to the iridium dimers, the rhodium analogue is lemon-yellow. The electronic absorption spectrum of $[\text{Rh}(\mu\text{-pz})(\text{COD})]_2$ in benzene solution is shown in Figure 2.13. While the iridium dimers are luminescent in fluid solution at ambient temperature from both singlet and triplet excited states, $[\text{Rh}(\mu\text{-pz})(\text{COD})]_2$ is not emissive at ambient temperature. This complex is luminescent at 77 K in a 2-methyltetrahydrofuran glass, but the emission is broad, as shown in Figure 2.14, and bears no similarity to that observed at 77 K for any of the pyrazolyl-bridged iridium dimers. Presumably the metal-metal interactions in the analogous ground and excited states of $[\text{Rh}(\mu\text{-pz})(\text{COD})]_2$ are not as strong as those of the iridium complex because of the smaller radial extension of the valence orbitals of rhodium relative to iridium. This is consistent with the very different spectral properties of the pyrazolyl-bridged dirhodium(I) complex and the pyrazolyl-bridged diiridium(I) complexes.

In summary, the pyrazolyl-bridged iridium(I) cyclooctadiene complexes appear to have the same types of metal-metal interactions in the ground and low-energy excited states as those documented for the $d^8\text{-}d^8$ binuclear rhodium(I), iridium(I), and platinum(II) complexes.

Figure 2.13 Electronic absorption spectrum of $[\text{Rh}(\mu\text{-pz})(\text{COD})]_2$
(benzene solution, $22 \pm 2^\circ\text{C}$).

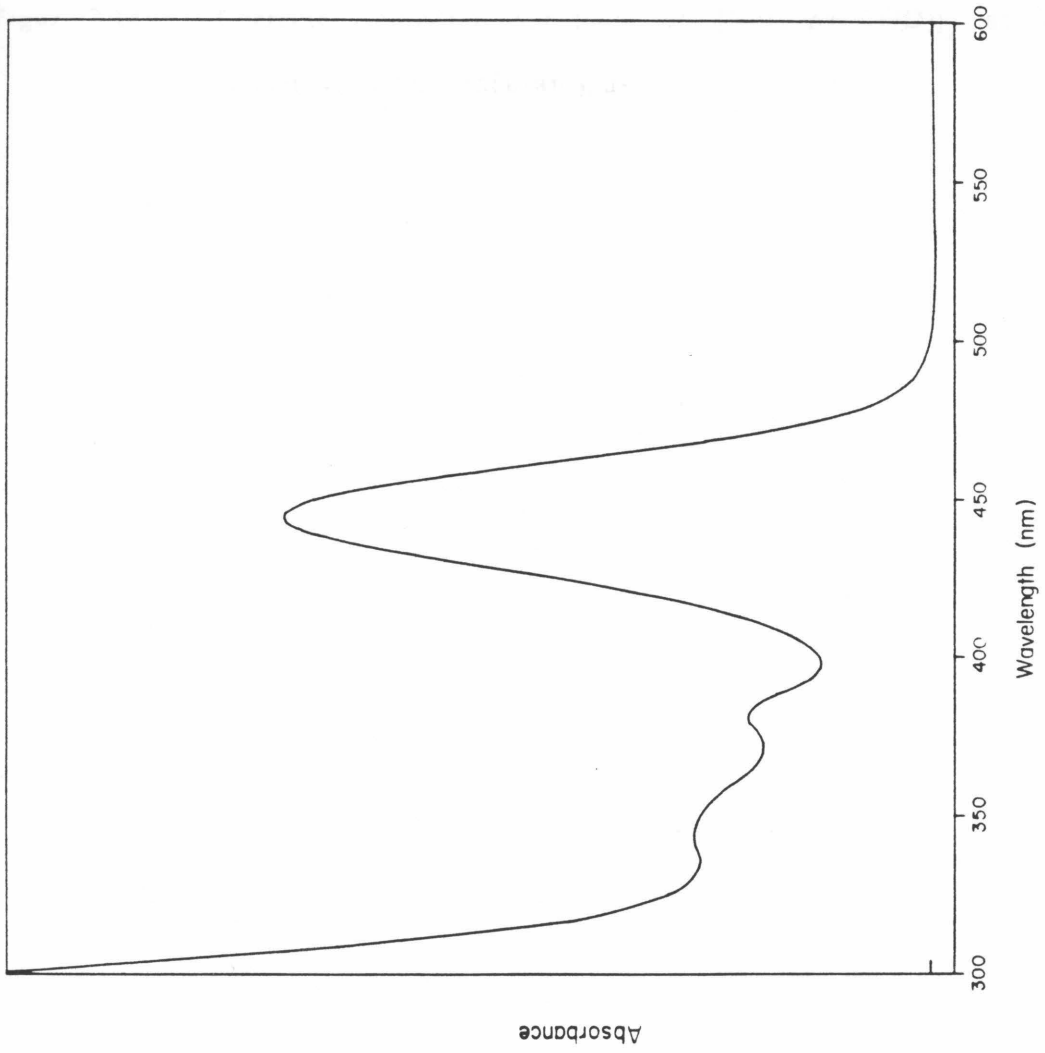
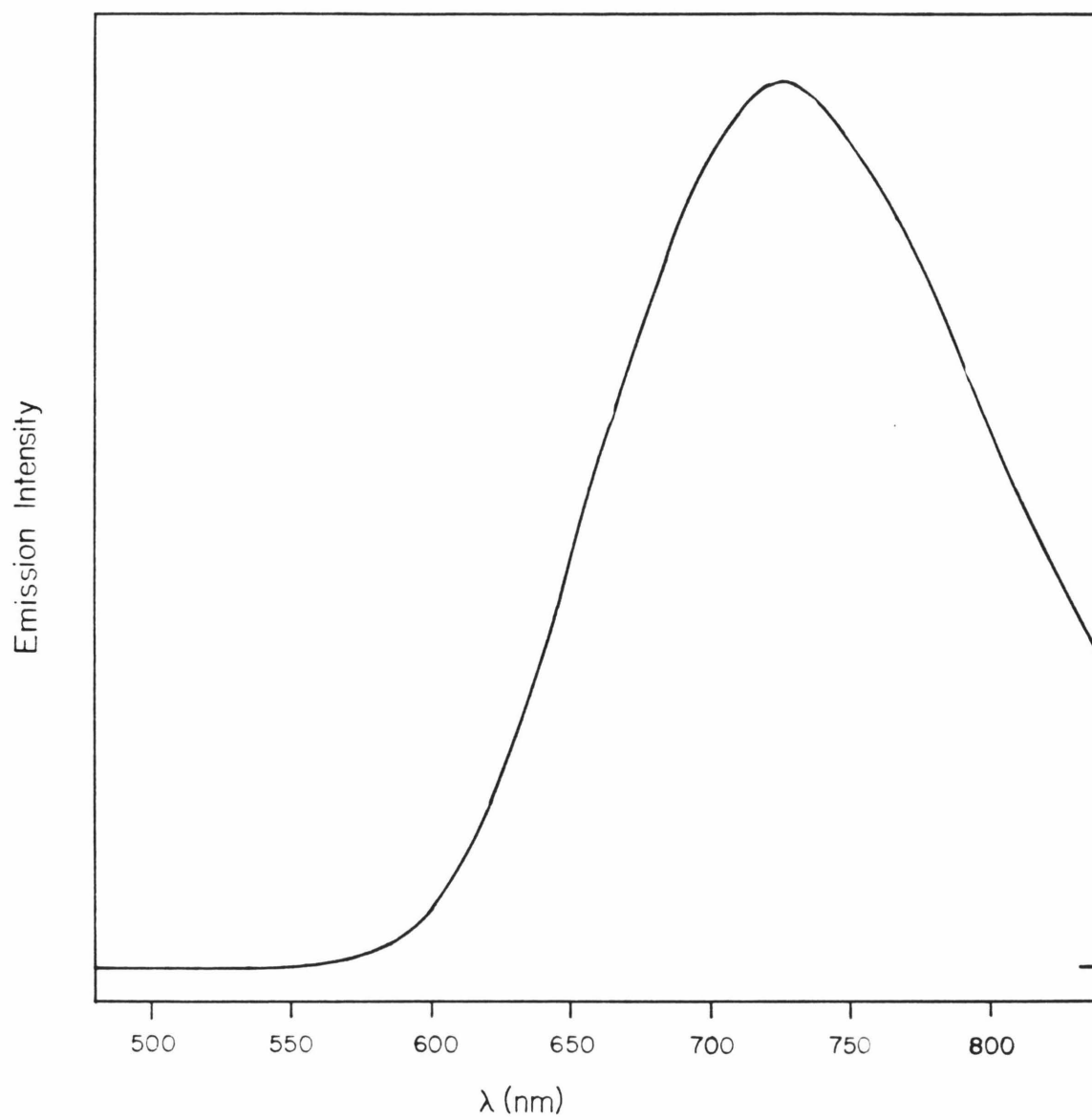


Figure 2.14 Corrected emission spectrum of $[\text{Rh}(\mu\text{-pz})(\text{COD})]_2$ at 77 K (2-methyltetrahydrofuran glass).



Even though the symmetry of the pyrazolyl-bridged iridium complexes (C_{2v}) is much lower than that of the "face-to-face" binuclear complexes (D_{4h}), the same metal-metal bonding interactions adequately describe the electronic absorption and emission spectral and photo-physical properties of these complexes. Analogous to studies for two of the higher-symmetry binuclear complexes, ground-state resonance Raman studies of the pyrazolyl-bridged iridium(I) dimers suggest the presence of a reasonable metal-metal bonding interaction in the formally nonbonded binuclear center.

Because of the unique shape of these dimers, the metal-metal interaction has both a distance and an angular dependence, as has been observed from comparisons of the absorption and emission spectra of the unsubstituted-pyrazolyl-bridged and the 3,5-disubstituted-pyrazolyl-bridged iridium(I) cyclooctadiene complexes. The energies of the $^1A_1 \rightarrow ^{1,3}B_2$ ($d\sigma^* \rightarrow p\sigma$) absorption and $^{1,3}B_2 \rightarrow ^1A_1$ ($p\sigma \rightarrow d\sigma^*$) emission bands of these five complexes appear to be largely determined by the metal-metal separation, as expected for predominantly metal-metal localized transitions. Interestingly, several of the photo-physical properties seem to be strongly influenced by the substituents on the pyrazolyl bridge. The complexes that contain substituted-pyrazolyl ligands all have shorter lifetimes and lower quantum yields for phosphorescence than $[Ir(\mu\text{-pz})(COD)]_2$. Furthermore, the two complexes with trifluoromethyl-substituted-pyrazolyl ligands have considerably lower ambient-temperature lifetimes and quantum yields for the $^3B_2(d\sigma^* p\sigma)$ excited state than either the unsubstituted or exclusively methyl-substituted-pyrazolyl complexes. This suggests that the

trifluoromethyl group influences the deactivation of the ${}^3B_2(d\sigma^* p\sigma)$ excited state. Certainly, these pyrazolyl-bridged iridium(I) complexes are ideally suited to a study of ligand effects on the properties of the $(d\sigma^* p\sigma)$ excited states since a variety of substituted-pyrazolyl-bridged iridium(I) complexes are easily prepared.²⁰

References and Notes

1. Mann, K.R.; Gray, H.B. *Adv. Chem. Ser.* 1979, 173, 225-235.
2. Rice, S.F.; Milder, S.J.; Gray, H.B.; Goldbeck, R.A.; Kliger, D.S. *Coord. Chem. Rev.* 1982, 43, 349-354.
3. Rice, S.F.; Gray, H.B. *J. Am. Chem. Soc.* 1981, 103, 1593-1595.
4. Dallinger, R.F.; Miskowski, V.M.; Gray, H.B.; Woodruff, W.H. *J. Am. Chem. Soc.* 1981, 103, 1595-1596.
5. Rice, S.F.; Gray, H.B. *J. Am. Chem. Soc.* 1983, 105, 4571-4575.
6. Che, C.-M.; Butler, L.G.; Gray, H.B.; Crooks, R.M.; Woodruff, W.H. *J. Am. Chem. Soc.* 1983, 105, 5492-5494.
7. Smith, T.P. Ph.D. Dissertation, California Institute of Technology, Pasadena, 1982.
8. Rice, S.F. Ph.D. Dissertation, California Institute of Technology, Pasadena, 1982.
9. Mann, K.R.; Thich, J.A.; Bell, R.A.; Coyle, C.L.; Gray, H.B. *Inorg. Chem.* 1980, 19, 2462-2468.
10. Miskowski, V.M.; Nobinger, G.L.; Kliger, D.S.; Hammond, G.S.; Lewis, N.S.; Mann, K.R.; Gray, H.B. *J. Am. Chem. Soc.* 1978, 100, 485-488.
11. Sperline, R.P.; Dickson, M.K.; Roundhill, D.M. *J. Chem. Soc., Chem. Commun.* 1977, 62-63.
12. Fordyce, W.A.; Brummer, J.G.; Crosby, G.A. *J. Am. Chem. Soc.* 1981, 103, 7061-7064.
13. Che, C.-M.; Butler, L.S.; Gray, H.B. *J. Am. Chem. Soc.* 1981, 103, 7796-7797.

14. Parker, W.L.; Crosby, G.A. *Chem. Phys. Lett.* **1984**, *105*, 544-546.
15. Nocera, D.G.; Maverick, A.W.; Winkler, J.R.; Che, C.-M.; Gray, H.B. *ACS Symp. Ser.* **1983**, *211*, 21-33.
16. Wiley, R.H.; Hexner, P.E. *Org. Syn.* **1951**, *31*, 43-44.
17. Herde, J.L.; Lambert, J.C.; Senoff, C.V. *Inorg. Syn.* **1974**, *15*, 18-20.
18. Atwood, J.L.; Beveridge, K.A.; Bushnell, G.W.; Dixon, K.R.; Eadie, D.T.; Stobart, S.R.; Zaworotko, M.J. *Inorg. Chem.* **1984**, *23*, 4050-4057.
19. Beveridge, K.A.; Bushnell, G.W.; Dixon, K.R.; Eadie, D.T.; Stobart, S.R.; Atwood, J.L. Zaworotko, M.J. *J. Am. Chem. Soc.* **1982**, *104*, 920-922.
20. Bushnell, G.W.; Fjeldsted, D.O.K.; Stobart, S.R.; Zaworotko, M.J.; Knox, S.A.R.; Macpherson, K.A. *Organometallics* **1985**, *4*, 1107-1114.
21. Coleman, A.W.; Eadie, D.T.; Stobart, S.R.; Zaworotko, M.J.; Atwood, J.L. *J. Am. Chem. Soc.* **1982**, *104*, 922-923.
22. Stobart, S.R.; Coleman, A.W.; Harrison, D.G.; Atwood, J.L.; Zaworotko, M.J. *J. Am. Chem. Soc.*, submitted.
23. Caspar, J.V.; Gray, H.B. *J. Am. Chem. Soc.* **1984**, *106*, 3029-3030.
24. Gordon, A.J.; Ford, R.A. "The Chemist's Companion"; John Wiley and Sons: New York, 1972; p 436.
25. Demas, J.N.; Crosby, G.A. *J. Phys. Chem.* **1971**, *75*, 991-1024.
26. Caspar, J.V.; Meyer, T.J. *J. Am. Chem. Soc.* **1983**, *105*, 5583-5590.
27. Parker, C.A.; Rees, W.T. *Analyst* **1960**, *85*, 587-600.
28. Nocera, D.G.; Winkler, J.R.; Yocom, K.M.; Bordignon, E.; Gray, H.B. *J. Am. Chem. Soc.* **1984**, *106*, 5145-5150.

29. Powell, J.; Kuksis, A.; Nyburg, S.C.; Ng, W.W. *Inorg. Chim. Acta* 1982, 64, L211-L212.
30. Nussbaum, S.; Rettig, S.J.; Storr, A.; Trotter, J. *Can. J. Chem.* 1985, 63, 692-702.
31. Uson Lacal, R.; Oro Giral, L.A.; Ciriano Lopez, M.A.; Pinillos, M.T.; Royo Macia, M.; Pastor Martinez, E. Spanish Patent ES 497,900, 1981; *Chem. Abstr.* 1982, 97, 55306n.
32. Bushnell, G.W.; Fjeldsted, D.O.K.; Stobart, S.R.; Zaworotko, M.J. *J. Chem. Soc., Chem. Commun.* 1983, 580-581.
33. Beveridge, K.A.; Bushnell, G.W.; Stobart, S.R.; Atwood, J.L.; Zaworotko, M.J. *Organometallics* 1983, 2, 1447-1451.
34. Bushnell, G.W.; Stobart, S.R.; Vefghi, R.; Zaworotko, M.J. *J. Chem. Soc., Chem. Commun.* 1984, 282-284.
35. Fjeldsted, D.O.K.; Stobart, S.R.; Zaworotko, M.J. *J. Am. Chem. Soc.* 1985, 107, 8258-8259.
36. Fjeldsted, D.O.K.; Stobart, S.R. *J. Chem. Soc., Chem. Commun.* 1985, 908-909.
37. Bushnell, G.W.; Decker, M.J.; Eadie, D.T.; Stobart, S.R.; Vefghi, R.; Atwood, J.L.; Zaworotko, M.J. *Organometallics* 1985, 4, 2106-2111.
38. Harrison, D.G.; Stobart, S.R. *J. Chem. Soc., Chem. Commun.* 1986, 285-286.
39. Hoffman, D.M.; Hoffman, R. *Inorg. Chem.* 1981, 20, 3543-3555 and references therein.
40. The absorption spectra of these complexes are the same in a variety of solvents. An additional band is observed at 227 nm for

the pyrazolyl-bridged complex and at ~ 236 nm for the substituted-pyrazolyl-bridged complexes in solvents with low UV absorption, such as cyclohexane.

41. The emission spectra of these complexes are the same in solvents such as acetonitrile, cyclohexane, benzene, and 2-methyltetrahydrofuran.
42. Winkler, J.R.; Marshall, J.L.; Netzel, T.L.; Gray, H.B. *J. Am. Chem. Soc.* **1986**, *108*, 2263-2266.
43. Milder, S.J. *Inorg. Chem.* **1985**, *24*, 3376-3378.
44. Turro, N.J. "Modern Molecular Photochemistry"; Benjamin/Cummings: Menlo Park, California, 1978; pp 146-148.
45. Birks, J.B. "Photophysics of Aromatic Molecules"; John Wiley and Sons: New York, 1970; pp 372-402.
46. Parker, C.A. *Adv. Photochem.* **1964**, *2*, 305-383.
47. The Raman spectrum of tetrahydrofuran has a very weak band at ~ 280 cm^{-1} (Strommen, D.P.; Nakamoto, K. "Laboratory Raman Spectroscopy"; John Wiley and Sons: New York, 1984; p 117).
48. Clark, R.J.H.; Williams, C.S. *Inorg. Chem.* **1965**, *4*, 350-357.
49. Bennett, M.A.; Clark, R.J.H.; Milner, D.L. *Inorg. Chem.* **1967**, *6*, 1647-1652.
50. Andrews, D.C.; Davidson, G. *J. Organomet. Chem.* **1973**, *55*, 383-393.
51. Quicksall, C.O.; Spiro, T.G. *Inorg. Chem.* **1969**, *8*, 2011-2013.
52. Shriver, D.F.; Cooper, C.B., III *Adv. Infrared Raman Spectrosc.* **1980**, *6*, 127-156.
53. Miskowski, V.M.; Smith, T.P.; Loehr, T.M.; Gray, H.B. *J. Am. Chem. Soc.* **1985**, *107*, 7925-7934.

54. Lewis, N.S.; Mann, K.R.; Gordon, J.G., II; Gray, H.B. *J. Am. Chem. Soc.* 1976, 98, 7461-7463.
55. Trofimenko, S. *Inorg. Chem.* 1971, 7, 1372-1376.

Chapter 3
Electron-Transfer Reactivity of the ${}^3B_2(d\sigma^* p\sigma)$ Excited State of
 $[\text{Ir}(\mu\text{-pz})(\text{COD})]_2$

Introduction

An electronic excited state of a transition metal complex that is sufficiently long-lived to be in thermal equilibrium with its surroundings is a new species with chemical and physical properties that can be quite different from those of the ground state. In particular, the increased electron affinity and decreased ionization potential of an excited state relative to the ground state lead to the prediction that an excited state should be a better oxidant and reductant than the corresponding ground state.^{1,2} Consequently, excited-state complexes that have lifetimes of at least 0.1 to 1 ns in fluid solution can participate in bimolecular electron-transfer reactions with appropriate electron donors and acceptors.^{3,4}

Research in photoinduced electron-transfer reactions of inorganic complexes includes studies aimed at developing and understanding the theoretical aspects of electron-transfer reactions,⁵⁻⁹ in addition to work concerning the photochemical conversion and storage of solar energy.¹⁰⁻¹² Along these lines, extensive investigations of the electron-transfer reactivity of the excited states of $[\text{Ru}(\text{bpy})_3]^{2+}$ (bpy = 2,2'-bipyridine) and related ruthenium(II) polypyridyl complexes,¹³⁻¹⁷ osmium (II) polypyridyl complexes,¹⁸ $[\text{Cr}(\text{bpy})_3]^{3+}$ (bpy = 2,2'-bipyridine),^{1,19} and $[\text{Re}_2\text{Cl}_8]^{2-}$ ^{20,21} have been reported. Clearly, fundamental studies of this type are important in understanding the factors that govern homogeneous electron transfer and may lead to systems in which the excited states of inorganic complexes are employed in energy conversion and storage processes.

The relatively long lifetime of the ${}^3B_2(d\sigma^* p\sigma)$ excited state of $[Ir(\mu\text{-pz})(COD)]_2$ (pzH = pyrazole, COD = 1,5-cyclooctadiene) in fluid solution suggests that it should be able to participate in bimolecular electron-transfer reactions with suitable electron acceptors or donors. In light of the favorable absorption and emission properties of this complex, we have been interested in examining the possibilities for the conversion of visible light to net chemical energy through a photoinduced electron-transfer process. In addition, we have been interested in examining the electron-transfer reactivity of this excited state in the context of classical Marcus theory predictions for outer-sphere electron transfer. The results of our efforts toward these goals are reported herein.

Experimental

Syntheses

Materials.

Acetone (EM Science), absolute ethanol (U.S. Industrial), 1,2-dichloroethane (Burdick and Jackson), methanol (Baker), diethyl ether (Baker), and N,N-dimethylacetamide (Aldrich) were reagent grade or better and used without further purification. Potassium hexafluorophosphate (Aldrich, 98%), ammonium hexafluorophosphate (Ozark-Mahoning), iodomethane (Aldrich, 99%), iodoethane (Aldrich, 99%), benzyl chloride (Aldrich, 97%), and dimethyl sulfate (MCB, 98%) were used as received. 4-Cyanopyridine (Aldrich, 98%), methyl isonicotinate (Aldrich, 98%), isonicotinamide (Aldrich, 99%), nicotinamide (Aldrich, 98%), pyridine (Burdick and Jackson), 2-methoxypyridine (Aldrich, 98%), 4-picoline (Aldrich, 98%), 4-*tert*-butylpyridine (Aldrich, 99%), 2,6-lutidine (Kodak), 2,3,6-collidine (ICN Pharmaceuticals), 2,4,6-collidine (Aldrich, 99+%), 2,6-dimethyl- γ -pyrone (Aldrich, 99%), sodium iodide (Baker), methylamine (Aldrich, 40 wt. % solution in water), and methyl viologen dichloride hydrate (Aldrich) were used as received.

Pyridinium Hexafluorophosphates.

The general method outlined below was used for the preparation of the pyridinium hexafluorophosphates, except where noted. Approximately 3-5 g of pyridine or substituted pyridine and a 4-fold molar excess of alkylating agent were dissolved in 80-100 mL of a 1:1 (v/v) acetone/ethanol solution. The mixture was refluxed from 4 - 24 h,

depending upon the difficulty of alkylation. Often the pyridinium halide would precipitate during the reaction or upon cooling, but if not, the solvents were removed on a rotary evaporator. The halide salt was isolated and dissolved in a minimum of water. A filtered, saturated, aqueous solution of either potassium hexafluorophosphate or ammonium hexafluorophosphate was added, with stirring, to precipitate the pyridinium hexafluorophosphate. This salt was filtered, washed well with water, and recrystallized from a 2:1:1 (v/v/v) water/acetone/ethanol solution to give a white, crystalline solid. The yields of the pyridinium hexafluorophosphates varied from 20-80%. The ^1H NMR spectra of the pyridinium hexafluorophosphates in acetone- d_6 agree with related data reported in the literature.^{2,2,23}

4-Cyano-N-methylpyridinium hexafluorophosphate (1) was synthesized from 4-cyanopyridine and iodomethane by the above general procedure. Anal. Calcd for $\text{C}_7\text{H}_7\text{N}_2\text{PF}_6$: C, 31.83; H, 2.67; N, 10.61. Found: C, 31.84; H, 2.67; N, 10.63. ^1H NMR (acetone- d_6): δ 9.43 (d, 2 H, 2,6-H), 8.60-8.80 (m, 2 H, 3,5-H), 4.77 (s, 3 H, CH_3).

4-Carbomethoxy-N-methylpyridinium hexafluorophosphate (2) was synthesized from methyl isonicotinate and iodomethane by the above general procedure. Anal. Calcd for $\text{C}_8\text{H}_{10}\text{NO}_2\text{PF}_6$: C, 32.34; H, 3.39; N, 4.71. Found: C, 32.32; H, 3.38; N, 4.72. ^1H NMR (acetone- d_6): δ 9.33 (d, 2 H, 2,6-H), 8.55-8.75 (m, 2 H, 3,5-H), 4.73 (s, 3 H, NCH_3), 4.07 (s, 3 H, COOCH_3).

4-Amido-N-ethylpyridinium hexafluorophosphate (3) was synthesized from isonicotinamide and iodoethane by the above general procedure. Anal. Calcd for $\text{C}_8\text{H}_{11}\text{N}_2\text{OPF}_6$: C, 32.45; H, 3.74; N, 9.46. Found: C,

32.45; H, 3.73; N, 9.47. ^1H NMR (acetone- d_6): δ 9.33 (d, 2 H, 2,6-H), 8.50-8.67 (m, 2 H, 3,5-H), 4.97 (q, 2 H, CH_2), 1.80 (t, 3 H, CH_3), unable to locate the resonance for the amide protons.

3-Amido-N-benzylpyridinium hexafluorophosphate was (4) synthesized from nicotinamide and benzyl chloride by the above general procedure. Anal. Calcd for $\text{C}_{13}\text{H}_{13}\text{N}_2\text{OPF}_6$: C, 43.59; H, 3.66; N, 7.82. Found: C, 43.61; H, 3.67; N, 7.82. ^1H NMR (acetone- d_6): δ 9.63 (s, 1 H, 2-H), 9.03-9.37 (m, 2 H, 4,6-H), 8.40 (dd, 1 H, 5-H), 7.43-7.77 (m, 5 H, C_6H_5), 6.13 (s, 2 H, CH_2), unable to locate the resonance for the amide protons.

3-Amido-N-methylpyridinium hexafluorophosphate (5) was synthesized from nicotinamide and iodomethane by the above general procedure. Anal. Calcd for $\text{C}_7\text{H}_9\text{N}_2\text{OPF}_6$: C, 29.80; H, 3.22; N, 9.93. Found: C, 29.85; H, 3.23; N, 9.94. ^1H NMR (acetone- d_6): δ 9.50 (s, 1 H, 2-H), 9.00-9.23 (m, 2 H, 4,6-H), 8.33 (dd, 1 H, 5-H), 4.67 (s, 3 H, CH_3), broad resonances at 7.30-8.10 for the amide protons.

N-Ethylpyridinium hexafluorophosphate (6) was synthesized from pyridine and iodoethane by the above general procedure. Anal. Calcd for $\text{C}_7\text{H}_{10}\text{NPF}_6$: C, 33.21; H, 3.98; N, 5.53. Found: C, 33.25; H, 3.90; N, 5.49. ^1H NMR (acetone- d_6): δ 9.13 (d, 2 H, 2,6-H), 8.73 (t, 1 H, 4-H), 8.13-8.40 (m, 2 H, 3,5-H), 4.85 (q, 2 H, CH_2), 1.75 (t, 3 H, CH_3).

2-Methoxy-N-methylpyridinium hexafluorophosphate (7) was synthesized using a slight modification of a published procedure^{2,4} from 2-methoxypyridine and dimethyl sulfate instead of methyl fluorosulfonate. The pyridinium methyl sulfate salt was dissolved in a minimum

of water and metathesized to the hexafluorophosphate by addition of a filtered, saturated, aqueous solution of ammonium hexafluorophosphate. The precipitated pyridinium hexafluorophosphate was filtered, washed well with water, and recrystallized from a 2:1:1 (v/v/v) water/acetone/ethanol solution. Anal. Calcd for $C_7H_{10}NOPF_6$: C, 31.24; H, 3.75; N, 5.20. Found: C, 31.23; H, 3.69; N, 5.22. 1H NMR (acetone- d_6): δ 8.43-8.70 (m, 2 H, 3,6-H), 7.50-7.87 (m, 2 H, 4,5-H), 4.40 (s, 3 H, OCH_3), 4.20 (s, 3 H, NCH_3).

4-Methyl-N-methylpyridinium hexafluorophosphate (8) was synthesized from 4-picoline and iodomethane by the above general procedure. Anal. Calcd for $C_7H_{10}NPF_6$: C, 33.21; H, 3.98; N, 5.53. Found: C, 33.26; H, 3.96; N, 5.52. 1H NMR (acetone- d_6): δ 8.83 (d, 2 H, 2,6-H), 8.03 (d, 2 H, 3,5-H), 4.50 (s, 3 H, NCH_3), 2.73 (s, 3 H, 4- CH_3).

4-*tert*-Butyl-N-ethylpyridinium hexafluorophosphate (9) was synthesized from 4-*tert*-butylpyridine and iodoethane by the above general procedure. Anal. Calcd for $C_{11}H_{18}NPF_6$: C, 42.73; H, 5.87; N, 4.53. Found: C, 42.63; H, 5.74; N, 4.47. 1H NMR (acetone, d_6): δ 9.02 (d, 2 H, 2,6-H), 8.28 (d, 2 H, 3,5-H), 4.72 (q, 2 H, CH_2), 1.72 (t, 3 H, NCH_2CH_3), 1.40 (s, 9 H, $C(CH_3)_3$).

2,6-Dimethyl-N-methylpyridinium hexafluorophosphate (10) was synthesized from 2,6-lutidine and iodomethane by the above general procedure. Anal. Calcd for $C_8H_{12}NPF_6$: C, 35.97; H, 4.53; N, 5.24. Found: C, 35.84; H, 4.41; N, 5.23. 1H NMR (acetone- d_6): δ 8.40 (t, 1 H, 4-H), 7.93 (d, 2 H, 3,5-H), 4.30 (s, 3 H, NCH_3), 2.97 (s, 6 H, 2,6- CH_3).

2,3,6-Trimethyl-N-methylpyridinium hexafluorophosphate (11) was

synthesized from 2,3,6-collidine and iodomethane by the above general procedure. Anal. Calcd for $C_9H_{14}NPF_6$: C, 38.44; H, 5.02; N, 4.98. Found: C, 38.45; H, 4.97; N, 4.98. 1H NMR (acetone- d_6): δ 8.23 (d, 1 H, 4-H), 7.77 (d, 1 H, 5-H), 4.25 (s, 3 H, NCH_3), 2.88 (s, 3 H, 2- CH_3 or 6- CH_3), 2.82 (s, 3 H, 2- CH_3 or 6- CH_3), 2.55 (s, 3 H, 3- CH_3).

2,4,6-Trimethyl-N-methylpyridinium hexafluorophosphate (12) was synthesized from 2,4,6-collidine and iodomethane by the above general procedure. Anal. Calcd for $C_9H_{14}NPF_6$: C, 38.44; H, 5.02; N, 4.98. Found: C, 38.67; H, 4.89; N, 4.95. 1H NMR (acetone- d_6): δ 7.78 (s, 2 H, 3,5-H), 4.20 (s, 3 H, NCH_3), 2.90 (s, 6 H, 2,6- CH_3), 2.60 (s, 3 H, 4- CH_3).

2,6-Dimethyl-4-methoxy-N-methylpyridinium hexafluorophosphate (13) was prepared by treating an aqueous solution of 2,6-dimethyl-4-methoxy-N-methylpyridinium iodide, synthesized by the method of King and Ozog,²⁵ with a filtered, saturated, aqueous solution of ammonium hexafluorophosphate. The precipitated 2,6-dimethyl-4-methoxy-N-methylpyridinium hexafluorophosphate was filtered, washed well with water, and recrystallized from a 2:1:1 (v/v/v) water/acetone/ethanol solution. Anal. Calcd for $C_9H_{14}NOPF_6$: C, 36.37; H, 4.75; N, 4.71. Found: C, 36.45; H, 4.74; N, 4.72. 1H NMR (acetone- d_6): δ 7.45 (s, 2 H, 3,5-H), 4.25 (s, 3 H, NCH_3 or OCH_3), 4.20 (s, 3 H, NCH_3 or OCH_3), 2.85 (s, 6 H, 2,6- CH_3).

Additional Compounds.

Bis(1,5-cyclooctadiene)bis(μ -pyrazolyl)diiridium(I), $[Ir(\mu\text{-pz})\text{-}(\text{COD})]_2$, was prepared by the method outlined in Chapter 2.

N,N' -Dimethyl-4,4'-bipyridinium di(hexafluorophosphate), methyl

viologen di(hexafluorophosphate) or $MV^{2+}(PF_6^-)_2$, was prepared by treating an aqueous solution of methyl viologen dichloride hydrate with a filtered, saturated, aqueous solution of ammonium hexafluorophosphate. The precipitated $MV^{2+}(PF_6^-)_2$ was filtered, washed well with water, and recrystallized from a 2:1:1 (v/v/v) water/acetone/ethanol solution to give white needles. Anal. Calcd for $C_{12}H_{14}N_2P_2F_{12}$: C, 30.27; H, 2.96; N, 5.88. Found: C, 30.32; H, 2.93; N, 5.84.

2,6-Dimethyl-N-methylpyridinium iodide was synthesized by refluxing 2,6-lutidine (3.0 mL, 0.026 mol) and excess iodomethane (8.0 mL, 0.13 mol) in a 1:1 (v/v) acetone/ethanol solution (60 mL) for 24 h. The pyridinium iodide precipitated during the reaction. The solution was cooled, and the product was filtered and recrystallized from N,N-dimethylacetamide to give a white, crystalline solid. Yield: 1.6 g (25%). Anal. Calcd for $C_8H_{12}NI$: C, 38.58; H, 4.86; N, 5.62. Found: C, 38.63; H, 4.74; N, 5.68.

Physical Measurements

Materials.

Solvents and liquid reagents for the quenching, flash photolysis, and steady-state photolysis experiments were purified, if necessary, degassed with a minimum of five freeze-pump-thaw cycles on a high-vacuum line (limiting pressure $< 10^{-3}$ torr), and bulb-to-bulb distilled into glass round-bottomed storage flasks equipped with Teflon vacuum valves. The solvents and reagents were stored over either alumina (Woelm N, Activity Grade 1, obtained from ICN Nutritional Biochemicals) or Linde 4A molecular sieves (Union Carbide) that were

activated by heating under dynamic vacuum ($< 10^{-3}$ torr) for 24 h. Acetonitrile (Burdick and Jackson, UV Grade) and cyclohexane (Aldrich, 99+%, Gold Label) were used as received and stored over alumina and molecular sieves, respectively. 1,2-Dibromoethane (Aldrich, 99+%, Gold Label) and 1-bromo-2-chloroethane (Aldrich, 98%) were distilled from calcium hydride (Aldrich, 95+%, -40 mesh) and stored over molecular sieves. The halocarbon solvents' storage flasks were wrapped with foil to prevent exposure to room light.

Acetonitrile (Burdick and Jackson, UV Grade) for the electrochemical experiments was obtained from a freshly opened bottle and used as received.

Tetra-*n*-butylammonium hexafluorophosphate was prepared from tetra-*n*-butylammonium iodide (Kodak) and potassium hexafluorophosphate (Aldrich, 98%) by addition of a saturated, aqueous solution of the iodide salt to a filtered, saturated, aqueous solution of the potassium salt. The precipitated tetra-*n*-butylammonium hexafluorophosphate was recrystallized from absolute ethanol (U.S. Industrial) to give white needles.

Tetra-*n*-butylammonium iodide (Kodak) was recrystallized from acetone (EM Science) before use. Tetra-*n*-butylammonium fluoroborate (Southwestern Analytical Chemicals), acetone- d_6 (Aldrich, 99+atom% D, Gold Label), and tetramethylsilane (Aldrich, 99.9+%, NMR Grade) were used as received.

Electrochemical Measurements.

Cyclic voltammetric measurements were conducted with a Princeton Applied Research (PAR) 173 potentiostat/galvanostat and a PAR 175 uni-

versal programmer using a Pt button working electrode, a Pt wire auxiliary electrode, and a sodium saturated calomel electrode (SSCE) as the reference. Cyclic voltammograms of the pyridinium hexafluorophosphates were measured for acetonitrile solutions under argon that contained 0.1 M tetra-*n*-butylammonium hexafluorophosphate as the supporting electrolyte and $5-7 \times 10^{-3}$ M compound. Cyclic voltammograms of $[\text{Ir}(\mu\text{-pz})(\text{COD})]_2$ were measured under the same conditions on solutions containing 5×10^{-4} M complex with 0.1 M tetra-*n*-butylammonium fluoroborate as the supporting electrolyte.

Stern-Volmer Quenching Procedures.

For the experiments with methyl viologen di(hexafluorophosphate) and the pyridinium hexafluorophosphate quenchers, acetonitrile solutions of $[\text{Ir}(\mu\text{-pz})(\text{COD})]_2$ (10^{-4} - 10^{-5} M) and tetra-*n*-butylammonium hexafluorophosphate ($\mu = 0.1$ M) were prepared on a high-vacuum line (limiting pressure $< 10^{-3}$ torr) in a two-compartment spectrophotometric cell consisting of a 1 cm pathlength square cuvette of quartz or Pyrex and a 10 mL Pyrex bulb.²⁶ Acetonitrile was first vacuum-distilled from its storage flask to a calibrated volumetric cylinder then to the evacuated cell containing the iridium complex and electrolyte. Addition of solid quencher to one compartment of the cell was followed by re-evacuation of the cell to maintain the oxygen-free conditions of the experiment. Rate constants for the quenching of the triplet excited state of $[\text{Ir}(\mu\text{-pz})(\text{COD})]_2$ (${}^3[\text{Ir}(\mu\text{-pz})(\text{COD})]_2^*$) were determined by measuring its lifetime as a function of quencher concentration. The emission lifetime measurements were conducted with a Nd:YAG pulsed laser system that has been described previously²⁷ using 532 nm

excitation.

Rate constants for the quenching of $^3[\text{Ir}(\mu\text{-pz})(\text{COD})]_2^*$ with 2,6-dimethyl-N-methylpyridinium iodide and 2,6-dimethyl-N-methylpyridinium hexafluorophosphate in the absence of added electrolyte were determined by measuring its emission intensity as a function of quencher concentration. The emission intensity measurements were conducted with an emission spectrophotometer constructed at Caltech which has been described previously.²⁸ Since the luminescence band shape did not change with quencher addition, the emission intensities were measured from the emission band maxima of the uncorrected spectra. Sample orientation and instrument stability were monitored to insure confidence in the quenching data. The method of preparation of these solutions was the same as that described for the samples containing 0.1 M tetra-*n*-butylammonium hexafluorophosphate.

Absorption spectra of the solutions were measured with a Cary 17 spectrophotometer before and after the quenching experiments to insure that the quenching was reversible and that no reaction, either thermal or photochemical, was occurring between $[\text{Ir}(\mu\text{-pz})(\text{COD})]_2$ and the quenchers during the course of the experiments.

Microsecond Flash Photolysis Procedures.

Flash photolysis experiments were conducted on an apparatus constructed at Caltech which has been described previously²⁹ with the noted modifications.²⁷ A Corning 3-73 cut-off filter was used for excitation filtering. Acetonitrile solutions of $[\text{Ir}(\mu\text{-pz})(\text{COD})]_2$ (1×10^{-4} M), methyl viologen di(hexafluorophosphate) (5×10^{-3} M), and tetra-*n*-butylammonium hexafluorophosphate ($\mu = 0.1$ M) were prepared on

a high vacuum line (limiting pressure $< 10^{-3}$ torr) in a cell consisting of a cylindrical Pyrex compartment (15 cm pathlength, 0.8 cm diameter) connected to a 50 mL Pyrex bulb used for condensation of solvent and a 1 cm pathlength square quartz cuvette with each compartment oriented 90° from its neighbor. Acetonitrile was first vacuum-distilled from its storage flask into a calibrated volumetric cylinder followed by distillation into the evacuated cell containing the iridium complex, quencher, and electrolyte. The solution was then blanketed with argon.

Steady-State Photolysis Procedures.

Steady-state photolysis experiments were conducted on solutions prepared on a high-vacuum line (limiting pressure $< 10^{-3}$ torr) in a two-compartment cell consisting of a 10 mL Pyrex bulb and a 1 cm pathlength square quartz cuvette.²⁶ Solvent was bulb-to-bulb distilled into the cell containing the $[\text{Ir}(\mu\text{-pz})(\text{COD})]_2$ from the appropriate solvent storage flask followed by addition of the reactant in the dark. Liquid reactants were bulb-to-bulb distilled into the cell, and solid reactants were added to one compartment of the cell followed by re-evacuation of the cell to maintain oxygen-free conditions.

Acetonitrile solutions of $[\text{Ir}(\mu\text{-pz})(\text{COD})]_2$ (1×10^{-4} M), 2,6-dimethyl-N-methylpyridinium iodide (2×10^{-2} M), and $(n\text{-C}_4\text{H}_9)_4\text{NI}$ (2×10^{-2} M) were irradiated for at least 24 h with $\lambda_{\text{ex}} > 420$ nm and showed no visible absorbance changes. Solutions of $[\text{Ir}(\mu\text{-pz})(\text{COD})]_2$ and 1,2-dibromoethane, in either neat 1,2-dibromoethane or diluted with acetonitrile or cyclohexane, were irradiated with $\lambda_{\text{ex}} > 450$ nm and

showed rapid formation of $[\text{Ir}(\mu\text{-pz})(\text{COD})(\text{Br})]_2$. Solutions kept in the dark showed no formation of the oxidative addition product. Solutions of $[\text{Ir}(\mu\text{-pz})(\text{COD})]_2$ and 1-bromo-2-chloroethane, in either neat 1-bromo-2-chloroethane or diluted with acetonitrile or cyclohexane, were irradiated with $\lambda > 450$ nm and showed rapid formation of either $[\text{Ir}(\mu\text{-pz})(\text{COD})(\text{Br})]_2$ or $\text{Ir}_2(\mu\text{-pz})_2(\text{COD})_2(\text{Br})(\text{Cl})$ as discussed in the text. Solutions kept in the dark showed no formation of the oxidative addition products. The iridium oxidative addition products were identified by their absorption spectra; the organic products were not identified.

Either a 1000 W high-pressure Hg/Xe arc lamp or a 200 W medium-pressure Hg/Xe arc lamp equipped with Corning cut-off filters was used for the irradiations. Spectrophotometric monitoring of both photolysis and thermal-blank experiments was done with either a Cary 17 or Hewlett-Packard 8450A spectrophotometer.

Additional Measurements.

^1H NMR spectra were recorded at 90 MHz on a Varian EM 390 spectrometer. Chemical shifts are reported in ppm (δ) vs. tetramethylsilane.

Elemental analyses were obtained by Mr. Larry Henling at the Caltech Analytical Laboratory.

Results and Discussion

A long-lived excited state of a transition metal complex has enhanced redox properties relative to the ground state. If the entropy difference between the ground and excited state is small, the reduction and oxidation potentials of the excited state can be estimated from the redox potentials of the ground state ($E^\circ(\text{M}^+/\text{M})$ and $E^\circ(\text{M}/\text{M}^-)$) and the spectroscopic energy of the excited state. The distortion (size, shape, solvation) of an excited state relative to the ground state is reflected in the Stokes shift between absorption and emission.^{3,0} If this shift is small, the entropy difference is usually neglected, and the spectroscopic energy may be taken as a free energy. In this situation, the redox potentials of the excited state ($E^\circ(\text{M}^+/\text{M}^*)$ and $E^\circ(\text{M}^*/\text{M}^-)$) can be estimated using equations (1) and (2) where $E_{0-0}(\text{M}/\text{M}^*)$ is the spectroscopic energy of the 0-0 transition.^{1,4}

$$E^\circ(\text{M}^+/\text{M}^*) \cong E^\circ(\text{M}^+/\text{M}) - E_{0-0}(\text{M}/\text{M}^*) \quad (1)$$

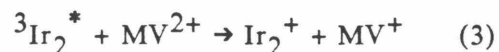
$$E^\circ(\text{M}^*/\text{M}^-) \cong E^\circ(\text{M}/\text{M}^-) + E_{0-0}(\text{M}/\text{M}^*) \quad (2)$$

Since the entropy corrections to these equations are very difficult to evaluate, the Stokes shift is used to gauge the validity of the approximations. From the band maxima corresponding to the ${}^1\text{A}_1 \leftrightarrow {}^3\text{B}_2$ electronic transitions in the absorption and emission spectra of $[\text{Ir}(\mu\text{-pz})(\text{COD})]_2$ in acetonitrile at ambient temperature, the Stokes shift for the ${}^3\text{B}_2(\text{d}\sigma^* \text{p}\sigma)$ excited state is $\sim 2500 \text{ cm}^{-1}$,

suggesting that equations (1) and (2) can be used to obtain estimates of the excited-state potentials. The spectroscopic energy of the ${}^3B_2(d\sigma^* p\sigma)$ excited state is estimated to be ~ 2.05 eV from the ambient-temperature acetonitrile solution spectra. The electrochemistry of $[\text{Ir}(\mu\text{-pz})(\text{COD})]_2$ (Ir_2) in acetonitrile is rather complex, however, since the oxidation to the mono-cation and the oxidation of this species to the di-cation are near the same potential and are complicated by acetonitrile coordination.³¹ Therefore, an estimate of $E^\circ(\text{Ir}_2^{+/0}) = 0.30 \pm 0.05$ V vs. SSCE is suggested. No reduction of $[\text{Ir}(\mu\text{-pz})(\text{COD})]_2$ is observed to -1.8 V vs. SSCE. These estimates for the various terms in equations (1) and (2) suggest that the ${}^3B_2(d\sigma^* p\sigma)$ excited state of $[\text{Ir}(\mu\text{-pz})(\text{COD})]_2$ (${}^3\text{Ir}_2^*$) is a powerful reductant in acetonitrile with $E^\circ(\text{Ir}_2^+ / {}^3\text{Ir}_2^*)$ about -1.7 V to -1.8 V vs. SSCE. Given a limit for $E^\circ(\text{Ir}_2^0 / -)$ of < -1.8 V, the value of $E^\circ({}^3\text{Ir}_2^* / \text{Ir}_2^-)$ is < 0.25 V vs. SSCE, implying that this excited state is a poor oxidant.

Since the long-lived (250 ns) ${}^3B_2(d\sigma^* p\sigma)$ excited state of $[\text{Ir}(\mu\text{-pz})(\text{COD})]_2$ is predicted to be a very strong reductant in acetonitrile, we initially studied its electron-transfer reactivity with N,N' -dimethyl-4,4'-bipyridinium (methyl viologen, MV^{2+}).³² In acetonitrile solution, the phosphorescence of ${}^3[\text{Ir}(\mu\text{-pz})(\text{COD})]_2^*$ is dramatically quenched in the presence of $\text{MV}^{2+}(\text{PF}_6^-)_2$. The triplet energy of MV^{2+} (3.10 eV)³³ is too high for energy-transfer quenching to be competitive with electron-transfer quenching of ${}^3[\text{Ir}(\mu\text{-pz})(\text{COD})]_2^*$, and energy transfer can be ruled out. Further evidence for electron transfer is obtained from a measurement of the rate of the quenching

reaction shown in equation (3).



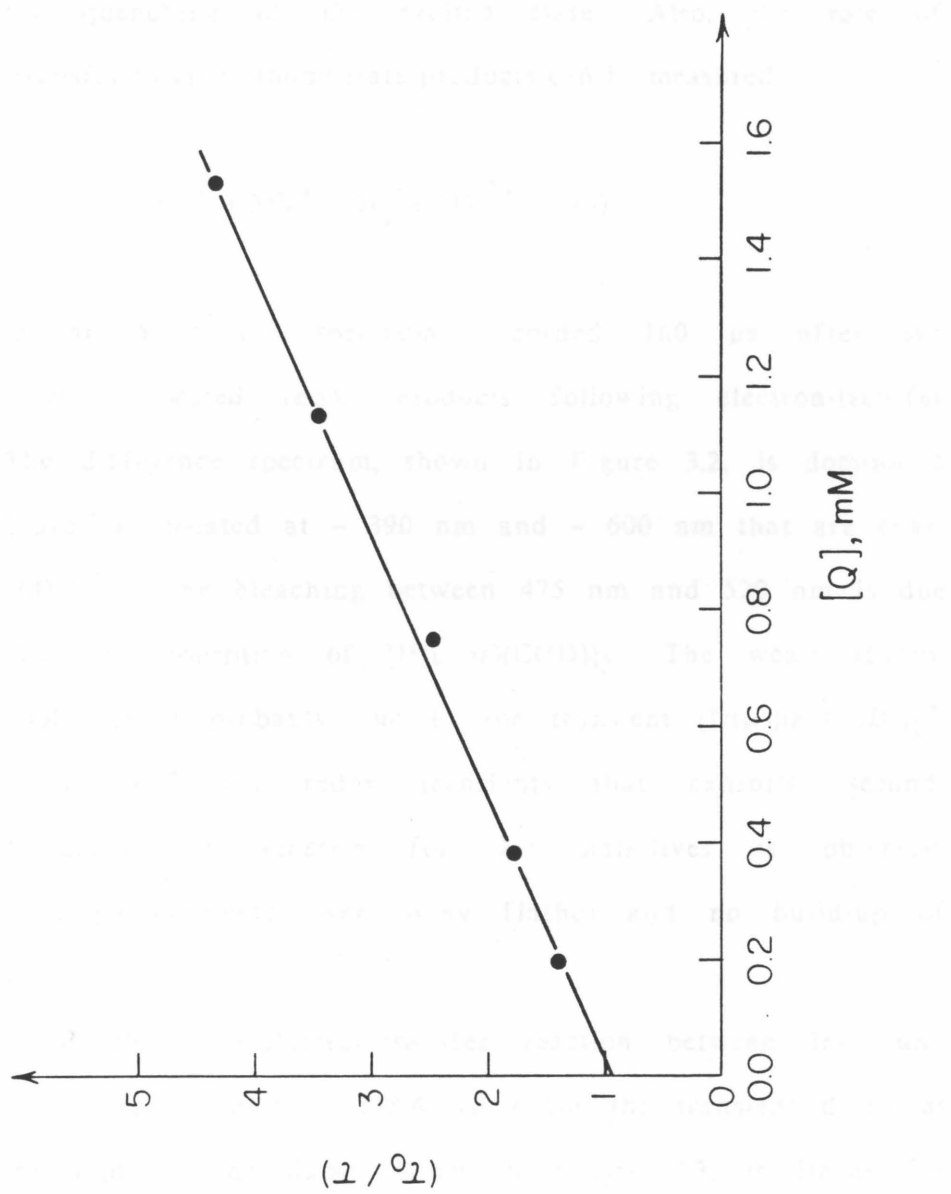
The reaction obeys Stern-Volmer quenching kinetics^{3 4} and is studied by monitoring the lifetime of the triplet excited state as a function of methyl viologen concentration. By analyzing the data according to the Stern-Volmer equation, shown below in equation (4), where τ_0 and τ are the lifetimes of the ${}^3\text{B}_2(d\sigma^* p\sigma)$ excited state in the absence and presence of quencher (Q), respectively, the value of the quenching rate constant (k_q) can be extracted from the slope of a plot of (τ_0/τ) vs. [Q].

$$(\tau_0/\tau) = 1 + k_q\tau_0[\text{Q}] \quad (4)$$

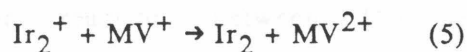
The Stern-Volmer plot of the data for the quenching of ${}^3[\text{Ir}(\mu\text{-pz})(\text{COD})]_2^*$ by methyl viologen in acetonitrile solution ($22 \pm 2^\circ\text{C}$, $\mu = 0.1 \text{ M } (n\text{-C}_4\text{H}_9)_4\text{NPF}_6$) is shown in Figure 3.1. The measured rate constant for the reaction is $8.7 \pm 0.9 \times 10^9 \text{ M}^{-1}\text{s}^{-1}$, which increases to $1.6 \pm 0.3 \times 10^{10} \text{ M}^{-1}\text{s}^{-1}$ after correction for diffusional effects.^{3 5} The rate of the reaction is near the diffusion limit for acetonitrile,^{3 6} which is reasonable for electron-transfer quenching between ${}^3[\text{Ir}(\mu\text{-pz})(\text{COD})]_2^*$ and methyl viologen, since MV^{2+} is easily reduced by one electron ($E_{1/2}(\text{MV}^{2+}/^+) = -0.45 \text{ V vs. SSCE}$, $\mu = 0.1 \text{ M } (n\text{-C}_4\text{H}_9)_4\text{NPF}_6, \text{CH}_3\text{CN}$).^{3 7}

Conventional microsecond flash-photolysis studies show that the

Figure 3.1 Stern-Volmer plot for the oxidative quenching of the ${}^3\text{B}_2(\text{d}\sigma^* \text{p}\sigma)$ excited state of $[\text{Ir}(\mu\text{-pz})(\text{COD})]_2$ by methyl viologen di(hexafluorophosphate) ($[\text{Ir}_2] = 5 \times 10^{-5} \text{ M}$, $\mu = 0.1 \text{ M } (n\text{-C}_4\text{H}_9)_4\text{NPF}_6$, CH_3CN , $22 \pm 2^\circ\text{C}$).



expected redox products for electron-transfer quenching of ${}^3\text{Ir}_2^*$ by MV^{2+} are produced. An investigation of the back-electron-transfer reaction between the oxidized iridium dimer and reduced methyl viologen, shown in equation (5), provides very strong evidence for electron-transfer quenching of the excited state. Also, the rate of back electron transfer to give ground-state products can be measured.



The transient difference spectrum, recorded 160 μs after the flash, shows the expected redox products following electron-transfer quenching. The difference spectrum, shown in Figure 3.2, is dominated by intense absorptions located at ~ 390 nm and ~ 600 nm that are characteristic of MV^+ .³⁸ The bleaching between 475 nm and 520 nm is due to the ground-state absorption of $[\text{Ir}(\mu\text{-pz})(\text{COD})]_2$. The weak absorption around 450 nm is probably due to the transient $[\text{Ir}(\mu\text{-pz})(\text{COD})]_2^+$. Well-defined decay of the redox transients that exhibits second-order, equal-concentration kinetics for 2-3 half-lives is observed. The solution is photochromic over many flashes and no build-up of products is noted.

The rate of the back-electron-transfer reaction between Ir_2^+ and MV^+ is measured from a plot of $1/\Delta A$ vs. t for the transient decay at 605 nm. The plot of the data, shown in Figure 3.3, is linear for > 2.5 half-lives and corresponds to the decay expected for second-order, equal-concentration kinetics.³⁹ The rate constant for the back reaction (k_b) can be calculated from the slope (m) of this plot using

Figure 3.2 Transient difference spectrum observed 160 μ s after the microsecond flash photolysis for the back-electron-transfer reaction between $[\text{Ir}(\mu\text{-pz})(\text{COD})]_2^+$ and MV^+ ($[\text{Ir}_2] = 1 \times 10^{-4}$ M, $[\text{MV}^{2+}] = 5 \times 10^{-3}$ M, $\mu = 0.1$ M (*n*- C_4H_9) $_4\text{NPF}_6$, CH_3CN , $22 \pm 2^\circ\text{C}$, $\lambda_{\text{ex}} > 420$ nm). The data between 475 nm and 520 nm have $-\Delta\text{O.D.s}$ and are not shown.

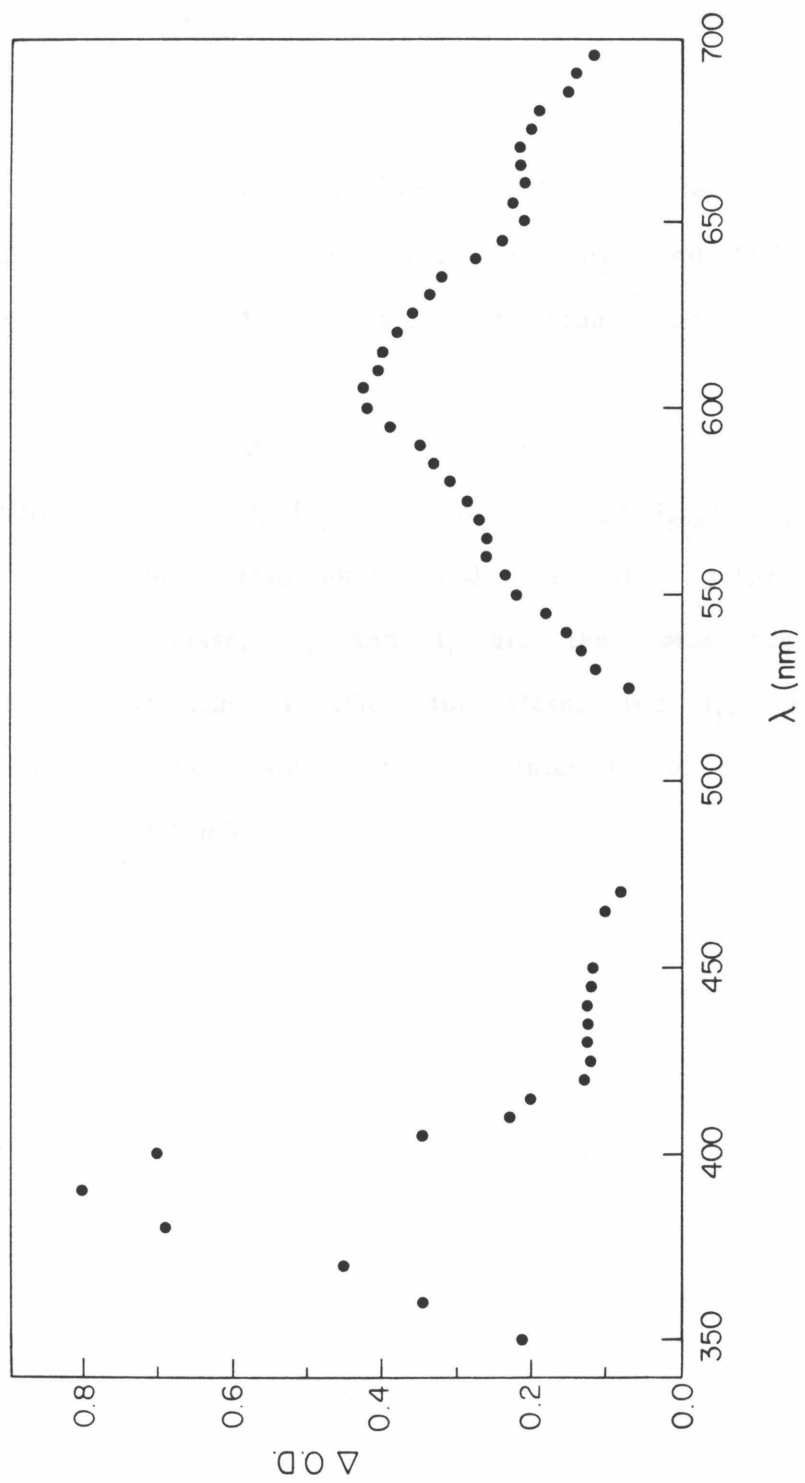
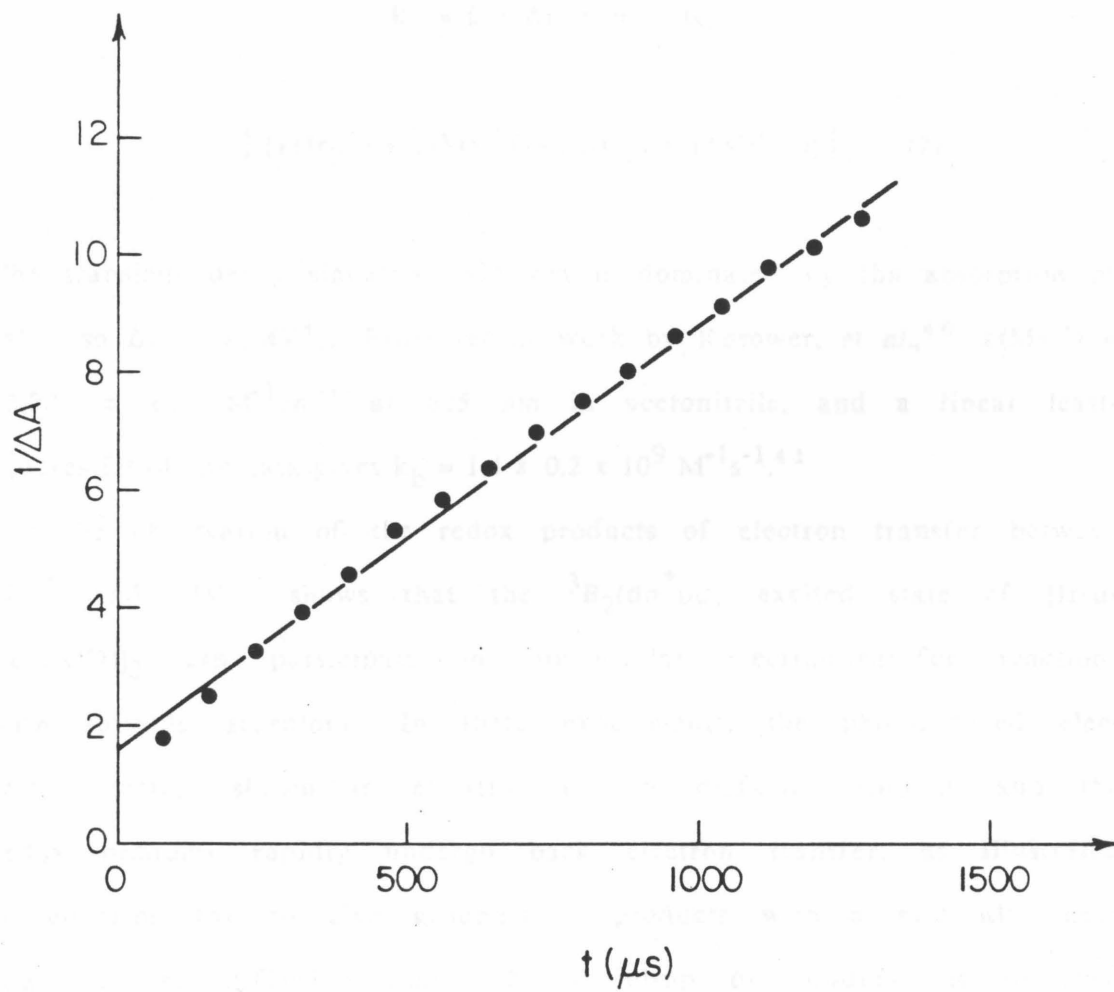


Figure 3.3 Plot of $1/\Delta A$ vs. t at 605 nm for the back-electron-transfer reaction between $[\text{Ir}(\mu\text{-pz})(\text{COD})]_2^+$ and MV^+ (see Figure 3.2). ΔA is calculated from the following equation

$$\Delta A = A_t - A_0 = -\log(I_t/I_0)$$

where $A_0 = -\log(I_0/I_{\text{ref}})$ and $A_t = -\log(I_t/I_{\text{ref}})$. A_0 and I_0 are the absorbance and intensity, respectively, before the flash, A_t and I_t are the absorbance and intensity at time t after the flash, and I_{ref} is an arbitrary value assigned to the intensity of the probe beam. $I_0 = 450 \text{ mV}$.



equation (6) where l is the cell pathlength (15 cm) and $\Delta\varepsilon$ is the absolute value of the difference between the sum of the redox product extinction coefficients and the sum of the extinction coefficients of the reactants at 605 nm as given in equation (7).

$$k_b = l \cdot \Delta\varepsilon \cdot m \quad (6)$$

$$\Delta\varepsilon = | \{ \varepsilon(\text{Ir}_2^+) + \varepsilon(\text{MV}^+) \} - \{ \varepsilon(\text{Ir}_2) + \varepsilon(\text{MV}^{2+}) \} | \quad (7)$$

The transient decay signal at 605 nm is dominated by the absorption of MV^+ , so $\Delta\varepsilon \cong \varepsilon(\text{MV}^+)$. From recent work by Kosower, *et al.*,⁴⁰ $\varepsilon(\text{MV}^+) = 13,000 \pm 600 \text{ M}^{-1}\text{cm}^{-1}$ at 605 nm in acetonitrile, and a linear least-squares fit of the data gives $k_b = 1.4 \pm 0.2 \times 10^9 \text{ M}^{-1}\text{s}^{-1}$.⁴¹

The observation of the redox products of electron transfer between ${}^3\text{Ir}_2^*$ and MV^{2+} shows that the ${}^3\text{B}_2(\text{d}\sigma^* \text{p}\sigma)$ excited state of $[\text{Ir}(\mu\text{-pz})(\text{COD})]_2$ can participate in bimolecular electron-transfer reactions with suitable acceptors. In these experiments, the photoinduced electron transfer, shown in equation (3), is diffusion limited, and the redox products rapidly undergo back electron transfer, as illustrated in equation (5), to give ground-state products with a rate also near that of the diffusion limit. No build-up of products is observed since the rapid back reaction of the redox products Ir_2^+ and MV^+ gives the ground state of $[\text{Ir}(\mu\text{-pz})(\text{COD})]_2$ and MV^{2+} . Consequently, this photoinduced electron transfer does not lead to net chemistry.

Our interests in further studying the electron-transfer reactivity of ${}^3[\text{Ir}(\mu\text{-pz})(\text{COD})]_2^*$ and examining this reactivity in the context of

classical Marcus-theory predictions for outer-sphere electron transfer prompted us to investigate the quenching of the ${}^3B_2(d\sigma^*p\sigma)$ excited state with a series of pyridinium acceptors of variable reduction potentials. The pyridinium quenchers and the measured values of $E_{1/2}(A^{+/o})$ or $E_{p,c}(A^{+/o})$ for the one-electron reductions of these acceptors are shown in Table 3.1. Because of a lack of acceptors with reversible couples of appropriate reduction potentials, a number of electrochemically irreversible pyridinium acceptors were used for the quenching study. Therefore, the reduction potentials reported in Table 3.1 for these pyridiniums are the cathodic peak potentials $E_{p,c}(A^{+/o})$ measured at a scan rate of 200 mV/s under the same experimental conditions ($22 \pm 2^\circ\text{C}$, $\mu = 0.1 \text{ M } (n\text{-C}_4\text{H}_9)_4\text{NPF}_6$, CH_3CN).

A recent study by Meyer and co-workers gives estimates for the values of $E_{1/2}(A^{+/o})$ for 3-amido-N-benzylpyridinium hexafluorophosphate and 3-amido-N-methylpyridinium hexafluorophosphate of $-1.07 \pm 0.03 \text{ V}$ and $-1.19 \pm 0.03 \text{ V}$ vs. SCE ($\mu = 0.1 \text{ M } (\text{C}_2\text{H}_5)_4\text{NClO}_4$), respectively, in acetonitrile solution.¹⁸ These reduction potentials are estimated by using the method of Olmstead, *et al.*,⁴⁵ as described elsewhere.¹⁵ The values of $E_{p,c}(A^{+/o})$ measured by us for these acceptors seem to be in agreement with the estimated $E_{1/2}(A^{+/o})$ values given by Meyer and co-workers. Furthermore, a recent study by Espenson⁴⁶ shows a good correlation of several of the pyridinium reduction potentials, both $E_{1/2}(A^{+/o})$ and $E_{p,c}(A^{+/o})$, with the Hammett parameter σ in a linear-free-energy analysis of substituent effects. Based on these studies, the relative trends in the reduction potentials for the electrochemically reversible and irreversible pyridinium

Table 3.1 Reduction potentials of the pyridinium quenchers.

	Quencher ^a	$E(A^{+/o})$, V vs. SSCE ^b
(1)	4-cyano-N-methylpyridinium	-0.67
(2)	4-carbomethoxy-N-methylpyridinium	-0.78
(3)	4-amido-N-ethylpyridinium	-0.93
(4)	3-amido-N-benzylpyridinium	-1.07
(5)	3-amido-N-methylpyridinium	-1.14
(6)	N-ethylpyridinium	-1.36
(7)	2-methoxy-N-methylpyridinium	-1.48
(8)	4-methyl-N-methylpyridinium	-1.49
(9)	4- <i>tert</i> -butyl-N-ethylpyridinium	-1.52
(10)	2,6-dimethyl-N-methylpyridinium	-1.52
(11)	2,3,6-trimethyl-N-methylpyridinium	-1.57
(12)	2,4,6-trimethyl-N-methylpyridinium	-1.67
(13)	2,6-dimethyl-4-methoxy-N-methylpyridinium	-1.85

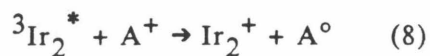
a. All of the compounds are hexafluorophosphate salts.

b. For pyridiniums 1-3, $E(A^{+/o}) = E_{1/2}(A^{+/o})$. For pyridiniums 4-13, the reductions are irreversible; therefore, the values of $E(A^{+/o})$ are the cathodic peak potentials, $E_{p,c}(A^{+/o})$, measured at a scan rate of 200 mV/s. Both $E_{1/2}(A^{+/o})$ and $E_{p,c}(A^{+/o})$ were measured by cyclic voltammetry ($22 \pm 2^\circ\text{C}$, $\mu = 0.1 \text{ M } (n\text{-C}_4\text{H}_9)_4\text{NPF}_6$) in acetonitrile solution.

acceptors are probably self-consistent and agree with the qualitative electron-donating or electron-withdrawing effects of the substituents on the pyridinium ring.

A number of studies show that the irreversible electrochemical behavior of several of these pyridiniums is due to dimerization of the reduced radicals.^{40,42,43} However, this reaction of the reduced acceptors does not appear to interfere with our electron-transfer quenching studies. The back-electron-transfer reactions between the reduced pyridiniums and the oxidized iridium dimer are diffusion controlled, so the dimerization of the reduced pyridiniums is unlikely to be a competitive process. Other studies of photoinduced electron transfer with the luminescent excited states of ruthenium(II) and osmium(II) polypyridyl complexes have used some of the same pyridinium acceptors and likewise report no complications from this dimerization reaction.^{18,44}

The kinetics of the electron-transfer quenching reactions between $^3[\text{Ir}(\mu\text{-pz})(\text{COD})]_2^*$ and the pyridinium acceptors, shown in equation (8), were studied by the same methods used for the quencher methyl viologen, and the data were analyzed using the Stern-Volmer equation given in equation (4).



The quenching reactions were done in acetonitrile solution at $22 \pm 2^\circ\text{C}$ with $\mu = 0.1 \text{ M } (n\text{-C}_4\text{H}_9)_4\text{NPF}_6$ added to maintain pseudo-constant ionic strength. The Stern-Volmer plots of (τ_0/τ) vs. $[\text{Q}]$ for the data are

linear over the range of quencher concentrations. A representative plot of the data for the quenching of $^3[\text{Ir}(\mu\text{-pz})(\text{COD})]_2^*$ by 2,3,6-trimethyl-N-methylpyridinium hexafluorophosphate is shown in Figure 3.4. The measured quenching rate constants (k_q), shown in Table 3.2, were calculated from the slopes of linear-least-squares fits of the data and are uncorrected for diffusional effects.

Since the most rapid of the quenching reactions approach the diffusion-controlled limit, the measured rate constants need to be corrected for diffusional effects to obtain the activated rate constants.^{2,17} The relationship between these rate constants is given in equation (9) where k_q is defined above, k_q' is the rate constant corrected for diffusional effects, and k_D is the diffusion-limited rate constant in the medium of interest.

$$1/k_q = 1/k_q' + 1/k_D \quad (9)$$

The values of k_D for the electron-transfer reactions between the iridium complex and the pyridiniums are calculated using the Smoluchowski equation, given in equation (10), where r_1 and r_2 are the radii of the reactants, η is the viscosity of the solution, and the other terms have their usual definitions.⁴⁷

$$k_D = (2RT/3000\eta)(2 + r_1/r_2 + r_2/r_1) \quad (10)$$

The pyridinium radii are calculated by averaging the van der Waals radii along the three molecular axes and vary from 3.2 Å to 4.6 Å.⁴⁸

Figure 3.4 Stern-Volmer plot for the oxidative quenching of the ${}^3B_2(d\sigma^* p\sigma)$ excited state of $[Ir(\mu\text{-pz})(COD)]_2$ by 2,3,6-trimethyl-N-methylpyridinium hexafluorophosphate ($[Ir_2] = 8 \times 10^{-5}$ M, $\mu = 0.1$ M $(n\text{-C}_4\text{H}_9)_4\text{NPF}_6$, CH_3CN , $22 \pm 2^\circ\text{C}$).

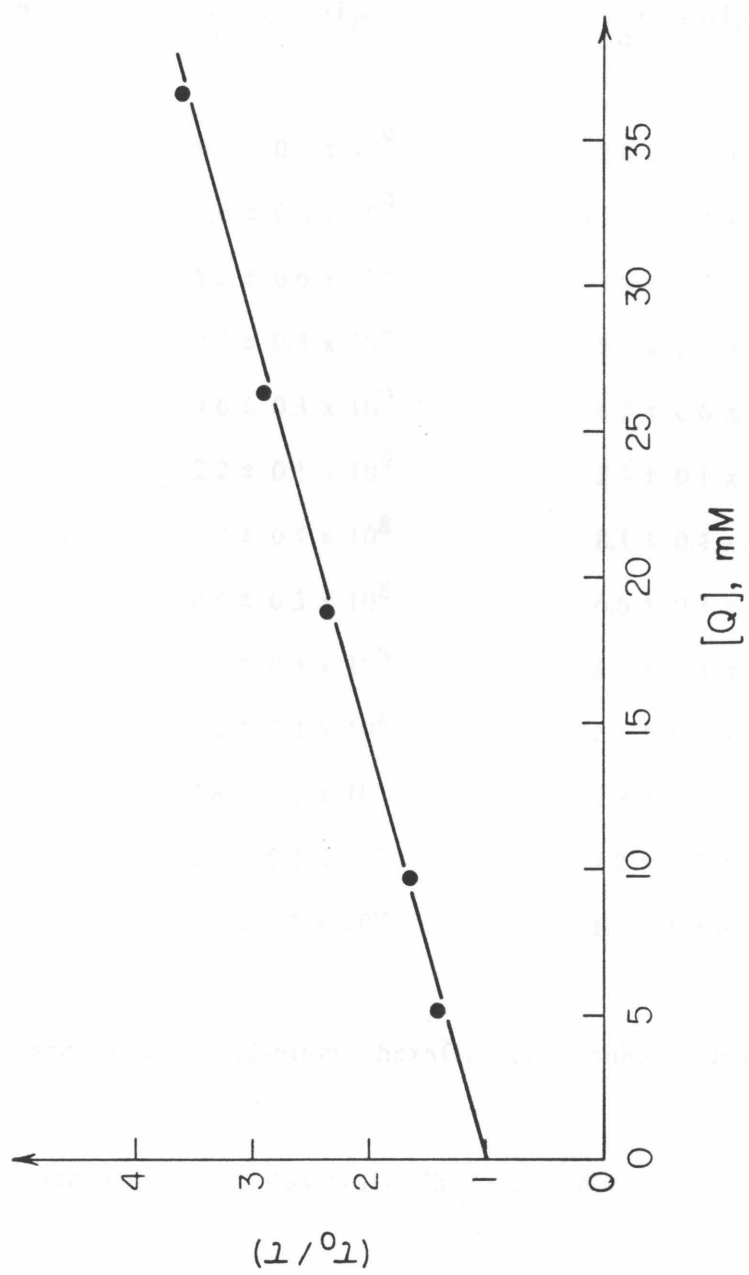


Table 3.2 Rate constants for the electron-transfer quenching of $^3[\text{Ir}(\mu\text{-pz})(\text{COD})]_2^*$ by pyridinium acceptors in acetonitrile solution at $22 \pm 2^\circ\text{C}$.

Pyridinium Acceptor ^a	$k_q, (\text{M}^{-1}\text{s}^{-1})^b$	$k_q', (\text{M}^{-1}\text{s}^{-1})^c$
1	$9.7 \pm 0.9 \times 10^9$	$2.0 \pm 0.4 \times 10^{10}$
2	$7.6 \pm 0.8 \times 10^9$	$1.3 \pm 0.2 \times 10^{10}$
3	$8.2 \pm 0.6 \times 10^9$	$1.5 \pm 0.2 \times 10^{10}$
4	$4.2 \pm 0.3 \times 10^9$	$5.5 \pm 0.5 \times 10^9$
5	$4.6 \pm 0.3 \times 10^9$	$6.2 \pm 0.6 \times 10^9$
6	$2.2 \pm 0.1 \times 10^9$	$2.5 \pm 0.1 \times 10^9$
7	$7.7 \pm 0.4 \times 10^8$	$8.1 \pm 0.4 \times 10^8$
8	$6.4 \pm 0.3 \times 10^8$	$6.6 \pm 0.3 \times 10^8$
9	$6.3 \pm 0.3 \times 10^8$	$6.5 \pm 0.3 \times 10^8$
10	$5.6 \pm 0.3 \times 10^8$	$5.8 \pm 0.3 \times 10^8$
11	$2.8 \pm 0.1 \times 10^8$	$2.9 \pm 0.1 \times 10^8$
12	$2.2 \pm 0.2 \times 10^7$	$2.2 \pm 0.2 \times 10^7$
13	$1.1 \pm 0.3 \times 10^6$	$1.1 \pm 0.3 \times 10^6$

a. The acceptors are the pyridinium hexafluorophosphates listed in Table 3.1.

b. The measured quenching rate constants (k_q) are not corrected for diffusional effects.

c. The quenching rate constants (k_q') are corrected for diffusional effects as discussed in the text.

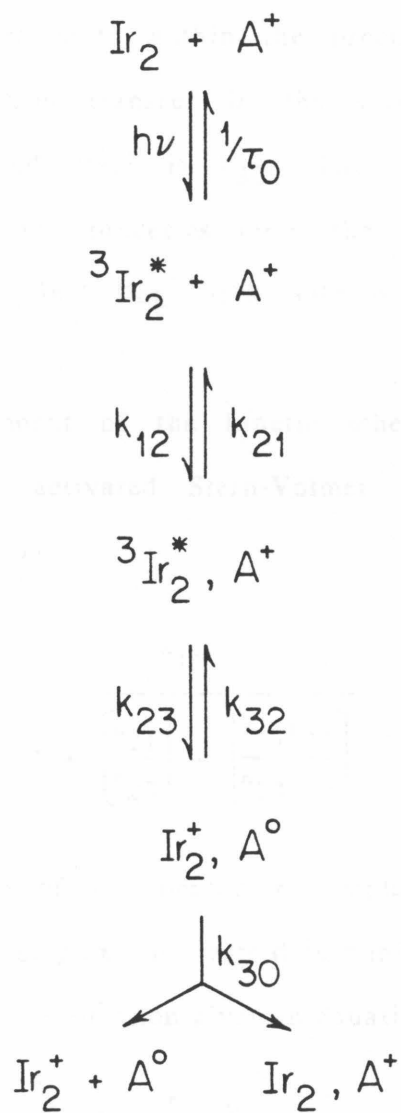
An average value of $r = 5.0 \text{ \AA}$ is calculated for $[\text{Ir}(\mu\text{-pz})(\text{COD})]_2$ from the crystal structure data.⁴⁹ A value of $k_D = 1.9 \times 10^{10} \text{ M}^{-1}\text{s}^{-1}$ is calculated from equation (10) for all the quenchers studied. Using equation (9), values of k_q' are calculated from k_q and are given in Table 3.2.

For the pyridinium acceptors with reduction potentials ranging from -0.67 V to -1.85 V vs. SSCE, the rates of electron-transfer quenching of $^3[\text{Ir}(\mu\text{-pz})(\text{COD})]_2^*$ range from a diffusion-limited rate of $k_q' = 2.0 \times 10^{10} \text{ M}^{-1}\text{s}^{-1}$ to $k_q' = 1.1 \times 10^6 \text{ M}^{-1}\text{s}^{-1}$ for the pyridinium that is the most difficult to reduce. The trend in these rates is consistent with electron-transfer quenching. Furthermore, studies by Meyer, *et al.*, have shown that several of these pyridiniums function as one-electron acceptors with the excited states of other inorganic complexes.^{18,44}

Since these pyridinium acceptors have variable reduction potentials but generally the same size, shape, charge, and electronic structure, this quenching study lends itself to a classical Marcus-theory treatment of the dependence of the electron-transfer quenching rate constant on the free-energy change of the quenching reaction.^{3,7} Following the treatment used for the electron-transfer quenching of the luminescent excited state of $[\text{Ru}(\text{bpy})_3]^{2+}$ (bpy = 2,2'-bipyridine) by Meyer, *et al.*,¹⁵ an analysis of the quenching of the $^3\text{B}_2(d\sigma^* p\sigma)$ excited state of $[\text{Ir}(\mu\text{-pz})(\text{COD})]_2$ by the pyridinium acceptors is discussed below.

The kinetic scheme for the quenching of $^3[\text{Ir}(\mu\text{-pz})(\text{COD})]_2^*$ by an acceptor A^+ is shown in Figure 3.5 and is based on a scheme originally

Figure 3.5 Kinetic scheme for the electron-transfer quenching of ${}^3[\text{Ir}(\mu\text{-pz})(\text{COD})]_2^*$ by pyridinium acceptors.



proposed by Rehm and Weller for the fluorescence quenching of a series of organic excited states.^{50,51} In this scheme, k_{12} and k_{21} are the rate constants for the formation and dissociation, respectively, of the precursor complex (${}^3\text{Ir}_2^*, \text{A}^+$) prior to electron transfer. The rate constant k_{23} is the unimolecular rate constant for electron-transfer quenching of the excited state within the precursor complex. The rate constant for back electron transfer in the successor complex ($\text{Ir}_2^+, \text{A}^\circ$) to regenerate the excited state is k_{32} . The rate constant k_{30} is a combined rate constant for processes from the successor complex which lead to net quenching including back electron transfer to give the ground-state reactants.

A steady-state treatment of the kinetic scheme in Figure 3.5 gives the expression for the activated Stern-Volmer quenching rate constant (k_q') shown in equation (11).

$$k_q' = \frac{k_{12}}{1 + \left[\frac{k_{21}}{k_{23}} \right] + \left[\frac{k_{21}k_{32}}{k_{23}k_{30}} \right]} \quad (11)$$

Assuming that formation of the precursor complex is rapid and electron transfer within this complex is rate-determining, *i.e.*, $k_{12} \gg k_{23}$, equation (11) reduces to the expression given in equation (12).

$$k_q' = \frac{k_{23}k_{12}}{k_{21}} \left[\frac{k_{30}}{k_{30} + k_{32}} \right] \quad (12)$$

The quenching rate constant (k_q') is proportional to the rate constant for electron transfer within the precursor complex (k_{23}) and the equi-

librium constant for formation of this complex ($K_{12} = k_{12}/k_{21}$). The term $[k_{30}/(k_{30} + k_{32})]$ represents the fraction of electron-transfer events that lead to net quenching. If back electron transfer to give the excited state is slow relative to processes that lead to net quenching from the successor complex,^{5,2} i.e., $k_{30} \gg k_{32}$, equation (12) reduces to the expression given in equation (13).

$$k_q' = k_{23}K_{12} \quad (13)$$

In the classical approach of Marcus theory for adiabatic electron transfer, the rate constant k_{23} can be expressed in terms of the free energy of activation (ΔG_{23}^*) and an effective frequency for nuclear motion (ν_{23}) for the electron transfer converting the precursor complex into the successor complex, as shown in equation (14).^{3,6}

$$k_{23} = \nu_{23} \exp(-\Delta G_{23}^*/RT) \quad (14)$$

According to this model, ΔG_{23}^* is related to the free-energy change for the electron transfer converting the precursor complex to the successor complex (ΔG_{23}) by the expression given in equation (15), where $\lambda/4$ is the contribution to the activation barrier for electron transfer involving reorganization of the inner and outer coordination spheres prior to electron transfer.^{5,3,5,4}

$$\Delta G_{23}^* = \frac{\lambda}{4} \left[1 + \left[\frac{\Delta G_{23}}{\lambda} \right] \right]^2 \quad (15)$$

The term λ is the sum of the inner (λ_i) and outer (λ_o) sphere reorganization energies for the electron-transfer process, and the expressions for λ_i and λ_o are based upon a harmonic oscillator model for the inner-sphere vibrations and a dielectric continuum model for the solvent, respectively.^{6,55} Substitution of equations (14) and (15) into equation (13) gives the expression shown in equation (16) that relates the rate constant k_q' to the free-energy change ΔG_{23} for the electron-transfer quenching of the excited state.

$$k_q' = \nu_{23} K_{12} \exp \left[- \frac{\lambda}{4} \left[1 + \frac{\Delta G_{23}}{\lambda} \right]^2 / RT \right] \quad (16)$$

Equation (16) expressed in logarithmic form gives equation (17).

$$RT \ln k_q' = \left[RT \ln \nu_{23} K_{12} - \frac{\lambda}{4} \right] - \frac{\Delta G_{23}}{2} \left[1 + \frac{\Delta G_{23}}{2\lambda} \right] \quad (17)$$

For a series of structurally and electronically related quenchers such as the pyridinium acceptors of Table 3.1, K_{12} , ν_{23} , and λ should be reasonably constant for electron-transfer reactions with the triplet excited state of $[\text{Ir}(\mu\text{-pz})(\text{COD})]_2$. Therefore, the expression $[RT \ln \nu_{23} K_{12} - (\lambda/4)]$ can be substituted by the term $RT \ln k_q'(0)$ where $k_q'(0)$ is the activated quenching rate constant for a hypothetical quencher with $\Delta G_{23} = 0$. The expression of equation (17) can then be simplified by the expression given in equation (18).

$$RT \ln k_q' = RT \ln k_q'(0) - \frac{\Delta G_{23}}{2} \left[1 + \frac{\Delta G_{23}}{2\lambda} \right] \quad (18)$$

When $|\Delta G_{23}| \ll 2\lambda$,^{5,6} the expression in equation (18) reduces to that of equation (19).

$$RT \ln k_q' = RT \ln k_q'(0) - (\Delta G_{23}/2) \quad (19)$$

The importance of equation (19) is apparent since values of ΔG_{23} can be calculated from the redox potentials for the excited-state couple $E^{\circ'}(\text{Ir}_2^+ / {}^3\text{Ir}_2^*)$ and the acceptors $E^{\circ'}(\text{A}^{+/0})$, provided that the electrostatic barriers involved in bringing the reactants and products of the quenching reaction together are included. Specifically, ΔG_{23} is related to the free-energy change for the quenching reaction ($\Delta G^{\circ'}$) of equation (8) as shown in equation (20) where w_p and w_r are the electrostatic work terms. The term $\Delta G^{\circ'}$ is related to the potentials of the reactants as shown below.⁷

$$\Delta G_{23} = \Delta G^{\circ'} + w_p - w_r \quad (20)$$

$$\Delta G^{\circ'} = - [E^{\circ'}(\text{A}^{+/0}) - E^{\circ'}(\text{Ir}_2^+ / {}^3\text{Ir}_2^*)] \quad (21)$$

Therefore, the values of ΔG_{23} for the oxidative quenching of ${}^3[\text{Ir}(\mu\text{-pz})(\text{COD})]_2^*$ by the pyridinium acceptors are given by equation (22).

$$\Delta G_{23} = - [E^{\circ'}(\text{A}^{+/0}) - E^{\circ'}(\text{Ir}_2^+ / {}^3\text{Ir}_2^*)] + w_p - w_r \quad (22)$$

The work terms can be evaluated using the Debye-Huckel expression¹ where w_p and w_r are directly proportional to the products of the ionic

charges of the products and reactants, respectively, of the electron-transfer reaction. In the electron-transfer quenching of ${}^3[\text{Ir}(\mu\text{-pz})(\text{COD})]_2^*$ by the pyridinium mono-cations, both the products and reactants include neutral species, so both w_p and w_r are equal to zero. Substitution of equation (22) into equation (19) with $w_p = w_r = 0$ gives an expression relating the experimentally determined values of k_q' to the reduction potentials $E^{\circ'}(A^{+/\circ})$ as shown in equation (23).

$$RT\ln k_q' = RT\ln k_q'(0) - 1/2[E^{\circ'}(\text{Ir}_2^{+}/{}^3\text{Ir}_2^*)] + 1/2[E^{\circ'}(A^{+/\circ})] \quad (23)$$

Both of the terms $RT\ln k_q'(0)$ and $1/2[E^{\circ'}(\text{Ir}_2^{+}/{}^3\text{Ir}_2^*)]$ of equation (23) are constants.

If the electron-transfer quenching of ${}^3[\text{Ir}(\mu\text{-pz})(\text{COD})]_2^*$ by the pyridinium acceptors follows the kinetic scheme of Figure 3.5 and obeys Marcus-theory predictions, a plot of $RT\ln k_q'$ vs. $E^{\circ'}(A^{+/\circ})$ should give a line of slope 0.5 in the region where $|\Delta G_{23}| \ll 2\lambda$.^{5,6} This plot of the data, presented in Table 3.3, for the quenching of the ${}^3B_2(d\sigma^*p\sigma)$ excited state of $[\text{Ir}(\mu\text{-pz})(\text{COD})]_2$ by pyridiniums 1-13 is shown in Figure 3.6. Because of the difficulty in finding acceptors with reversible reduction potentials as discussed, values of $E^{\circ'}(A^{+/\circ})$ are unavailable for the majority of the pyridiniums, so the values of $RT\ln k_q'$ are plotted vs. $E_{1/2}(A^{+/\circ})$ and $E_{p,c}(A^{+/\circ})$. The slope of 0.48 in the linear region of this curve (quenchers 7-13) is in excellent agreement with the theoretical value of 0.5. This suggests that the quenching of the ${}^3B_2(d\sigma^*p\sigma)$ excited state of $[\text{Ir}(\mu\text{-pz})(\text{COD})]_2$ follows classical Marcus-theory predictions for outer-sphere electron

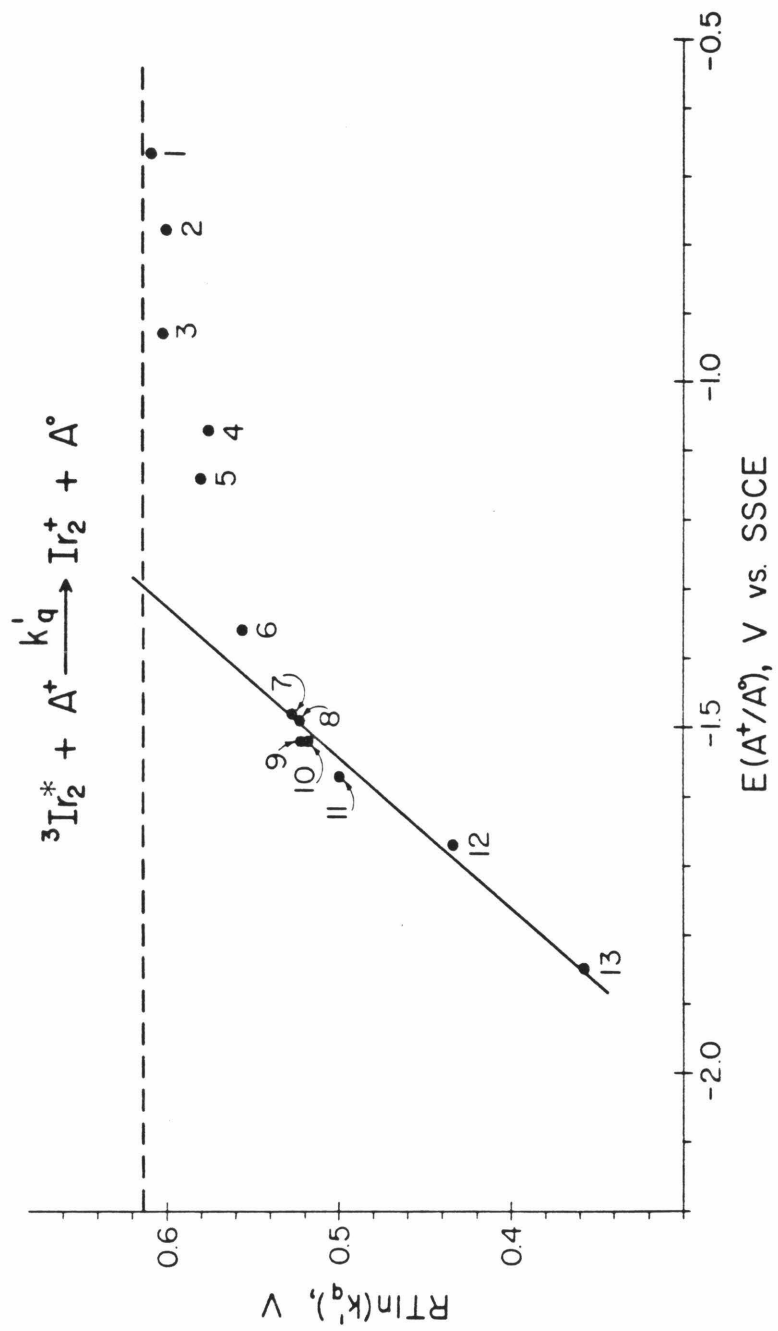
Table 3.3 $RT\ln k_q'$ vs. $E(A^{+/o})$ for the quenching of $^3[\text{Ir}(\mu\text{-pz})\text{-}(\text{COD})]_2^*$ by pyridinium acceptors.

Pyridinium Acceptor ^a	$RT\ln k_q'$, V	$E(A^{+/o})$, V vs. SSCE ^b
1	0.609	-0.67
2	0.598	-0.78
3	0.602	-0.93
4	0.576	-1.07
5	0.579	-1.14
6	0.556	-1.36
7	0.527	-1.48
8	0.522	-1.49
9	0.522	-1.52
10	0.518	-1.52
11	0.500	-1.57
12	0.434	-1.67
13	0.357	-1.85

a. The acceptors are the pyridinium hexafluorophosphates listed in Table 3.1.

b. The values of $E(A^{+/o})$ are given in Table 3.1.

Figure 3.6 Plot of $RT\ln k_q'$ (V) vs. $E(A^{+/0})$ (V) for the electron-transfer quenching of ${}^3[\text{Ir}(\mu\text{-pz})(\text{COD})]_2^*$ by the pyridinium acceptors in Table 3.1 ($\mu = 0.1 \text{ M}$ ($n\text{-C}_4\text{H}_9$) $_4\text{NPF}_6$, CH_3CN , $22 \pm 2^\circ\text{C}$).

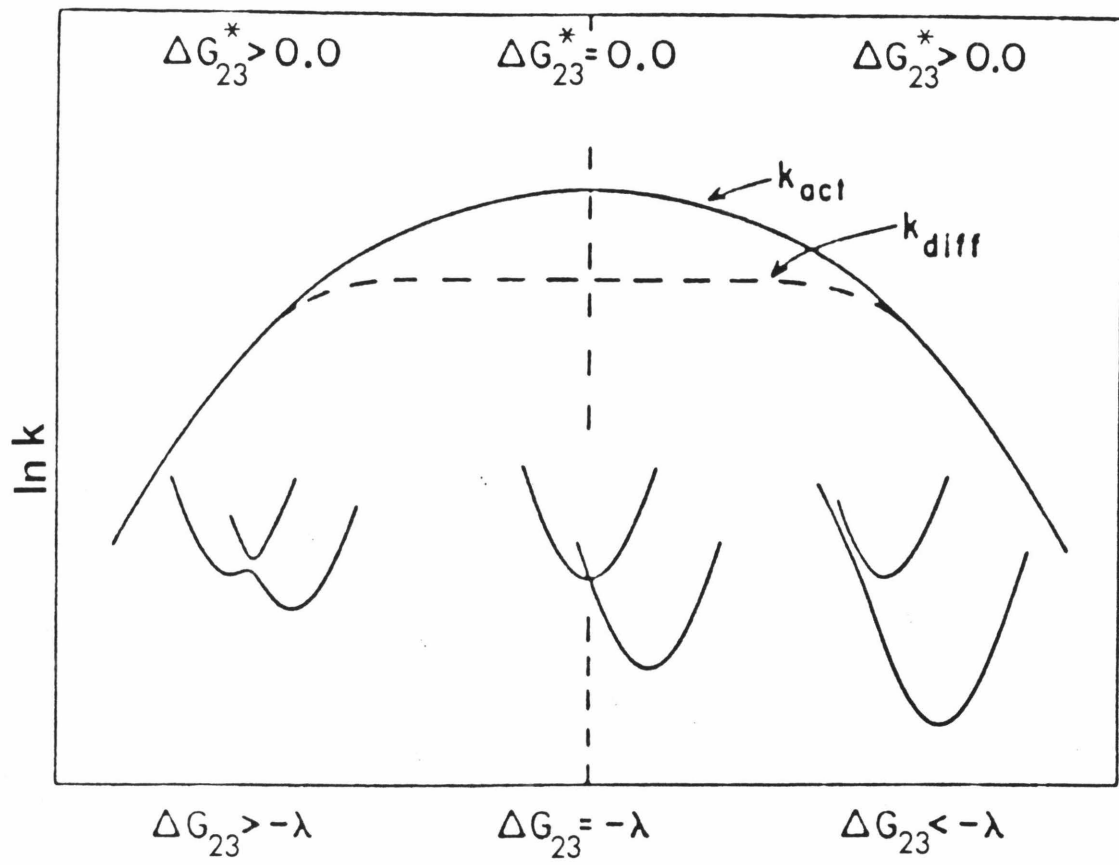


transfer. Furthermore, the rate constants for the quenching of $^3[\text{Ir}(\mu\text{-pz})(\text{COD})]_2^*$ by 2,6-dimethyl-4-methoxy-N-methylpyridinium (13) and 2,4,6-trimethyl-N-methylpyridinium (12), in particular, are consistent with the prediction that the excited state is a very strong reductant with $E^\circ(\text{Ir}_2^+ / ^3\text{Ir}_2^*)$ on the order of -1.7 to -1.8 V vs. SSCE in acetonitrile.

As given by equation (15), the dependence of ΔG_{23}^* on ΔG_{23} for a constant value of λ is such that as ΔG_{23} becomes more negative, ΔG_{23}^* at first decreases until $-\Delta G_{23}$ exceeds λ and ΔG_{23}^* begins to increase. As depicted in Figure 3.7, the region of the curve where $\Delta G_{23} > -\lambda$ is called the "normal region" and where $\Delta G_{23} < -\lambda$ is called the "inverted region." As given by the expression in equation (16), the rate of electron transfer is predicted to decrease with more negative values of ΔG_{23} .^{2,6}

In our quenching study, the rate constant k_q' does not decrease with increasing driving force, but instead becomes diffusion-limited. In practice, the behavior predicted for the "inverted region" has not been observed in a bimolecular electron-transfer reaction.^{3,7,57,58} Several explanations for this have been presented,^{3,7} including the suggestion that diffusion of the reactants limits the value of the observed quenching rate constant,^{58,59} as illustrated in Figure 3.7. Recent intramolecular electron-transfer experiments in organic systems where the "inverted region" has been observed seem to support this since the quenching rates are not diffusion-limited.⁵⁸⁻⁶⁰ Experiments designed to probe these questions in an inorganic system using a pyrazolyl-bridged iridium(I) dimer with metal-metal localized excited

Figure 3.7 Plot of the logarithm of the activation-controlled (k_{act}) and diffusion-limited (k_{diff}) electron-transfer quenching rate constants as a function of increasing driving force in the classical model. The normal free-energy region, $\Delta G_{23} > -\lambda$, is on the left, and the inverted free-energy region, $\Delta G_{23} < -\lambda$, is on the right. The dashed horizontal curve is for a diffusion-controlled reaction, and the case illustrated is for $k_{\text{act}} > k_{\text{diff}}$ when $\Delta G_{23} \sim -\lambda$; under these conditions, the observed rate constant will be equal to k_{diff} (taken from references 2, 5 and 6).



states by attaching the pyridinium acceptor to the complex, are currently underway in our laboratory.^{6 1}

As noted in Chapter 2, $[\text{Ir}(\mu\text{-pz})(\text{COD})]_2$ exhibits luminescence from both singlet and triplet excited states. The phosphorescent $^3\text{B}_2(\text{d}\sigma^* \text{p}\sigma)$ excited state is sufficiently long-lived to undergo bimolecular electron-transfer quenching, as we have demonstrated. The fluorescent $^1\text{B}_2(\text{d}\sigma^* \text{p}\sigma)$ excited state has a lifetime of < 20 ps, and recent experiments using picosecond laser spectroscopy strongly suggest that this excited state does not participate in intermolecular electron-transfer reactions.^{6 2}

Although the conversion of light to chemical energy via the electron-transfer reactivity of $^3[\text{Ir}(\mu\text{-pz})(\text{COD})]_2^*$ is rather facile, the photochemical products rapidly return to starting materials, because the back-electron-transfer reactions are very rapid. To utilize the strong reducing power of the $^3\text{B}_2(\text{d}\sigma^* \text{p}\sigma)$ excited state, the nonproductive back-electron-transfer reaction needs to be inhibited. Several experiments designed to accomplish this have been tried. The electron-transfer quenching of $^3[\text{Ir}(\mu\text{-pz})(\text{COD})]_2^*$ by the pyridinium acceptors leads to the transient mono-cation $[\text{Ir}(\mu\text{-pz})(\text{COD})]_2^+$. In an attempt to trap this cation by an added ligand, the quenching reaction of $^3[\text{Ir}(\mu\text{-pz})(\text{COD})]_2^*$ by 2,6-dimethyl-N-methylpyridinium iodide has been studied. The quenching rate constant k_q is measured by monitoring the decrease in intensity of the phosphorescence with increasing quencher concentration. The data are analyzed using the Stern-Volmer equation shown below where I_0 and I are the emission intensities in the absence and presence of a given amount of quencher (Q), respec-

tively, and τ_0 is the lifetime of the excited state in the absence of quencher (250 ns for ${}^3[\text{Ir}(\mu\text{-pz})(\text{COD})]_2^*$ in CH_3CN).

$$I_0/I = 1 + k_q \tau_0 [Q] \quad (24)$$

This rate has also been measured for the related quencher 2,6-dimethyl-N-methylpyridinium hexafluorophosphate. Both studies are done in acetonitrile solution in the absence of added electrolyte. The quenching rate constants are identical within experimental error ($6.0 \pm 0.3 \times 10^8 \text{ M}^{-1}\text{s}^{-1}$). Furthermore, no build-up of products is observed suggesting that the transient $[\text{Ir}(\mu\text{-pz})(\text{COD})]_2^+$ is not trapped by iodide ion in this experiment. Also, an acetonitrile solution containing $[\text{Ir}(\mu\text{-pz})(\text{COD})]_2$, 2,6-dimethyl-N-methylpyridinium iodide, and excess iodide ion in the form of $(n\text{-C}_4\text{H}_9)_4\text{NI}$ shows no visible absorbance change upon long-term irradiation.

As Caspar and Gray have shown, an effective way to inhibit the unproductive back-electron-transfer reaction is with acceptors that are thermally unstable after the initial electron transfer. The ${}^3\text{B}_2(d\sigma^* p\sigma)$ excited state of $[\text{Ir}(\mu\text{-pz})(\text{COD})]_2$ reacts with a number of halocarbons to give net two-electron Ir(II)-Ir(II) oxidative-addition products. For example, $[\text{Ir}(\mu\text{-pz})(\text{COD})(\text{Cl})]_2$ is formed upon irradiation of $[\text{Ir}(\mu\text{-pz})(\text{COD})]_2$ in the presence of 1,2-dichloroethane, and the complex $\text{Ir}_2(\mu\text{-pz})_2(\text{COD})_2(\text{Cl})(\text{CH}_2\text{Cl})$ is formed upon irradiation with dichloromethane.^{6,3} In addition to Caspar's results with these halocarbons, irradiation of $[\text{Ir}(\mu\text{-pz})(\text{COD})]_2$ in the presence of 1,2-dibromoethane results in a clean and rapid photoreaction to give the

dibromo dimer $[\text{Ir}(\mu\text{-pz})(\text{COD})(\text{Br})]_2$ and ethylene. The qualitative spectral changes observed during the irradiation are shown in Figure 3.8.

A mechanism that accounts for the oxidative addition of halocarbons such as 1,2-dichloroethane and 1,2-dibromoethane has been proposed.^{6 3,6 4} This mechanism involves the oxidative quenching of the triplet excited state as the primary photoprocess to give a radical-anion species that dissociates a halide ion, thereby producing an organic radical. The dissociated halide ion adds to the partially oxidized metal dimer to form a mixed-valence Ir(I)-Ir(II)-X intermediate. In light of recent studies by Saveant, *et al.*,^{6 5} concerning the "extreme instability, if not the inexistence of the RX^\cdot radical anion," the formation of the Ir(I)-Ir(II)-X intermediate might be viewed better as an inner-sphere or atom-transfer process involving electron transfer concomitant with R-X bond cleavage and Ir-X bond formation. This intermediate would then react further with the organic radical (presumably in a second, thermal electron transfer) to form the final X-Ir(II)-Ir(II)-X dihalide dimer.

This mechanism is supported by the product distribution found for the photochemical reactions with 1-bromo-2-chloroethane.^{6 4} At high concentrations of this substrate, the resulting iridium dimer is the dibromide species, $[\text{Ir}(\mu\text{-pz})(\text{COD})(\text{Br})]_2$, exclusively. Low concentrations of 1-bromo-2-chloroethane, however, yield the mixed halide dimer $\text{Ir}_2(\mu\text{-pz})_2(\text{COD})_2(\text{Br})(\text{Cl})$. This result is predicted by the proposed mechanism shown in Figure 3.9 with a concerted electron-transfer, R-Br breaking, Ir-Br forming step leading to the Ir(I)-Ir(II)-Br

Figure 3.8 Spectral changes upon irradiation of a cyclohexane solution of $[\text{Ir}(\mu\text{-pz})(\text{COD})]_2$ and 1,2-dibromoethane ($[\text{Ir}_2] = 3 \times 10^{-5} \text{ M}$, $[\text{C}_2\text{H}_4\text{Br}_2] = 2 \text{ M}$, $22 \pm 2^\circ\text{C}$, $\lambda > 450 \text{ nm}$, spectra recorded approximately 3 minutes apart).

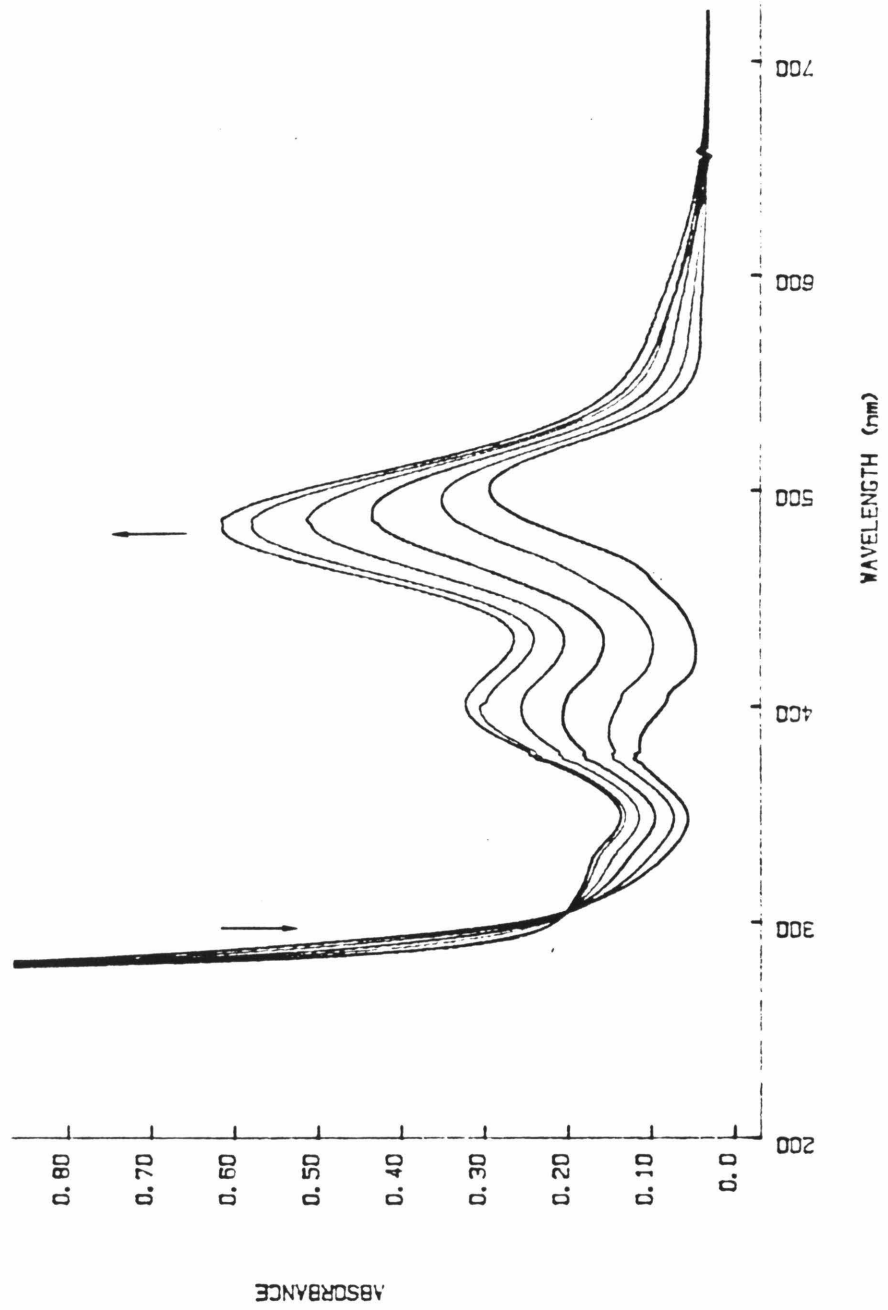
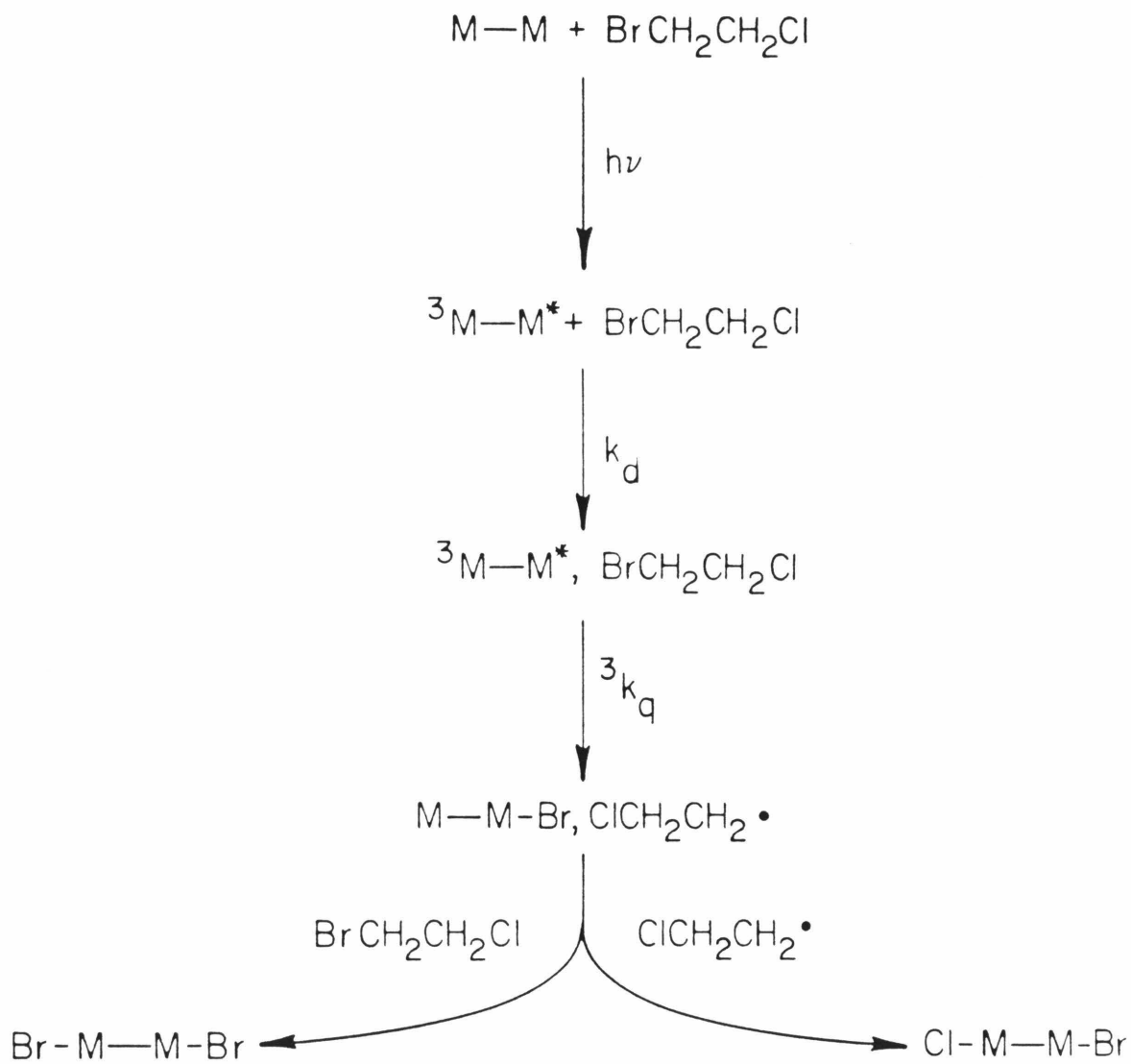


Figure 3.9 Proposed pathways for 1-bromo-2-chloroethane photo-induced oxidative addition to $[\text{Ir}(\mu\text{-pz})(\text{COD})]_2$.



intermediate, consistent with the fact that the C-Br bond is weaker than the C-Cl bond.^{6,6} Photolysis results in formation of $\text{Ir}_2(\mu\text{-pz})_2(\text{COD})_2(\text{Br})$ as the intermediate that can react with another 1-bromo-2-chloroethane molecule, as it does when the latter species is in high concentration, to yield the dibromide dimer, or it can react with the chloroethane radical to yield the mixed halide species. The latter pathway becomes competitive at low halocarbon concentrations. In general, the photoinduced oxidative addition of halocarbons is typical of the photochemistry arising from electron transfer from d^8 - d^8 dimers with the final product being the stable d^7 - d^7 metal-metal bonded dimers. In particular, this same type of photochemistry has been documented for the platinum(II) dimer $[\text{Pt}_2(\text{pop})_4]^{4-}$ ($\text{pop} = \text{P}_2\text{O}_5\text{H}_2^{2-}$)^{6,4,6,7,6,8} suggesting that this reaction may be general for long-lived, strongly reducing excited states of this electronic configuration.

In conclusion, the strongly reducing $^3\text{B}_2(d\sigma^*p\sigma)$ excited state of $[\text{Ir}(\mu\text{-pz})(\text{COD})]_2$ undergoes photoinduced electron transfer with a variety of substrates. Electron transfer to one-electron acceptors such as methyl viologen or pyridinium mono-cations readily occurs with quenchers that have reduction potentials as negative as -1.8 V vs. SSCE.^{6,4,6,9} As has been shown for the series of electronically and structurally related pyridinium hexafluorophosphates in Table 3.1, this reactivity obeys Marcus-theory predictions for adiabatic, outer-sphere electron transfer. With these acceptors, however, back electron transfer to give ground-state products prevents net photochemistry. With acceptors such as halocarbons that are thermally un-

stable after the initial electron transfer, the unproductive back-electron-transfer reaction can be circumvented, and net two-electron, photoinduced electron transfer yields iridium(II)-iridium(II) oxidative addition products.

References and Notes

1. Balzani, V.; Bolletta, F.; Gandolfi, M.T.; Maestri, M. *Top. Curr. Chem.* **1978**, *75*, 1-64.
2. Sutin, N.; Creutz, C. *J. Chem. Ed.* **1983**, *60*, 809-814.
3. Balzani, V.; Scandola, F. in "Energy Resources through Photochemistry and Catalysis"; Gratzel, M., Ed.; Academic Press: New York, 1983; Chapter 1.
4. Julliard, M.; Chanon, M. *Chem. Brit.* **1982**, *18*, 558-562.
5. Sutin, N. *Accts. Chem. Res.* **1982**, *15*, 275-282.
6. Sutin, N. *Prog. Inorg. Chem.* **1983**, *30*, 441-498.
7. Meyer, T.J. *Prog. Inorg. Chem.* **1983**, *30*, 389-441.
8. Balzani, V.; Bolletta, F.; Scandola, F.; Ballardini, R. *Pure Appl. Chem.* **1979**, *51*, 299-311.
9. Balzani, V.; Scandola, F. in "Photochemical Conversion and Storage of Solar Energy"; Connolly, J.S., Ed.; Academic Press: New York, 1981; Chapter 4.
10. Rabani, J., Ed. "Photochemical Conversion and Storage of Solar Energy"; Weizmann Science Press: Jerusalem, 1982.
11. Gratzel, M., Ed. "Energy Resources through Photochemistry and Catalysis"; Academic Press: New York, 1983.
12. Connolly, J.S., Ed. "Photochemical Conversion and Storage of Solar Energy"; Academic Press: New York, 1981.
13. Kalyanasundaram, K. *Coord. Chem. Rev.* **1982**, *46*, 159-244 and references therein.
14. Watts, R.J. *J. Chem. Ed.* **1983**, *60*, 834-842 and references therein.

15. Bock, C.R.; Connor, J.A.; Gutierrez, A.R.; Meyer, T.J.; Whitten, D.G.; Sullivan, B.P.; Nagle, J.K. *J. Am. Chem. Soc.* **1979**, *101*, 4815-4824 and references therein.
16. Sutin, N. *J. Photochem.* **1979**, *10*, 19-40 and references therein.
17. Whitten, D.G. *Accts. Chem. Res.* **1980**, *13*, 83-90 and references therein.
18. Kober, E.M.; Marshall, J.L.; Dressick, W.J.; Sullivan, B.P.; Caspar, J.V.; Meyer, T.J. *Inorg. Chem.* **1985**, *24*, 2755-2763.
19. Sutin, N.; Creutz, C. *Pure Appl. Chem.* **1980**, *52*, 2717-2738 and references therein.
20. Nocera, D.G.; Gray, H.B. *J. Am. Chem. Soc.* **1981**, *103*, 7349-7350.
21. Nocera, D.G.; Gray, H.B. *Inorg. Chem.* **1984**, *23*, 3686-3688.
22. Batterham, T.J. "NMR Spectra of Simple Heterocycles"; John Wiley and Sons: New York, 1973; Chapter 2, Part I.
23. Biellmann, J.F.; Callot, H. *Bull. Soc. Chim. Fr.* **1967**, 397-402.
24. Beak, P.; Mueller, D.S.; Lee, J. *J. Am. Chem. Soc.* **1974**, *96*, 3867-3874.
25. King, L.C.; Ozog, F.J. *J. Org. Chem.* **1955**, *20*, 448-454.
26. For a description of the two-compartment spectrophotometric cell see: Marshall, J.L.; Hopkins, M.D.; Gray, H.B. *ACS Symp. Ser.*, submitted.
27. Nocera, D.G.; Winkler, J.R.; Yocom, K.M.; Bordignon, E.; Gray, H.B. *J. Am. Chem. Soc.* **1984**, *106*, 5145-5150.
28. Rice, S.F.; Gray, H.B. *J. Am. Chem. Soc.* **1983**, *105*, 4571-4575.
29. Milder, S.J.; Goldbeck, R.A.; Kliger, D.S.; Gray, H.B. *J. Am. Chem. Soc.* **1980**, *102*, 6761-6764.

30. Forster, L.S. in "Concepts of Inorganic Photochemistry"; Adamson, A.W.; Fleischauer, P.D., Eds.; John Wiley and Sons: New York, 1975; Chapter 1.
31. Boyd, D.C.; Rodman, G.S.; Mann, K.R. *J. Am. Chem. Soc.* **1986**, *108*, 1779-1784.
32. Bird, C.L.; Kuhn, A.T. *Chem. Soc. Rev.* **1981**, *10*, 49-82.
33. Ledwith, A. *Accts. Chem. Res.* **1972**, *5*, 133-139.
34. Balzani, V.; Moggi, L.; Manfrin, M.F.; Bolletta, F.; Laurence, G.S. *Coord. Chem. Rev.* **1975**, *15*, 321-433.
35. The correction for diffusional effects for the measured electron-transfer quenching rate constant using $r(\text{MV}^{2+}) = 7.8 \text{ \AA}$ and $r(\text{Ir}_2) = 5.0 \text{ \AA}$ is discussed later in this chapter.
36. Turro, N.J. "Modern Molecular Photochemistry"; Benjamin/Cummings: Menlo Park, California, 1978; pp 311-316.
37. Bock, C.R.; Meyer, T.J.; Whitten, D.G. *J. Am. Chem. Soc.* **1974**, *96*, 4710-4712.
38. Kosower, E.M.; Cotter, J.L. *J. Am. Chem. Soc.* **1964**, *86*, 5524-5527.
39. Espenson, J.H. "Chemical Kinetics and Reaction Mechanisms"; McGraw-Hill: New York, 1981; pp 16-21.
40. Hermolin, J.; Levin, M.; Ikegami, Y.; Sawayanagi, M.; Kosower, E.M. *J. Am. Chem. Soc.* **1981**, *103*, 4795-4800.
41. This value of k_b is higher than that previously reported (reference 69). An updated value of $\epsilon(\text{MV}^+) = 13,000 \pm 600 \text{ M}^{-1}\text{cm}^{-1}$ at 605 nm was used to calculate k_b instead of the previously reported value of $\epsilon(\text{MV}^+) = 10,700 \text{ M}^{-1}\text{cm}^{-1}$ (reference 38), and the difference in the two values of k_b reflects this.

42. Janik, B.; Elving, P.J. *Chem. Rev.* **1968**, *68*, 295-319 and references therein.
43. Kosower, E.M. *Top. Curr. Chem.* **1983**, *112*, 117-162 and references therein.
44. Nagle, J.K.; Dressick, W.J.; Meyer, T.J. *J. Am. Chem. Soc.* **1979**, *101*, 3993-3995.
45. Olmstead, M.L.; Hamilton, R.G.; Nicholson, R.S. *Anal. Chem.* **1969**, *41*, 260-267.
46. Connolly, P.; Espenson, J.H.; Bakac, A. *Inorg. Chem.* **1986**, *25*, 2169-2175.
47. Smoluchowski, M. *Z. Phys. Chem.* **1917**, *92*, 129-168.
48. Gordon, A.J.; Ford, R.A. "The Chemist's Companion"; John Wiley and Sons: New York, 1972; pp 107-109.
49. Beveridge, K.A.; Bushnell, G.W.; Stobart, S.R.; Atwood, J.L.; Zaworotko, M.J. *Organometallics* **1983**, *2*, 1447-1451.
50. Rehm, D.; Weller, A. *Isr. J. Chem.* **1970**, *8*, 259-271.
51. Rehm, D.; Weller, A. *Ber. Bunsenges. Chem.* **1969**, *73*, 834-839.
52. Electron-transfer quenching of the excited states of $[\text{Ru}(\text{bpy})_3]^{2+}$ (bpy = 2,2'-bipyridine) and a number of osmium(II) polypyridyl complexes by methyl viologen and several of the pyridinium quenchers listed in Table 3.1 is known to follow the kinetic scheme presented here with back electron transfer to give the ground states of the metal complexes more rapidly than back electron transfer to give the excited states, *i.e.*, $k_{30} \gg k_{32}$ (references 15, 18, and 44). By analogy, electron-transfer quenching of ${}^3[\text{Ir}(\mu\text{-pz})(\text{COD})]_2^*$ by methyl viologen and the pyridinium

acceptors is expected to exhibit this behavior. Further proof of this is that the linear region of the plot of $RT \ln k_q'$ vs. $E(A^{+/o})$ has a slope = 0.48, consistent with the assumption that $k_{30} \gg k_{32}$. If this were not the case, i.e., $k_{32} \gg k_{30}$, the linear region of this plot should have a slope = 1 as discussed in reference 15.

53. Marcus, R.A. *J. Chem. Phys.* **1965**, *43*, 679-701.
54. Marcus, R.A. *J. Chem. Phys.* **1956**, *24*, 966-978.
55. Brunschwig, B.S.; Logan, J.; Newton, M.D.; Sutin, N. *J. Am. Chem. Soc.* **1980**, *102*, 5798-5809.
56. The part of this curve defined by quenchers 7 - 13 is well within the region where $|\Delta G_{23}| \ll 2\lambda$. For quencher 7, $\Delta G_{23} = -0.25$ V, which is less than an estimated value of λ that can be calculated from an unweighted, nonlinear least-squares, three-parameter fit of the data of Tables 3.1 and 3.2 to the logarithmic form of equation (16). Although there is some error in fitting an equation that is approximately parabolic to data for only half of the function, a calculated value of $\lambda \sim 0.97$ V is physically reasonable for the quenching of $^3[\text{Ir}(\mu\text{-pz})(\text{COD})]_2^*$ by the pyridinium quenchers in acetonitrile solution. For comparison, a value of $\lambda = 0.74$ V is estimated for the quenching of the excited state of $[\text{Ru}(\text{bpy})_3]^{2+}$ (bpy = 2,2'-bipyridine) by the bipyridinium quenchers given in Table II of reference 15.
57. Creutz, C.; Sutin, N. *J. Am. Chem. Soc.* **1977**, *99*, 241-243.
58. Miller, J.R.; Beitz, J.V.; Huddleston, R.K. *J. Am. Chem. Soc.* **1984**, *106*, 5057-5068.

59. Miller, J.R.; Calcaterra, L.T.; Closs, G.L. *J. Am. Chem. Soc.* **1984**, *106*, 3047-3049.
60. Calcaterra, L.T.; Closs, G.L.; Miller, J.R. *J. Am. Chem. Soc.* **1983**, *105*, 670-671.
61. Fox, L.S.; Marshall, J.L.; Winkler, J.R.; Gray, H.B., unpublished results.
62. Winkler, J.R.; Marshall, J.L.; Netzel, T.L.; Gray, H.B. *J. Am. Chem. Soc.* **1986**, *108*, 2263-2266.
63. Caspar, J.V.; Gray, H.B. *J. Am. Chem. Soc.* **1984**, *106*, 3029-3030.
64. Marshall, J.L.; Stiegman, A.E.; Gray, H.B. *ACS Symp. Ser.*, **1986**, *307*, 166-176.
65. Andrieux, C.P.; Merz, A.; Saveant, J.M. *J. Am. Chem. Soc.* **1985**, *107*, 6097-6103.
66. Benson, S.W. "Thermochemical Kinetics", 2nd ed.; John Wiley and Sons: New York, 1976; p 309.
67. Roundhill, D.M. *J. Am. Chem. Soc.* **1985**, *107*, 4354-4356.
68. Roundhill, D.M.; Atherton, S.F. *Inorg. Chem.* **1986**, *25*, 4071-4072.
69. Marshall, J.L.; Stobart, S.R.; Gray, H.B. *J. Am. Chem. Soc.* **1984**, *106*, 3027-3029.

Chapter 4

Spectroscopic Studies of
Tetracarbonylbis(μ -pyrazolyl)diiridium(I)
and Related Complexes

Introduction

The synthetic versatility of the pyrazolyl-bridged iridium(I) dimers provides a general route to a variety of binuclear iridium(I) complexes.^{1,2} In addition to the large number of substituted-pyrazolyl-bridged iridium(I) cyclooctadiene dimers that can be prepared from $[\text{Ir}(\text{COD})(\text{Cl})]_2$,³⁻⁵ the displacement of the cyclooctadiene ligands in $[\text{Ir}(\mu\text{-pz})(\text{COD})]_2$ and the substituted-pyrazolyl analogues by carbon monoxide produces tetracarbonylbis(μ -pyrazolyl)diiridium(I) and related complexes.^{6,7} The reactions of these complexes with two equivalents of phosphine (PR_3) results in rapid displacement of one carbonyl ligand from each metal center to give *trans*- $[\text{Ir}(\mu\text{-pz}^*)(\text{CO})(\text{PR}_3)]_2$ (pz^*H = pyrazole or substituted-pyrazole) compounds in high yields.^{8,9}

Our spectroscopic studies of several of the pyrazolyl-bridged and substituted-pyrazolyl-bridged binuclear iridium(I) cyclooctadiene complexes, presented in Chapter 2, indicate that the description of the metal-metal interactions in previously studied D_{4h} d^8 - d^8 rhodium(I), iridium(I), and platinum(II) species¹⁰⁻¹⁷ may be extended to these lower-symmetry (C_{2v}) d^8 - d^8 complexes. Specifically, the ${}^1A_1(d\sigma)^2(d\sigma^*)^2$ ground state is weakly metal-metal bonding and the lowest electronic excited states are a singlet (1B_2) and triplet (3B_2) derived from the $(d\sigma)^2(d\sigma^*)^1(p\sigma)^1$ electronic configuration. Since the luminescent 1B_2 and 3B_2 excited states are derived from 1A_1 by predominantly metal-metal localized transitions, the pyrazolyl-bridged iridium complexes containing ancillary ligands such as carbon monoxide and phosphines

also are predicted to have long-lived luminescent excited states. In fact, luminescence has been observed for several of the tetracarbonyl and dicarbonyl diphosphine binuclear iridium(I) compounds.^{16,18}

This chapter focuses on spectroscopic studies of the series of complexes $[\text{Ir}(\mu\text{-pz})(\text{CO})_2]_2$, $[\text{Ir}(\mu\text{-3-CH}_3\text{pz})(\text{CO})_2]_2$, and $[\text{Ir}(\mu\text{-3,5-(CH}_3)_2\text{pz})(\text{CO})_2]_2$ (pzH = pyrazole, 3-CH₃pzH = 3-methylpyrazole, 3,5-(CH₃)₂pzH = 3,5-dimethylpyrazole). The metal-metal separation in these complexes decreases with increasing substitution of the bridging ligand, and the degree of metal-metal interaction is reflected in the visible absorption and emission spectra at both ambient temperature and 77 K. Photophysical studies of the emissive ${}^{1,3}\text{B}_2(\text{d}\sigma^*\text{p}\sigma)$ excited states suggest that an understanding of the higher-energy excited states is relevant to the photophysical properties of these complexes.

Experimental

Syntheses

Materials.

Acetonitrile (Burdick and Jackson), benzene (Burdick and Jackson), and *n*-hexane (Baker) were reagent grade or better and used as received. Tetrahydrofuran (EM Science) was distilled under nitrogen from calcium hydride (Aldrich, 95+%, -40 mesh) prior to use. Carbon monoxide (Matheson) and 3-methylpyrazole (Aldrich, 97%) were used as received. $[\text{Ir}(\text{COD})(\text{Cl})]_2$, $[\text{Ir}(\mu\text{-pz})(\text{COD})]_2$, and $[\text{Ir}(\mu\text{-3,5-}(\text{CH}_3)_2\text{pz})(\text{COD})]_2$ were prepared by the methods described in Chapter 2.

Inorganic Complexes.

Tetracarbonylbis(μ -pyrazolyl)diiridium(I), $[\text{Ir}(\mu\text{-pz})(\text{CO})_2]_2$, was prepared by a method related to published procedures.^{6,7,9} Under an argon atmosphere using standard Schlenk techniques, $[\text{Ir}(\mu\text{-pz})(\text{COD})]_2$ (0.220g, 0.299 mmol) was dissolved in tetrahydrofuran (50 mL) to give a dark red solution. Carbon monoxide was bubbled through the solution for 45 min at ambient temperature to give a bright yellow solution characteristic of $[\text{Ir}(\mu\text{-pz})(\text{CO})_2]_2$. The solvent was removed under vacuum, leaving a mixture of yellow crystals and blue-black residue that was dissolved in *n*-hexane (50 mL). This solution was filtered, and the product was recrystallized by slow evaporation of the hexane solution with a stream of argon to give yellow crystals of $[\text{Ir}(\mu\text{-pz})(\text{CO})_2]_2$ (0.050 g) and blue-black residue. The air-stable crystals were isolated and dried under vacuum. The residue was redissolved in *n*-hexane (40 mL) and additional product (0.080 g) was isolated in the

same manner. Yield: 0.130 g (69%). Anal. Calcd for $C_{10}H_6N_4O_4Ir_2$: C, 19.05; H, 0.96; N, 8.88. Found: C, 19.15; H, 0.98; N, 8.91. 1H NMR (acetone- d_6): δ 7.93 (d, 2 H, 3,5-H), 6.52 (t, 1 H, 4-H).

Tetracarbonylbis(μ -3-methylpyrazolyl)diiridium(I), $[Ir(\mu\text{-}3\text{-}CH_3\text{pz})\text{-}(CO)_2]_2$, was prepared using standard Schlenk techniques under an argon atmosphere. $[Ir(COD)(Cl)]_2$ (0.300 g, 0.447 mmol) was dissolved in tetrahydrofuran (30 mL) to give an orange-red solution. Excess triethylamine (0.25 mL, 1.8 mmol) and 3-methylpyrazole (0.080 mL, 0.994 mmol) were added to this solution against a counterflow of argon. The reaction mixture was stirred at ambient temperature for 20 h during which time the solution turned purple and solid precipitated. The solvent was removed under vacuum and the $[Ir(\mu\text{-}3\text{-}CH_3\text{pz})(COD)]_2$ product was dissolved in benzene (50 mL). This solution was filtered from the triethylammonium chloride by-product and evaporated to dryness. The solid $[Ir(\mu\text{-}3\text{-}CH_3\text{pz})(COD)]_2$ was dissolved in tetrahydrofuran (50 mL), and carbon monoxide was bubbled through the solution for 2 h at ambient temperature. The yellow-orange solution was evaporated to dryness under vacuum, and the residue was dissolved in acetonitrile (40 mL). This solution was filtered, and the $[Ir(\mu\text{-}3\text{-}CH_3\text{pz})(CO)_2]_2$ product was crystallized by slow evaporation of the solvent with a stream of argon. The air-stable, crystalline product was washed with ice-cold acetonitrile (2 mL) and dried under vacuum. Yield: 0.210 g (71%). Anal. Calcd for $C_{12}H_{10}N_4O_4Ir_2$: C, 21.88; H, 1.53; N, 8.51. Found: C, 22.08; H, 1.55; N, 8.51. 1H NMR (acetone- d_6): δ 7.72 (d, 1 H, 5-H), 7.71 (d, 1 H, 5-H), 6.31 (m, 2 H, 4-H), 2.42 (s, 3 H, 3- CH_3), 2.41 (s, 3 H, 3- CH_3).

Tetracarbonylbis(μ -3,5-dimethylpyrazolyl)diiridium(I), $[\text{Ir}(\mu\text{-3,5-}(\text{CH}_3)_2\text{pz})(\text{CO})_2]_2$, was prepared using standard Schlenk techniques under an argon atmosphere. Carbon monoxide was bubbled through a tetrahydrofuran solution (100 mL) of $[\text{Ir}(\mu\text{-3,5-}(\text{CH}_3)_2\text{pz})(\text{COD})]_2$ (0.925 g, 1.17 mmol) for 8 h at ambient temperature. The initial purple solution had turned orange by the end of the reaction, indicative of formation of $[\text{Ir}(\mu\text{-3,5-}(\text{CH}_3)_2\text{pz})(\text{CO})_2]_2$. The solvent was removed under vacuum and the residue was dissolved in *n*-hexane. This solution was filtered, slightly heated, and evaporated to give a saturated solution of the product at 40-45°C that was refrigerated for 24 h to give large orange crystals of $[\text{Ir}(\mu\text{-3,5-}(\text{CH}_3)_2\text{pz})(\text{CO})_2]_2$. The air-stable crystals were collected, washed with ice-cold hexane (5 mL), and dried under vacuum. The remaining solution was slowly evaporated with a stream of argon to yield a second crop of smaller crystals of the product that were dried under vacuum. Yield: 0.660 g (82%). Anal. Calcd for $\text{C}_{14}\text{H}_{14}\text{N}_4\text{O}_4\text{Ir}_2$: C, 24.49; H, 2.05; N, 8.16. Found: C, 24.50; H, 2.09; N, 8.24. ^1H NMR (acetone- d_6): δ 6.10 (s, 1 H, 4-H), 2.35 (s, 6 H, 3,5- CH_3).

Physical Measurements

Materials.

Solvents for the absorption, emission, and lifetime measurements were purified, if necessary, degassed with a minimum of five freeze-pump-thaw cycles on a high-vacuum line (limiting pressure $< 10^{-3}$ torr), and bulb-to-bulb distilled into glass round-bottomed storage flasks equipped with Teflon vacuum valves. Acetonitrile (Burdick and Jackson, UV Grade) was used as received, degassed, and stored over

alumina (Woelm N, Activity Grade 1, obtained from ICN Nutritional Biochemicals) that had been activated by heating under dynamic vacuum ($< 10^{-3}$ torr) for 24 h. 2-Methylpentane (Phillips Petroleum) was refluxed over lithium aluminum hydride (Alfa, 95%), degassed, and stored over lithium aluminum hydride.

For the measurement of several of the absorption spectra and the molar extinction coefficients of the iridium complexes, which are moderately air-stable in solution, *n*-hexane (Baker, "Photrex" Grade) from a freshly opened bottle was used.

Ruthenium tris(2,2'-bipyridine) di(hexafluorophosphate), $[\text{Ru}(\text{bpy})_3](\text{PF}_6)_2$, was obtained from Dr. Michael D. Hopkins and recrystallized from a solution of acetonitrile (Burdick and Jackson) and toluene (Baker) before use.

Carbon-13 monoxide (Monsanto, 99%), acetone- d_6 (Aldrich, 99+atom% D, Gold Label), and tetramethylsilane (Aldrich, 99.9+%, NMR Grade) were used as received.

The carbon-13 labeled $[\text{Ir}(\mu\text{-pz})(^{13}\text{CO})_2]_2$ complex was prepared *in situ* for the spectroscopic experiments by blanketing a 2-methylpentane solution of $[\text{Ir}(\mu\text{-pz})(\text{COD})]_2$ in a spectrophotometric cell with carbon-13 monoxide gas on a high-vacuum line. The exchange of the cyclooctadiene ligands for carbon monoxide was complete upon mixing of the solution.

Electronic Absorption Spectroscopy.

Electronic absorption spectra were measured using either a Cary 17 or Hewlett-Packard 8450A spectrophotometer. The samples were prepared by the methods given in Chapter 2. The electronic absorption spectra

at 77 K were measured using a quartz optical dewar of local design. The absorption spectra of the complexes in aerated solutions are identical with those in degassed solutions.

Electronic Emission Spectroscopy.

The emission spectra were measured using an emission spectrophotometer constructed at Caltech which has been described previously.¹⁴ The samples for both the ambient temperature and 77 K measurements were prepared by the methods given in Chapter 2. Highly dilute solutions of the complexes in 2-methylpentane were used for the quantum yield measurements.¹⁹ An acetonitrile solution of $[\text{Ru}(\text{bpy})_3](\text{PF}_6)_2$, which has a quantum yield for emission of 0.062 at ambient temperature,²⁰ was used as the standard. The indexes of refraction of 2-methylpentane (1.3716) and acetonitrile (1.3440) are very similar, so no correction (n_1^2/n_2^2) for the difference between them was made. For these measurements, the excitation wavelength was the 436 nm Hg line from a medium-pressure Hg/Xe arc lamp that was filtered with an Oriel 5645 interference filter. For the 77 K emission measurements, the samples were held in a liquid-nitrogen-filled quartz finger dewar. The emission intensities were corrected for spectrometer response²¹ by digitally recording the data *via* a computer interface (On Line Instrument Systems, Inc.; Model 3820 data collection system) and processing with an internal computer program.

Emission Lifetime Measurements.

Emission lifetime measurements were made with a Nd:YAG pulsed laser system which has been described previously²² using 532 nm excitation. The solutions for the ambient temperature, 77 K, and vari-

able temperature measurements were prepared by the procedures outlined in Chapter 2. All of the emission intensity decays exhibited first-order kinetics over at least 3 half-lives. For the measurements at 77 K, the samples were held in a liquid-nitrogen-filled quartz finger dewar. For the variable temperature measurements between 150 and 300 K, a continuous-flow nitrogen gas dewar was used. The sample temperature was monitored with a calibrated copper/constantan thermocouple. The laser was operated at low power to minimize local sample heating.

Additional Measurements.

^1H NMR spectra were recorded at 400 MHz on a JEOL GX-400 spectrometer. Chemical shifts are reported in ppm (δ) vs. tetramethylsilane.

Elemental analyses were obtained by Mr. Larry Henling at the Caltech Analytical Laboratory.

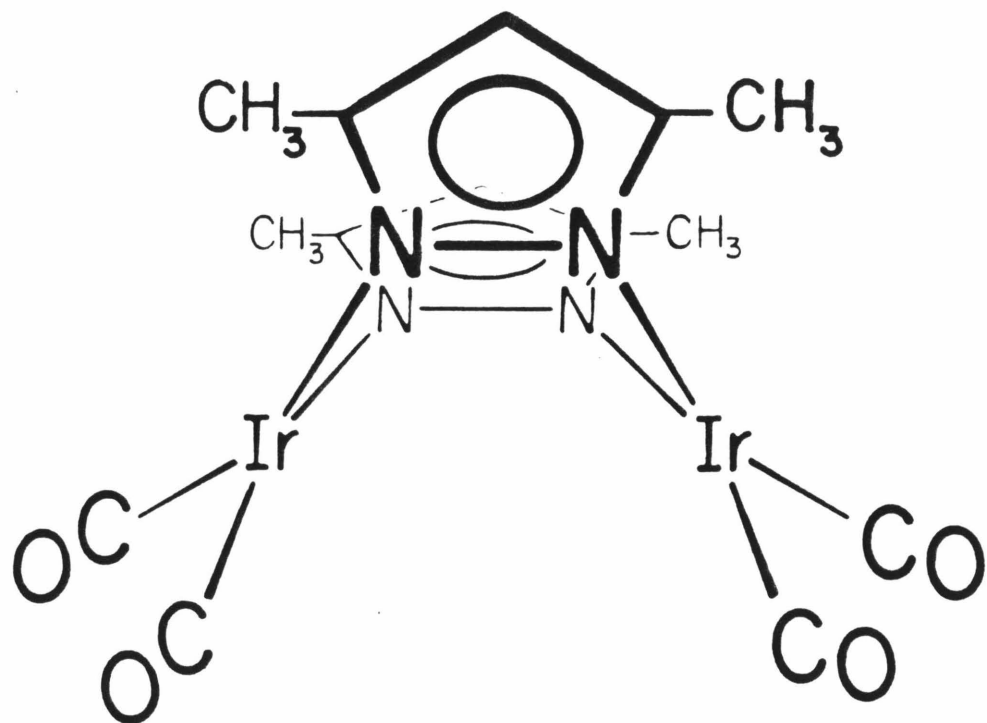
Results and Discussion

The complex $[\text{Ir}(\mu\text{-pz})(\text{CO})_2]_2$, obtained from the reaction between $[\text{Ir}(\mu\text{-pz})(\text{COD})]_2$ and carbon monoxide, was originally reported to be stable only in solution in the presence of excess carbon monoxide.⁹ Recently, however, $[\text{Ir}(\mu\text{-pz})(\text{CO})_2]_2$ has been isolated by slow evaporation or extended cooling of hexane solutions.^{6,7} In addition, X-ray crystal structure determinations of $[\text{Ir}(\mu\text{-pz})(\text{CO})_2]_2$ by two independent research groups have shown that this complex adopts a conformation similar to that of $[\text{Ir}(\mu\text{-pz})(\text{COD})]_2$ with an iridium-iridium separation of 3.510(1) Å.^{6,7,23} The substituted-pyrazolyl complex $[\text{Ir}(\mu\text{-3,5-(CH}_3)_2\text{pz})(\text{CO})_2]_2$ is easier to isolate, and an X-ray crystal structure determination has shown that it adopts a similar conformation but has a much shorter metal-metal distance (3.245 Å).⁷ The iridium-iridium distances are influenced by steric interactions of the ligands and are shortened with substitution at the 3- and 5-positions of the bridging-pyrazolyl ligands. From the structural data, the $\text{N}_1\text{-Ir-N}_2$, $\text{N}_2\text{-Ir-C}_1$, $\text{C}_1\text{-Ir-C}_2$, and $\text{C}_2\text{-Ir-N}_1$ angles are approximately 90° for both complexes. The average Ir-N-N angle in $[\text{Ir}(\mu\text{-3,5-(CH}_3)_2\text{pz})(\text{CO})_2]_2$ (117°) is smaller than that of $[\text{Ir}(\mu\text{-pz})(\text{CO})_2]_2$ (123°) and reflects the steric influence of the 3,5-dimethylpyrazolyl bridge.⁷ The structures of these compounds are shown in Figure 4.1.

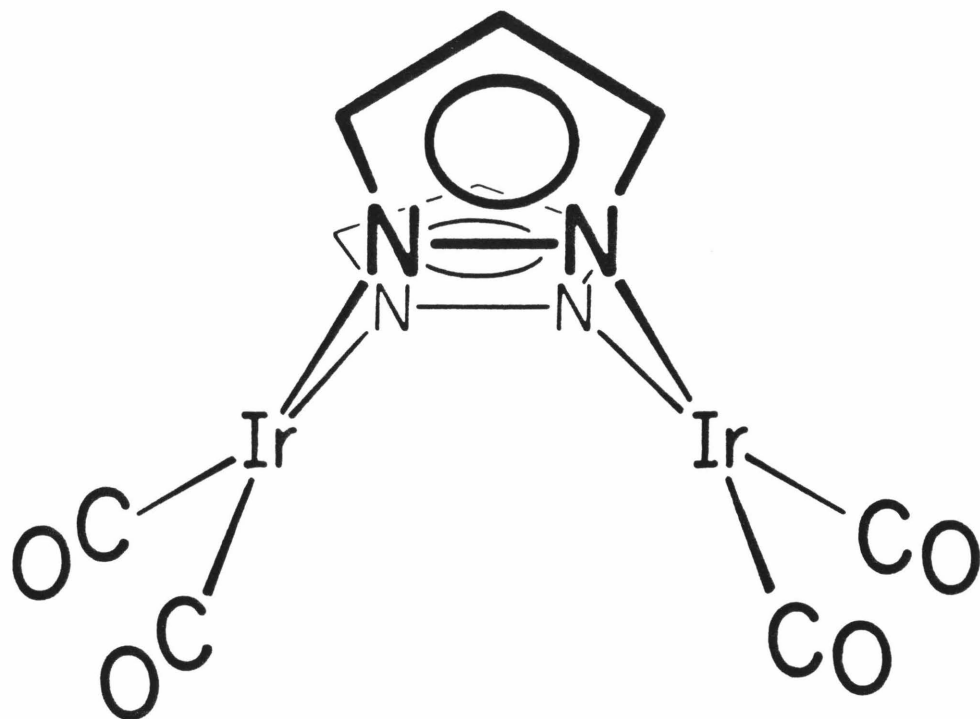
Because of our interest in systematically studying the metal-metal interactions of $d^8\text{-}d^8$ binuclear complexes in the ground and lowest-energy excited states, we also prepared $[\text{Ir}(\mu\text{-3-CH}_3\text{pz})(\text{CO})_2]_2$, which is expected to have an iridium-iridium separation between those of

Figure 4.1 Structures of (a) $[\text{Ir}(\mu\text{-}3,5\text{-}(\text{CH}_3)_2\text{pz})(\text{CO})_2]_2$ and (b) $[\text{Ir}(\mu\text{-pz})(\text{CO})_2]_2$.

A



B

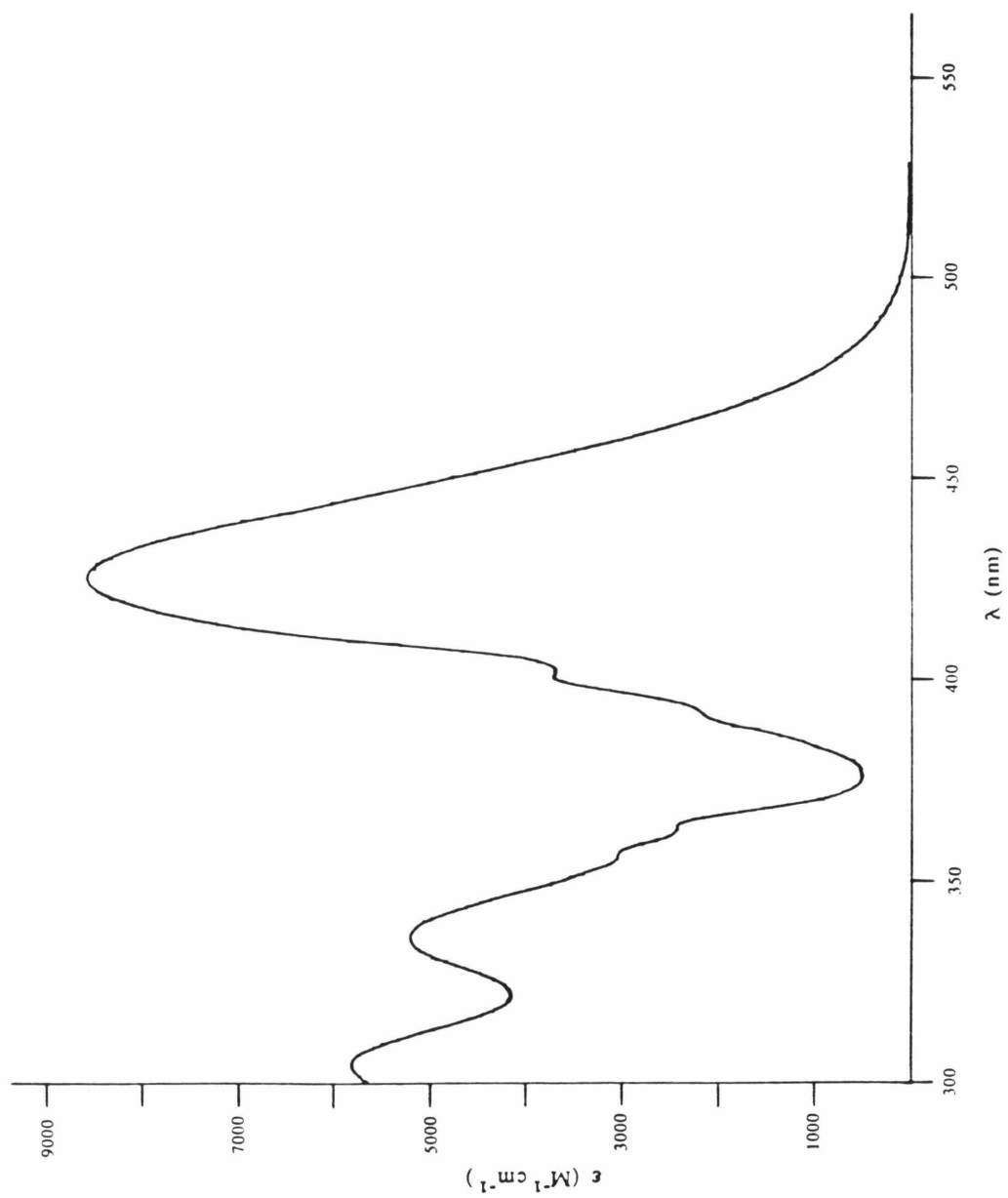


$[\text{Ir}(\mu\text{-pz})(\text{CO})_2]_2$ and $[\text{Ir}(\mu\text{-3,5-(CH}_3)_2\text{pz})(\text{CO})_2]_2$. The ^1H NMR spectrum of $[\text{Ir}(\mu\text{-3-CH}_3\text{pz})(\text{CO})_2]_2$ suggests that this compound is a mixture of diastereomers that results from the asymmetry of the 3-methylpyrazolyl bridge. In the ^1H NMR spectrum, doublets at δ 7.72 ppm and 7.71 ppm are assigned to the 5-H resonances of the 3-methylpyrazolyl ligand in the two isomers; singlets at δ 2.42 ppm and 2.41 ppm correspond to the 3-CH₃ protons of the two isomers. The 4-H bridge protons are not resolved; therefore, a multiplet at δ 6.31 ppm is observed. The integrated intensities of the 5-H and 3-CH₃ signals suggest a 1:1 ratio for the isomers. The ^1H NMR spectrum of $[\text{Ir}(\mu\text{-3-CH}_3\text{pz})(\text{CO})_2]_2$ is consistent with Stobart's observation that the complex $[\text{Ir}(\mu\text{-3-CH}_3\text{pz})(\text{COD})]_2$ is a 1:1 diastereomeric mixture.³ Even though $[\text{Ir}(\mu\text{-3-CH}_3\text{pz})(\text{CO})_2]_2$ is a mixture of two isomers, the spectroscopic and photophysical properties of each isomer are likely to be very similar, based on the spectroscopic studies of $[\text{Ir}(\mu\text{-3-CH}_3\text{-5-CF}_3\text{pz})(\text{COD})]_2$ that are presented in Chapter 2.

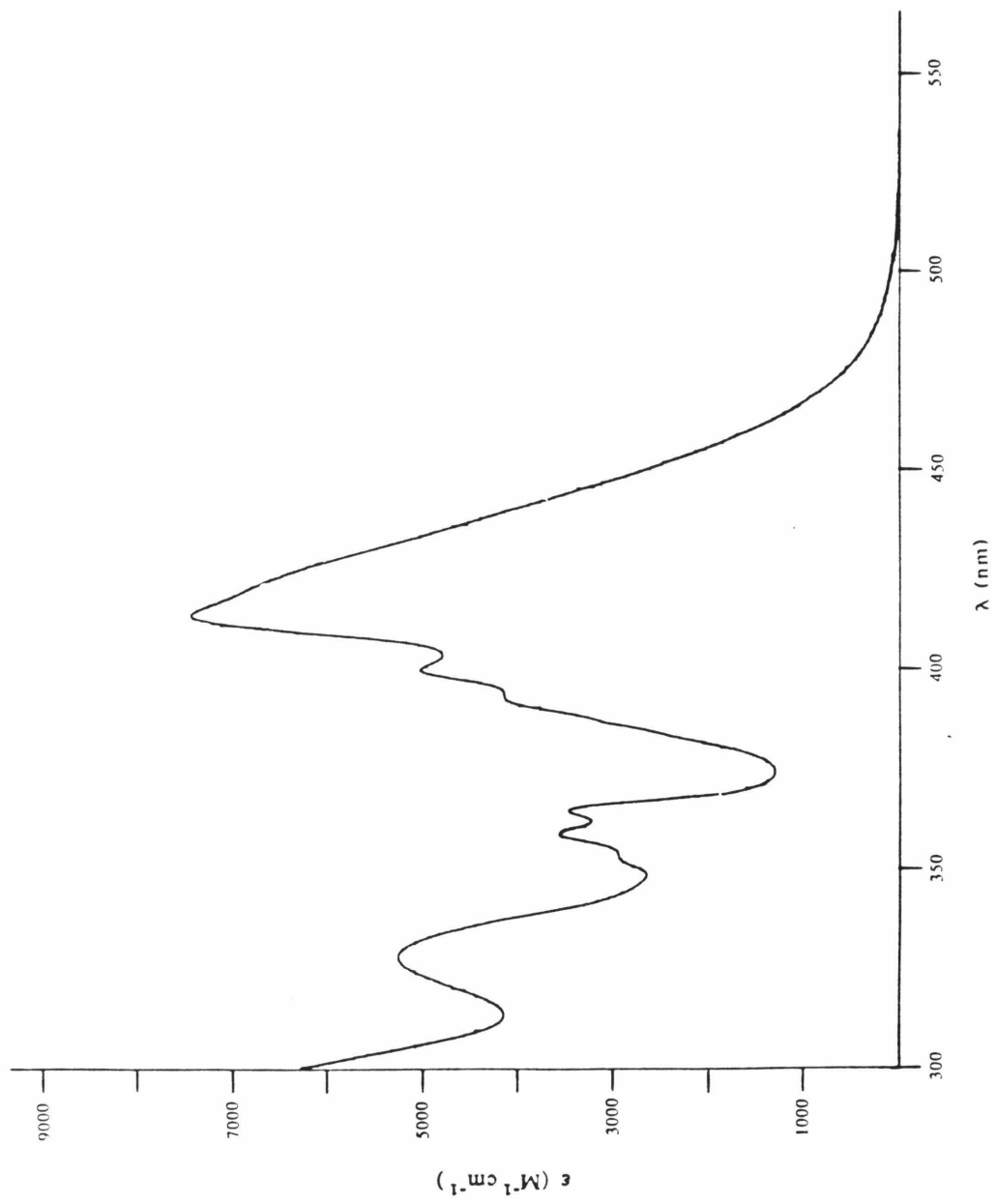
The electronic absorption spectra of $[\text{Ir}(\mu\text{-3,5-(CH}_3)_2\text{pz})(\text{CO})_2]_2$, $[\text{Ir}(\mu\text{-3-CH}_3\text{pz})(\text{CO})_2]_2$, and $[\text{Ir}(\mu\text{-pz})(\text{CO})_2]_2$ in *n*-hexane solutions at ambient temperature are shown in Figure 4.2. The absorption spectrum of $[\text{Ir}(\mu\text{-3,5-(CH}_3)_2\text{pz})(\text{CO})_2]_2$ resembles that of $[\text{Ir}(\mu\text{-pz})(\text{COD})]_2$, in some respects, and the lowest-energy intense band is suggested to correspond to the predominantly metal-metal localized $^1\text{A}_1 \rightarrow ^1\text{B}_2$ ($\sigma^*(d_{z^2}) \rightarrow [\sigma(p_z), \pi^*(\text{CO})]$) transition. Since the iridium-iridium separation in $[\text{Ir}(\mu\text{-3,5-(CH}_3)_2\text{pz})(\text{CO})_2]_2$ (3.245 Å) is similar to that of $[\text{Ir}(\mu\text{-pz})(\text{COD})]_2$ (3.216(1) Å),⁵ the energy of the $^1\text{A}_1 \rightarrow ^1\text{B}_2$ transition is not solely determined by the metal-metal distance but is

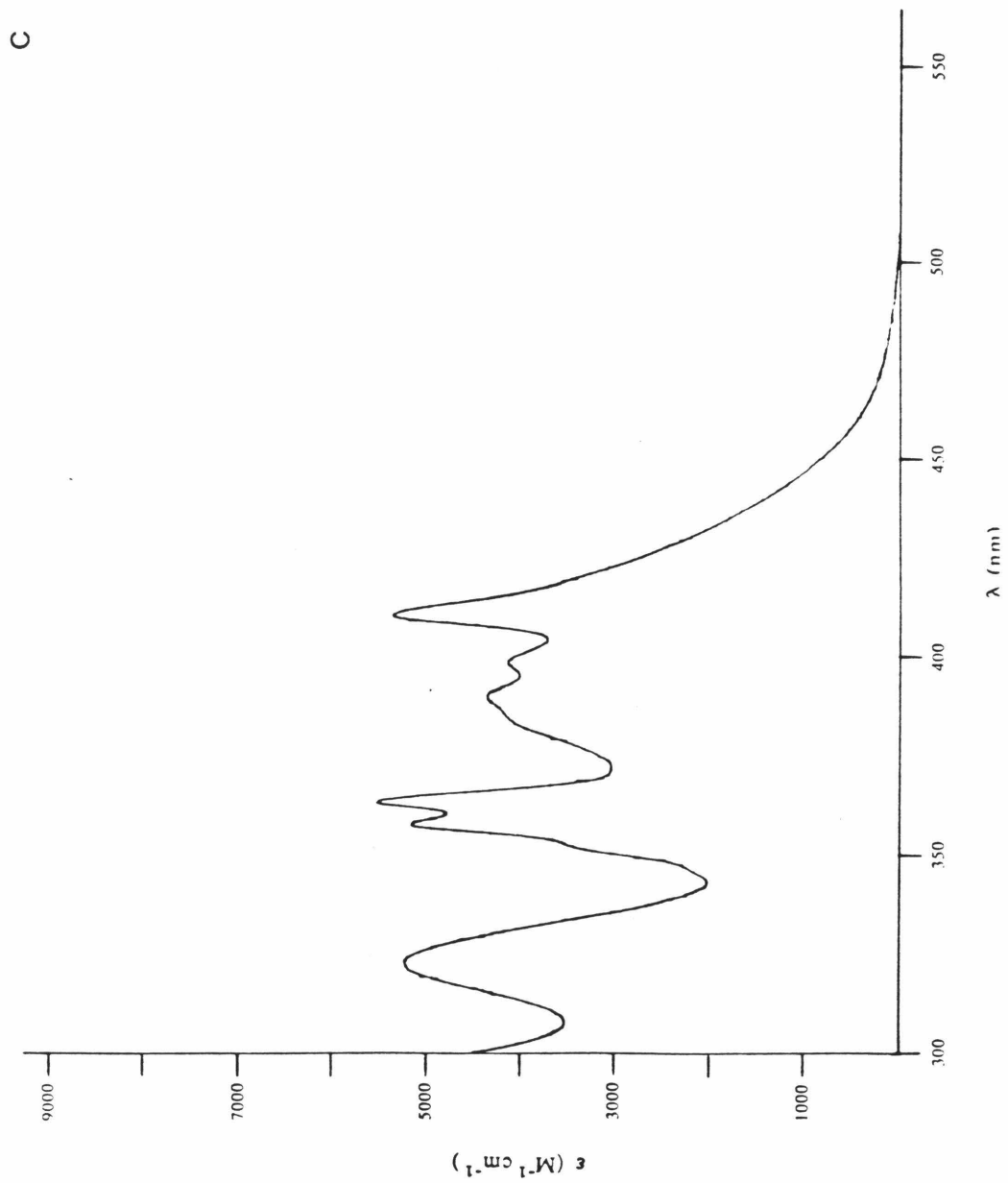
Figure 4.2 Electronic absorption spectra of (a) $[\text{Ir}(\mu\text{-3,5-}(\text{CH}_3)_2\text{pz})(\text{CO})_2]_2$, (b) $[\text{Ir}(\mu\text{-3-CH}_3\text{pz})(\text{CO})_2]_2$, and (c) $[\text{Ir}(\mu\text{-pz})(\text{CO})_2]_2$ at $22 \pm 2^\circ\text{C}$ (*n*-hexane solutions).

A



B





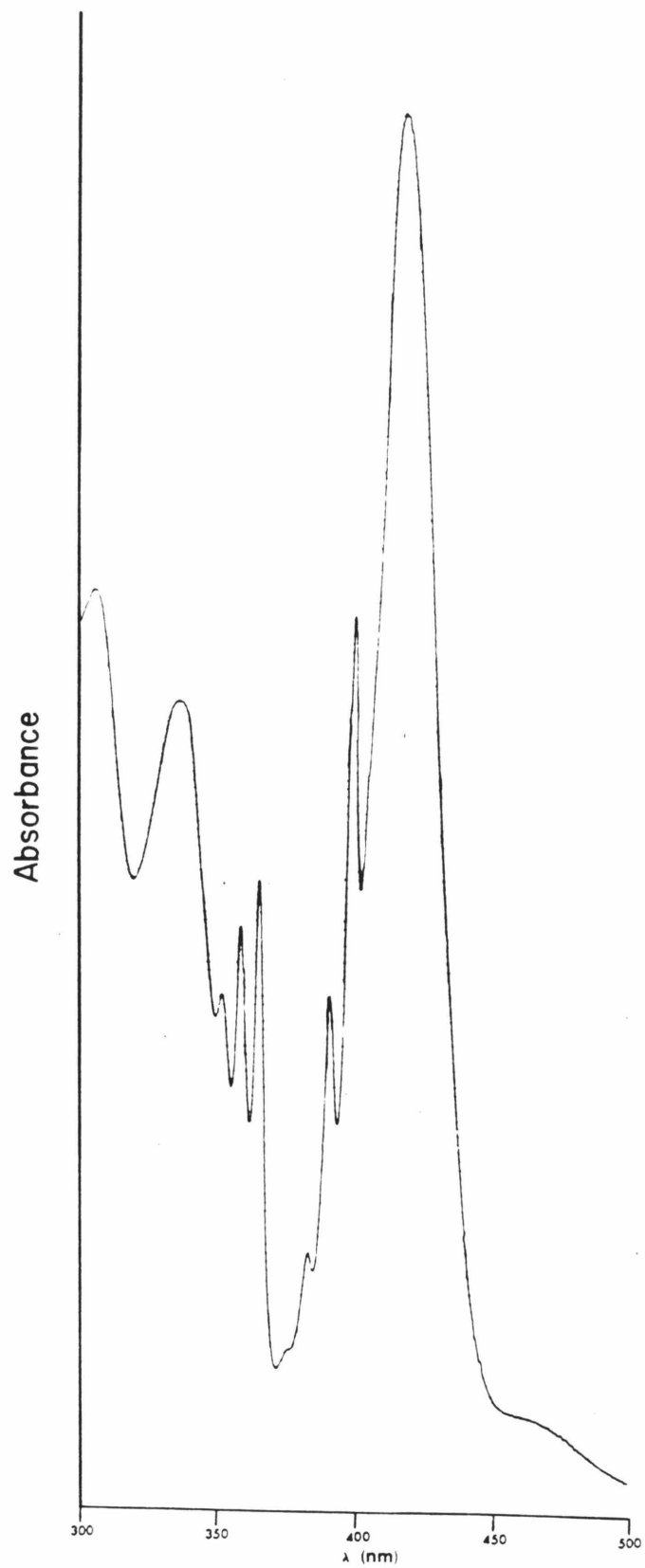
apparently influenced by the ancillary ligands.¹⁶ Interestingly, two bands that exhibit vibrational fine structure are shoulders on the high-energy side of the band corresponding to the ${}^1A_1 \rightarrow {}^1B_2$ transition and on the low-energy side of a band at ~ 336 nm. This becomes more apparent from a comparison of the electronic absorption spectra of $[\text{Ir}(\mu\text{-}3\text{-CH}_3\text{pz})(\text{CO})_2]_2$ and $[\text{Ir}(\mu\text{-pz})(\text{CO})_2]_2$, shown in Figure 4.2. The predominantly metal-metal localized $\sigma^*(d_z^2) \rightarrow [\sigma(p_z), \pi^*(\text{CO})]$ transition shifts to higher energy with increasing metal-metal separation, as expected, and begins to overlap the lowest-energy vibronically structured band.

Upon cooling to 77 K, the vibronically structured bands in the absorption spectrum of each complex sharpen considerably; the spectra are shown in Figure 4.3. The structured bands located at 365 nm in each spectrum, at 398 nm in the spectra of $[\text{Ir}(\mu\text{-}3,5\text{-(CH}_3)_2\text{pz})(\text{CO})_2]_2$ and $[\text{Ir}(\mu\text{-}3\text{-CH}_3\text{pz})(\text{CO})_2]_2$, and at 410 nm in the spectrum of $[\text{Ir}(\mu\text{-pz})(\text{CO})_2]_2$, show vibrational progressions of *ca.* 500 cm^{-1} that are attributed to $\nu(\text{Ir-C})$. Isotopic labeling of $[\text{Ir}(\mu\text{-pz})(\text{CO})_2]_2$ with ${}^{13}\text{CO}$ shows the expected decrease in $\nu(\text{Ir-C})$ in its 77 K absorption spectrum. The enhancement of the metal-metal interaction in these complexes is manifested by the shift of the $\sigma^*(d_z^2) \rightarrow [\sigma(p_z), \pi^*(\text{CO})]$ transition to lower energy with the increase in methyl-substitution of the pyrazolyl ligand. Cooling of a sample of $[\text{Ir}(\mu\text{-}3,5\text{-(CH}_3)_2\text{pz})(\text{CO})_2]_2$ in a Nujol mull to 16 K does not result in further resolution of the spectral features.²⁴

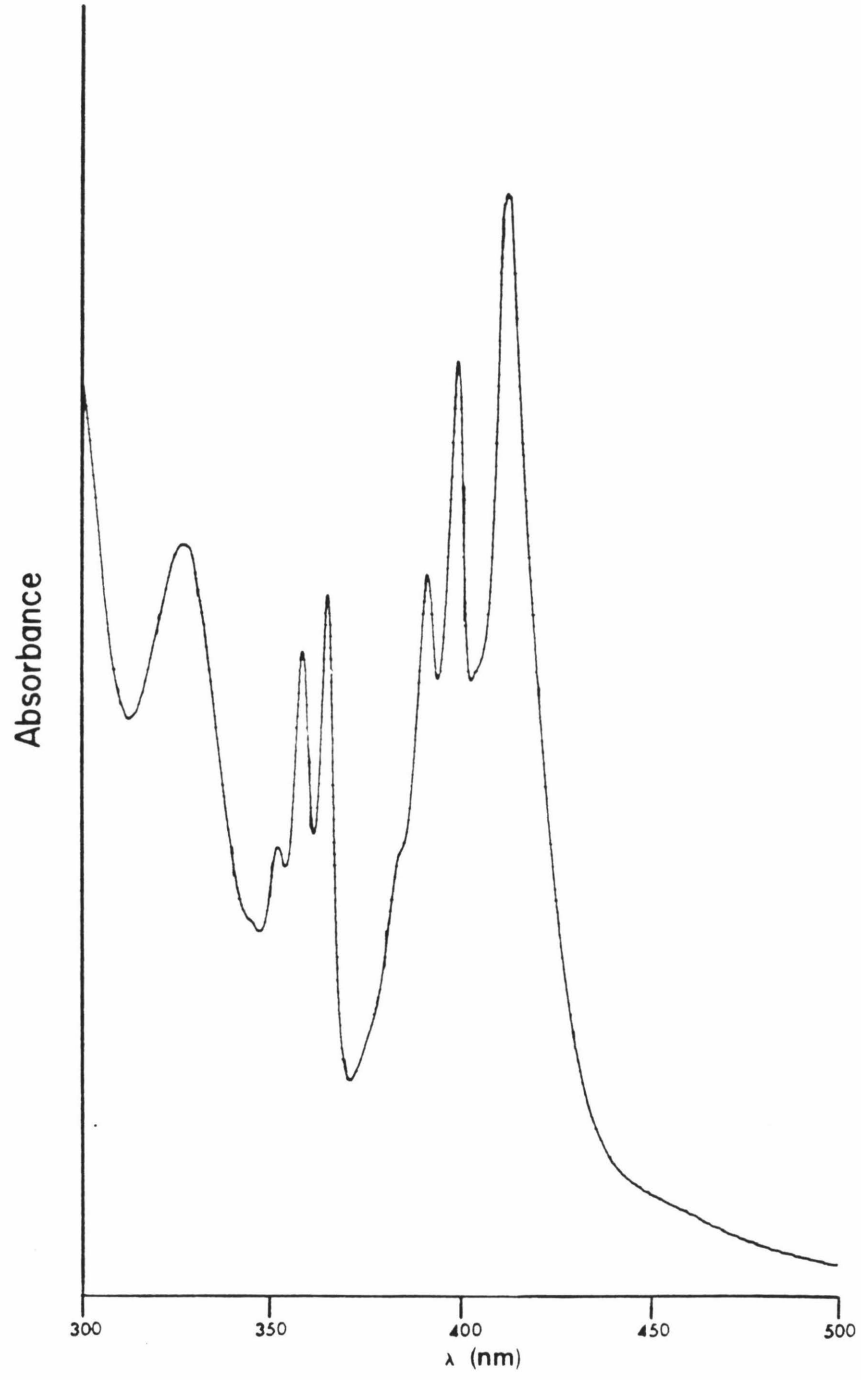
In the context of the molecular orbital diagram for the interaction of two d^8 metal ions complexed with carbon monoxide ligands,

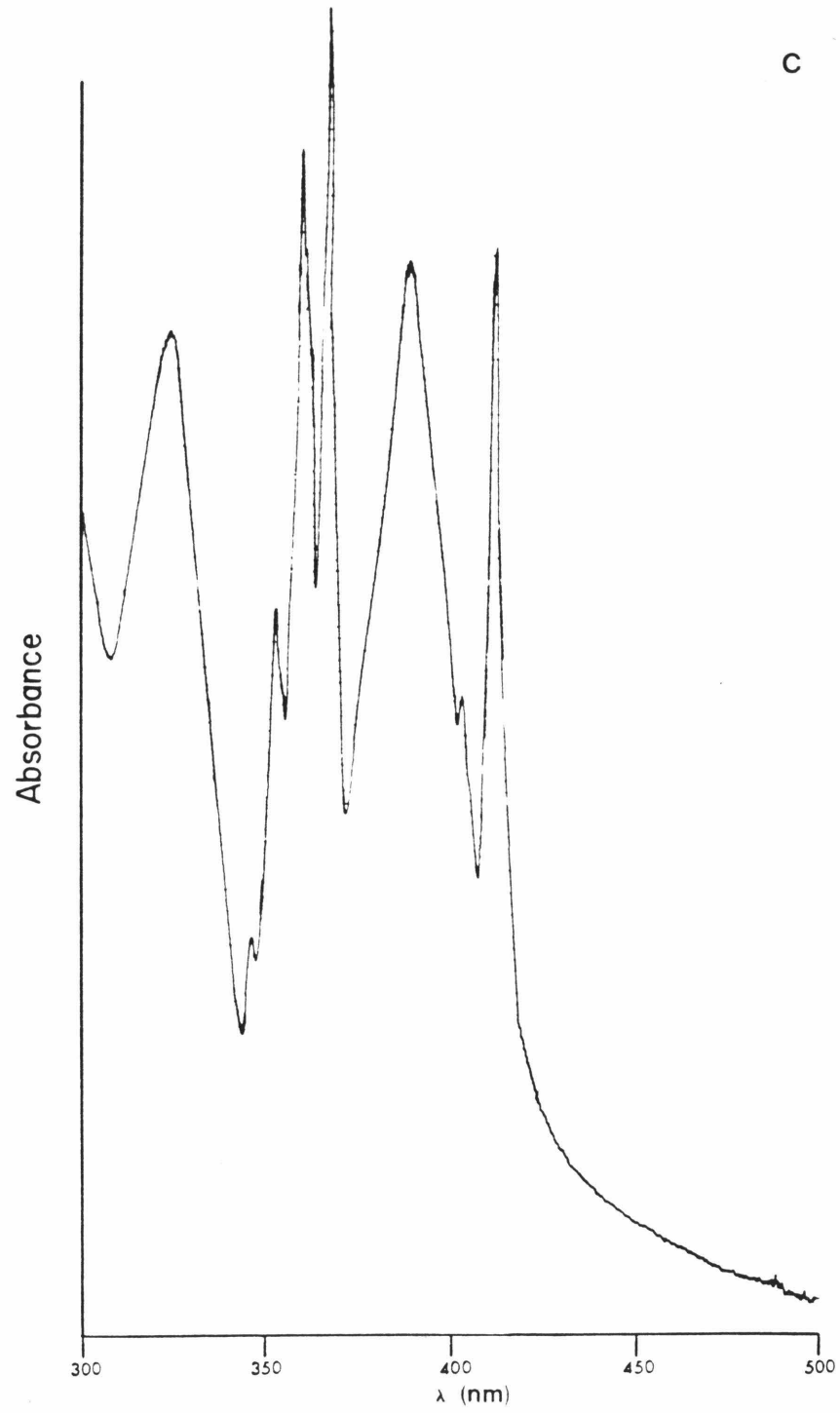
Figure 4.3 Electronic absorption spectra of (a) $[\text{Ir}(\mu\text{-}3,5\text{-}(\text{CH}_3)_2\text{pz})(\text{CO})_2]_2$, (b) $[\text{Ir}(\mu\text{-}3\text{-CH}_3\text{pz})(\text{CO})_2]_2$, and (c) $[\text{Ir}(\mu\text{-pz})(\text{CO})_2]_2$ at 77 K (2-methylpentane glasses).

A



B





shown in Figure 4.4,²⁵ assignments for the major bands in the spectra of these pyrazolyl-bridged binuclear iridium(I) carbonyl complexes may be suggested.²⁶ From the spectra recorded at 77 K, the bands at 415 nm for $[\text{Ir}(\mu\text{-}3,5\text{-}(\text{CH}_3)_2\text{pz})(\text{CO})_2]_2$, 411 nm for $[\text{Ir}(\mu\text{-}3\text{-CH}_3\text{pz})(\text{CO})_2]_2$, and 388 nm for $[\text{Ir}(\mu\text{-pz})(\text{CO})_2]_2$ are assigned to the predominantly metal-metal localized $\sigma^*(d_{z^2}) \rightarrow [\sigma(p_z), \pi^*(\text{CO})]$ transition. The two vibronically structured bands, which are less dependent on the metal-metal separation, are proposed to correspond to $d\pi(xz, yz) \rightarrow [\sigma(p_z), \pi^*(\text{CO})]$ transitions.²⁷

The $[\text{Ir}(\mu\text{-}3,5\text{-}(\text{CH}_3)_2\text{pz})(\text{CO})_2]_2$, $[\text{Ir}(\mu\text{-}3\text{-CH}_3\text{pz})(\text{CO})_2]_2$, and $[\text{Ir}(\mu\text{-pz})(\text{CO})_2]_2$ complexes are similar to the pyrazolyl-bridged iridium(I) cyclooctadiene dimers in that both fluorescence and phosphorescence from the $^1\text{B}_2(d\sigma^* p\sigma)$ and $^3\text{B}_2(d\sigma^* p\sigma)$ excited states are observed at ambient temperature in fluid solution. The emission spectra are shown in Figure 4.5, and the corresponding band maxima and quantum yields for the luminescent excited states are listed in Table 4.1. Interestingly, both the fluorescence and phosphorescence quantum yields for these carbonyl complexes are considerably higher than those of the cyclooctadiene species, and the emission yields of the $^3\text{B}_2(d\sigma^* p\sigma)$ excited state of the carbonyl dimers rival that of $[\text{Ru}(\text{bpy})_3](\text{PF}_6)_2$.²⁸

The emission intensities and lifetimes of the $^3\text{B}_2(d\sigma^* p\sigma)$ excited states of $[\text{Ir}(\mu\text{-}3,5\text{-}(\text{CH}_3)_2\text{pz})(\text{CO})_2]_2$, $[\text{Ir}(\mu\text{-}3\text{-CH}_3\text{pz})(\text{CO})_2]_2$, and $[\text{Ir}(\mu\text{-pz})(\text{CO})_2]_2$ are temperature-dependent. Upon cooling to 77 K, the fluorescence and phosphorescence bands sharpen and shift to higher energies. The phosphorescence intensity shows a dramatic enhancement with the decrease in temperature. The corrected emission spectra of

Figure 4.4 Molecular orbital diagram for pyrazolyl-bridged binuclear iridium(I) carbonyl complexes of C_{2v} symmetry.

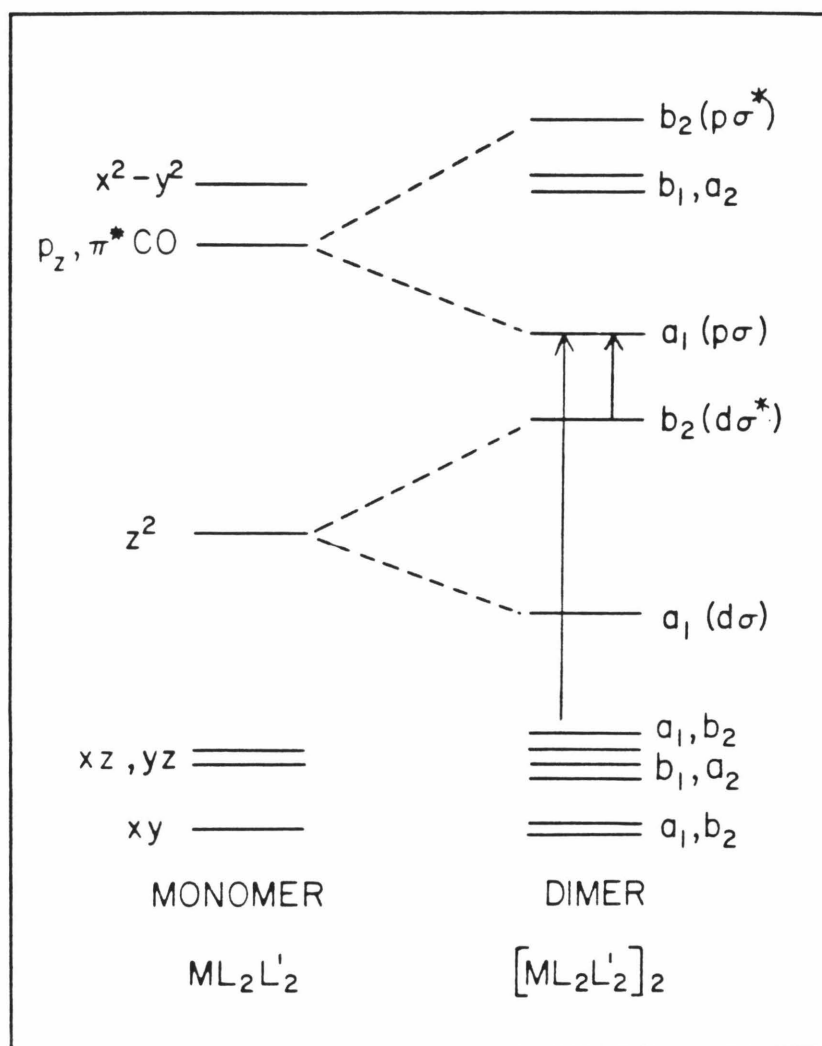


Figure 4.5 Corrected emission spectra of (1) $[\text{Ir}(\mu\text{-}3,5\text{-}(\text{CH}_3)_2\text{pz})(\text{CO})_2]_2$, (2) $[\text{Ir}(\mu\text{-}3\text{-CH}_3\text{pz})(\text{CO})_2]_2$, (3) $[\text{Ir}(\mu\text{-pz})(\text{CO})_2]_2$ at ambient temperature (2-methylpentane solutions). The spectra are scaled to the same sensitivity.

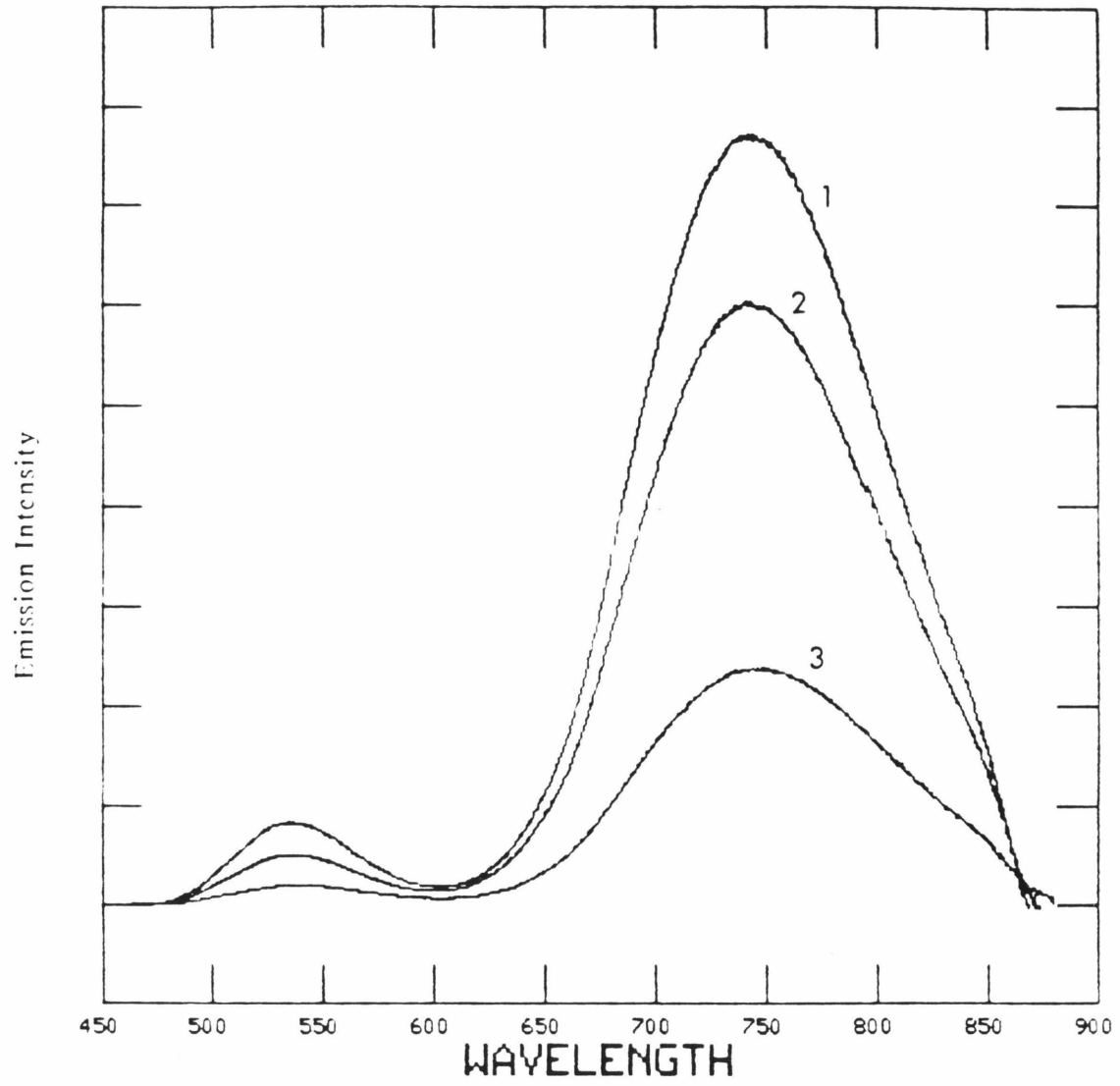


Table 4.1 Emission band maxima and quantum yields for the fluorescent $^1B_2(d\sigma^* p\sigma)$ and phosphorescent $^3B_2(d\sigma^* p\sigma)$ excited states of pyrazolyl-bridged binuclear iridium(I) carbonyl complexes.

Iridium Complex ^a	Emission Band Maxima (nm) ^b		Quantum Yields ^c	
	$^1B_2(d\sigma^* p\sigma)$	$^3B_2(d\sigma^* p\sigma)$	1B_2	3B_2
(μ -3,5-(CH ₃) ₂ pz)	535	740	0.0051	0.096
(μ -3-CH ₃ pz)	537	742	0.0035	0.079
(μ -pz)	540	743	0.0014	0.032

- a. The complex designations are abbreviated and represent [Ir(μ -pz)-(CO)₂]₂ and the substituted-pyrazolyl analogues.
- b. The emission band maxima and quantum yields were measured for 2-methylpentane solutions of these complexes.
- c. An acetonitrile solution of [Ru(bpy)₃](PF₆)₂, which has a quantum yield for emission of 0.062,²⁰ was used as the standard. The numbers are accurate to \pm 20%.

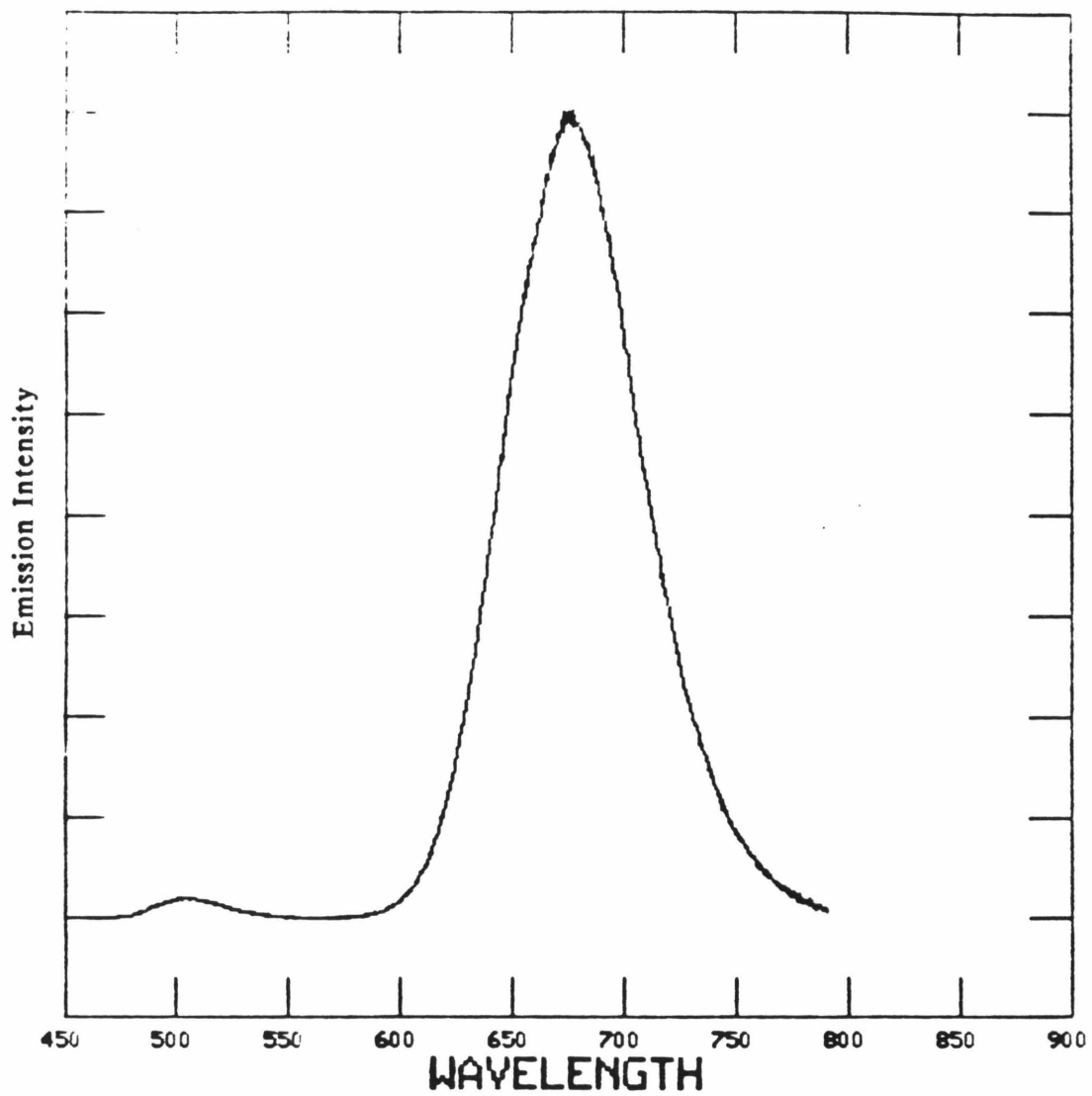
these three complexes at 77 K in 2-methylpentane glasses are shown in Figure 4.6. The ${}^3B_2(d\sigma^*p\sigma)$ excited-state lifetimes in 2-methylpentane solution parallel the luminescence and increase to 10.9 μs at 77 K for $[\text{Ir}(\mu\text{-}3,5\text{-}(\text{CH}_3)_2\text{pz})(\text{CO})_2]_2$ and $[\text{Ir}(\mu\text{-}3\text{-CH}_3\text{pz})(\text{CO})_2]_2$, from 3.3 μs and 580 ns, respectively, at ambient temperature, and to 10.2 μs at 77 K from 350 ns at ambient temperature for $[\text{Ir}(\mu\text{-pz})(\text{CO})_2]_2$. This implies that the temperature dependence of the lifetimes is primarily due to variations in the rate constant for nonradiative decay (k_{nr}) of the triplet excited state. Analogous to the study of $[\text{Ir}(\mu\text{-pz})(\text{COD})]_2$, $[\text{Ir}(\mu\text{-}3,4,5\text{-}(\text{CH}_3)_3\text{pz})(\text{COD})]_2$, and $[\text{Ir}(\mu\text{-}3\text{-CF}_3\text{-}5\text{-CH}_3\text{pz})(\text{COD})]_2$ outlined in Chapter 2, the observed lifetimes (τ_{obs}) of the ${}^3B_2(d\sigma^*p\sigma)$ excited states of the tetracarbonyl dimers are approximately equal to $(1/k_{\text{nr}})$, because $\Phi_{\text{em}} < 0.1$ at ambient temperature. The data for the temperature dependence of τ_{obs} for these three complexes, shown in Figure 4.7, can be fit to a modified-Arrhenius expression of the form given in equation (1).

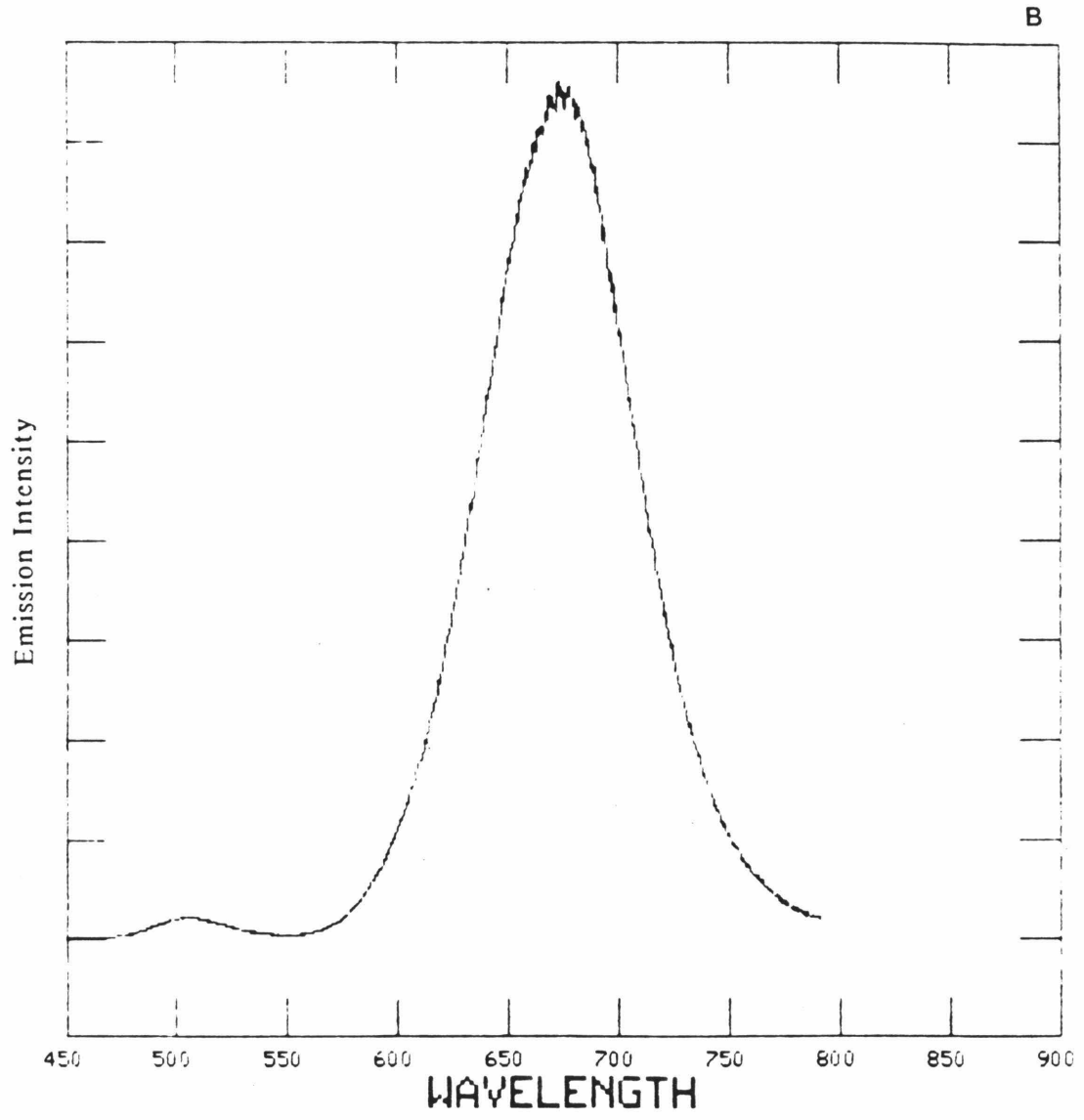
$$(1/\tau_{\text{obs}}) \approx k_{\text{nr}} = k_{\text{nr}}^{\circ} + k_{\text{nr}}' \exp(-E_a/k_bT) \quad (1)$$

In this expression, k_{nr}° and $k_{\text{nr}}' \exp(-E_a/k_bT)$ represent the nonradiative decay rate at low and high temperatures, respectively, and E_a is the activation energy for the thermally-accessible nonradiative pathway leading to deactivation of the excited state. The calculated values of E_a for the ${}^3B_2(d\sigma^*p\sigma)$ excited states of $[\text{Ir}(\mu\text{-}3,5\text{-}(\text{CH}_3)_2\text{pz})(\text{CO})_2]_2$, $[\text{Ir}(\mu\text{-}3\text{-CH}_3\text{pz})(\text{CO})_2]_2$, and $[\text{Ir}(\mu\text{-pz})(\text{CO})_2]_2$ are 1300, 550, and 650 cm^{-1} , respectively.²⁹

Figure 4.6 Corrected emission spectra of (a) $[\text{Ir}(\mu\text{-}3,5\text{-}(\text{CH}_3)_2\text{pz})(\text{CO})_2]_2$, (b) $[\text{Ir}(\mu\text{-}3\text{-CH}_3\text{pz})(\text{CO})_2]_2$, and (c) $[\text{Ir}(\mu\text{-pz})(\text{CO})_2]_2$ at 77 K (2-methylpentane glasses).

A





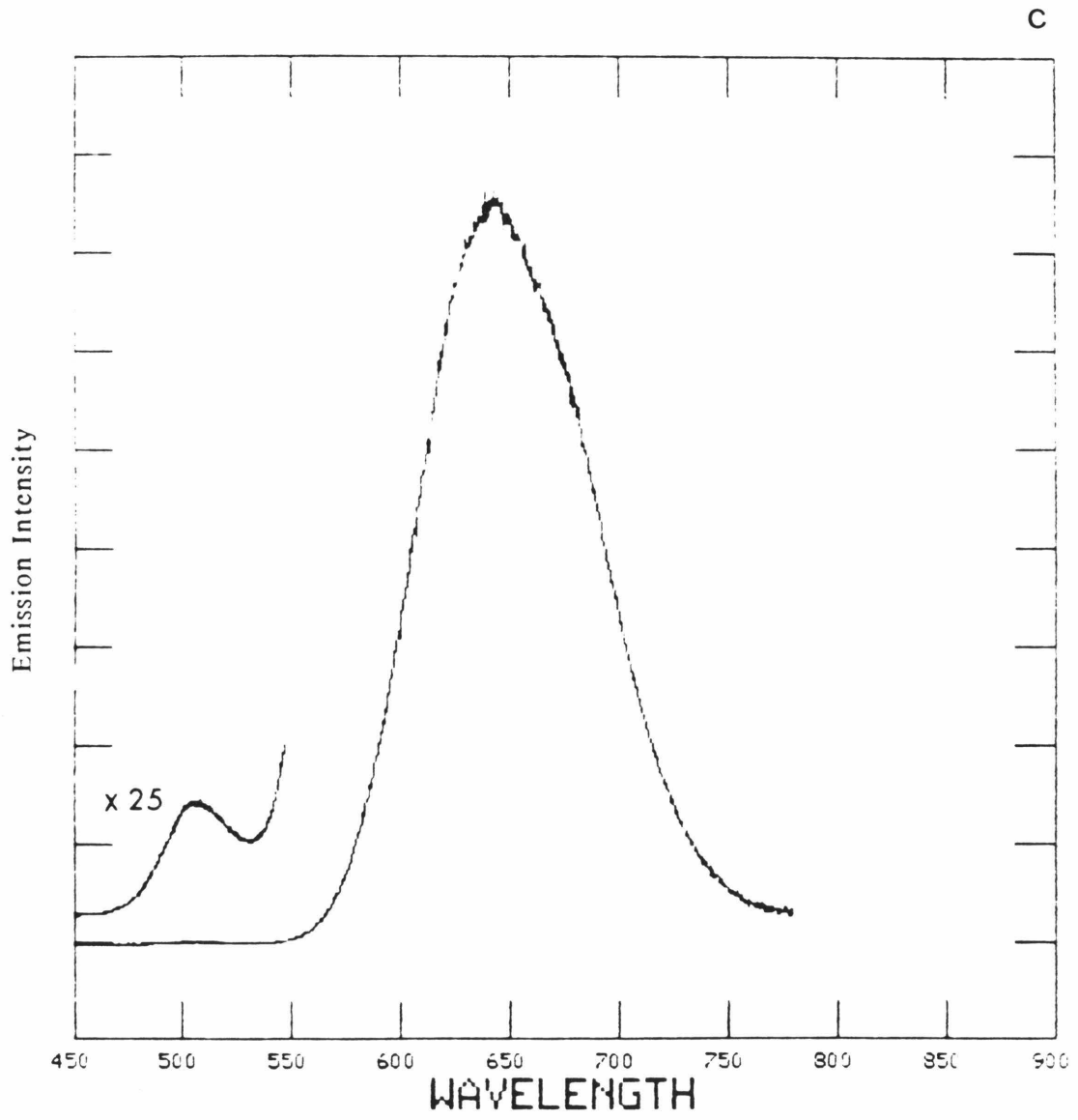
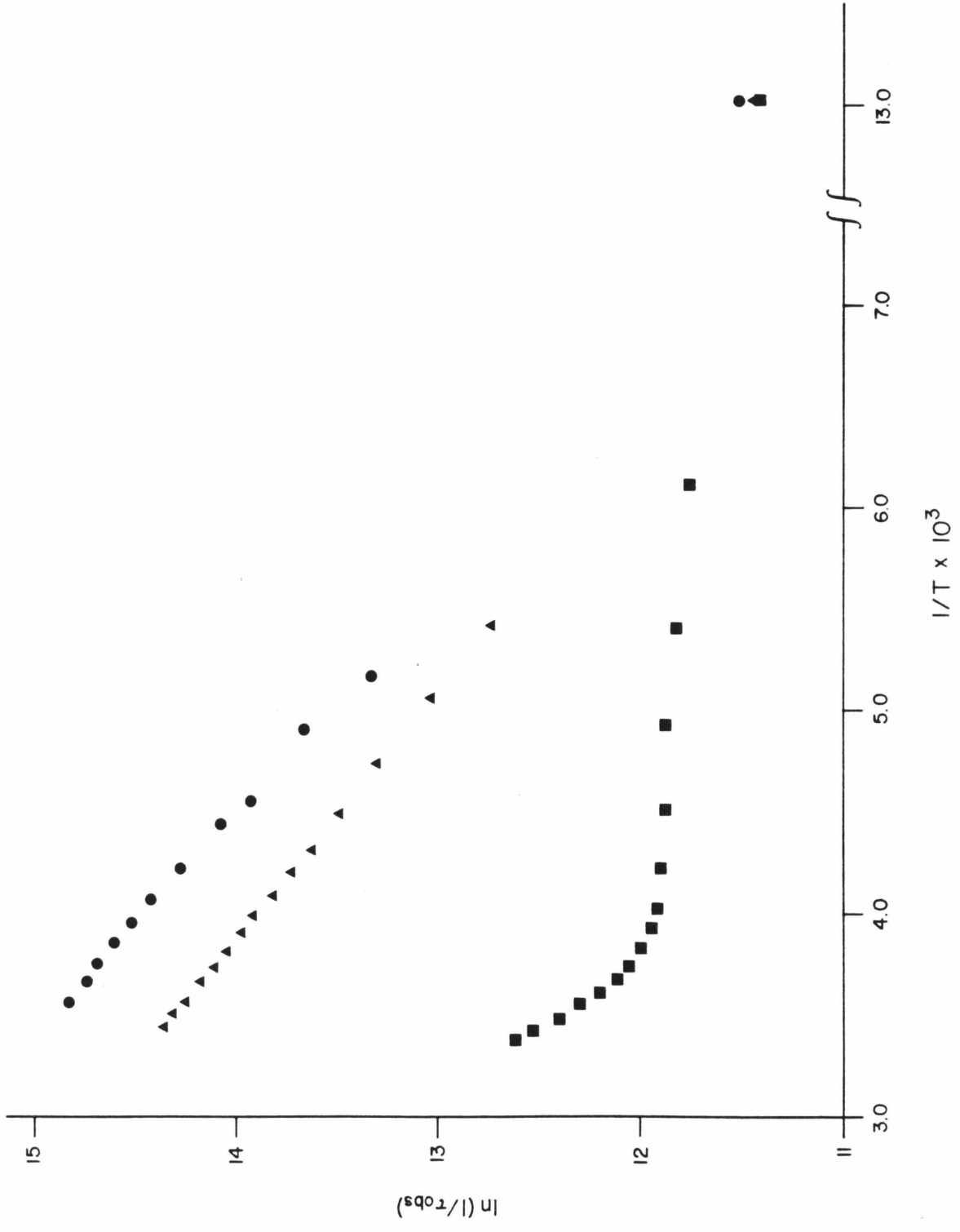


Figure 4.7 Arrhenius plots of the ${}^3B_2(d\sigma^*p\sigma)$ excited-state lifetimes of $[\text{Ir}(\mu\text{-}3,5\text{-}(\text{CH}_3)_2\text{pz})(\text{CO})_2]_2$ (■), $[\text{Ir}(\mu\text{-}3\text{-CH}_3\text{pz})(\text{CO})_2]_2$ (▲), and $[\text{Ir}(\mu\text{-pz})(\text{CO})_2]_2$ (●).



The activation energies for the thermal deactivation of the ${}^3B_2(d\sigma^*p\sigma)$ excited state for these carbonyl complexes are much lower than those of the cyclooctadiene species discussed in Chapter 2. Since the singlet-triplet splitting in these iridium carbonyl dimers is considerably larger than the measured activation energies, the possibility of thermally-activated delayed fluorescence is ruled out. Interestingly, both the ambient-temperature lifetimes of the triplet excited state and the emission quantum yields decrease with increasing metal-metal separation. Furthermore, the predominantly metal-metal localized $\sigma^*(d_z^2) \rightarrow [\sigma(p_z), \pi^*(CO)]$ transition shifts to higher energy with the increase in metal-metal separation. A reasonable mechanism for the nonradiative decay of the ${}^3B_2(d\sigma^*p\sigma)$ excited state, related to that proposed for the deactivation of the ${}^3A_{2u}(d\sigma^*p\sigma)$ excited state of the d^8 - d^8 rhodium isocyanide complexes,^{11,17} is thermal activation to a higher-energy d-d excited state derived from $d_{xz}, d_{yz} \rightarrow d_{x^2-y^2}$ excitation. This state, whose energy would be independent of the metal-metal separation, provides a pathway for rapid relaxation to the ground state.

The spectroscopic studies presented in this chapter of the series of complexes $[\text{Ir}(\mu\text{-}3,5\text{-(CH}_3)_2\text{pz})(\text{CO})_2]_2$, $[\text{Ir}(\mu\text{-}3\text{-CH}_3\text{pz})(\text{CO})_2]_2$, and $[\text{Ir}(\mu\text{-pz})(\text{CO})_2]_2$ reveal interesting features in the visible absorption and emission spectra at ambient temperature and 77 K. The metal-metal separation increases in the order $\mu\text{-}3,5\text{-(CH}_3)_2\text{pz} < \mu\text{-}3\text{-CH}_3\text{pz} < \mu\text{-pz}$, and the degree of metal-metal interaction is reflected in the predominantly metal-metal localized $d\sigma^*(d_z^2) \rightarrow [\sigma(p_z), \pi^*(CO)]$ transition. The photophysical studies of the emissive ${}^1,3B_2(d\sigma^*p\sigma)$ excited

states suggest that a higher-energy d-d excited state may provide a pathway for thermal deactivation of the luminescent ($d\sigma^* p\sigma$) excited states.

References and Notes

1. Beveridge, K.A.; Bushnell, G.W.; Dixon, K.R.; Eadie, D.T.; Stobart, S.R.; Atwood, J.L.; Zaworotko, M.J. *J. Am. Chem. Soc.* **1982**, *104*, 920-922.
2. Coleman, A.W.; Eadie, D.T.; Stobart, S.R.; Zaworotko, M.J.; Atwood, J.L. *J. Am. Chem. Soc.* **1982**, *104*, 922-923.
3. Bushnell, G.W.; Fjeldsted, D.O.K.; Stobart, S.R.; Zaworotko, M.J.; Knox, S.A.R.; Macpherson, K.A. *Organometallics* **1985**, *4*, 1107-1114.
4. Bushnell, G.W.; Fjeldsted, D.O.K.; Stobart, S.R.; Zaworotko, M.J. *J. Chem. Soc., Chem. Commun.* **1983**, 580-581.
5. Beveridge, K.A.; Bushnell, G.W.; Stobart, S.R.; Atwood, J.L.; Zaworotko, M.J. *Organometallics* **1983**, *2*, 1447-1451.
6. Harrison, D.G.; Stobart, S.R. *J. Chem. Soc., Chem. Commun.* **1986**, 285-286.
7. Nussbaum, S.; Rettig, S.J.; Storr, A.; Trotter, J. *Can J. Chem.* **1985**, *63*, 692-702.
8. Powell, J.; Kuksis, A.; Nyburg, S.C.; Wg, W.W. *Inorg. Chim. Acta* **1982**, *64*, L211-L212.
9. Atwood, J.L.; Beveridge, K.A.; Bushnell, G.W.; Dixon, K.R.; Eadie, D.T.; Stobart, S.R.; Zaworotko, M.J. *Inorg. Chem.* **1984**, *23*, 4050-4057.
10. Mann, K.R.; Gray, H.B. *Adv. Chem. Ser.* **1979**, *173*, 225-235.
11. Rice, S.F.; Milder, S.J.; Gray, H.B.; Goldbeck, R.A.; Kliger, D.S. *Coord. Chem. Rev.* **1982**, *43*, 349-354.
12. Rice, S.F.; Gray, H.B. *J. Am. Chem. Soc.* **1981**, *103*, 1593-1595.

13. Dallinger, R.F.; Miskowski, V.M.; Gray, H.B.; Woodruff, W.H. *J. Am. Chem. Soc.* **1981**, *103*, 1595-1596.
14. Rice, S.F.; Gray, H.B. *J. Am. Chem. Soc.* **1983**, *105*, 4571-4575.
15. Che, C.-M.; Butler, L.G.; Gray, H.B.; Crooks, R.M.; Woodruff, W.H. *J. Am. Chem. Soc.* **1983**, *105*, 5492-5494.
16. Smith, T.P. Ph.D. Dissertation, California Institute of Technology, Pasadena, 1982.
17. Rice, S.F. Ph.D. Dissertation, California Institute of Technology, Pasadena, 1982.
18. Marshall, J.L.; Fox, L.S.; Gray, H.B., unpublished results.
19. Demas, J.N.; Crosby, G.A. *J. Phys. Chem.* **1971**, *75*, 991-1024.
20. Caspar, J.V.; Meyer, T.J. *J. Am. Chem. Soc.* **1983**, *105*, 5583-5590.
21. Parker, C.A.; Rees, W.T. *Analyst* **1960**, *85*, 587-600.
22. Nocera, D.G.; Winkler, J.R.; Yocom, K.M.; Bordignon, E.; Gray, H.B. *J. Am. Chem. Soc.* **1984**, *106*, 5145-5150.
23. The iridium-iridium distance in $[\text{Ir}(\mu\text{-pz})(\text{CO})_2]_2$ is reported to be 3.510(1) Å in reference 6 and 3.506 Å in reference 7.
24. Hopkins, M.D.; Miskowski, V.M.; Marshall, J.L.; Gray, H.B., unpublished results.
25. In the molecular orbital diagram shown in Figure 4.4, the $a_1(d\sigma)$ orbital is higher in energy than the $d\pi(xz,yz)$ orbitals. Although the difference in energy between the $d\sigma$ and $d\pi$ orbitals is not known, the $d\sigma$ orbital is likely to be much closer in energy to the $d\pi$ orbitals than is suggested from this diagram.
26. For a discussion of the absorption spectra of square-planar, d^8 rhodium(I) and iridium(I) $\text{trans}-[\text{M}(\text{L})(\text{L}')_2(\text{CO})]$ complexes see:

- Brady, R.; Flynn, B.R.; Geoffroy, G.L.; Gray, H.B.; Peone, J., Jr.; Vaska, L. *Inorg. Chem.* **1976**, *15*, 1485-1488; Geoffroy, G.L.; Isci, H.; Litrenti, J.; Mason, W.R. *Inorg. Chem.* **1977**, *16*, 1950-1955.
27. See references 16 and 17 for a discussion of this transition in square-planar, d^8-d^8 complexes of rhodium(I) and iridium(I) with bridging isocyanide ligands.
28. Kalyanasundaram, K. *Coord. Chem. Rev.* **1982**, *46*, 159-244.
29. Because the transition between the high- and low-temperature regions of the lifetime data for $[\text{Ir}(\mu\text{-}3,5\text{-}(\text{CH}_3)_2\text{pz})(\text{CO})_2]_2$ is fairly close to ambient temperature, the number of data points for the thermally-activated process, from which E_a is determined, is limited, so the error in E_a for this complex is greater than for the other two complexes.